

Functional PVD-Coated/Textured Antimicrobial Surfaces

NIALL HALL

MPhil 2023

Functional Hybrid PVD-Coated/Textured Antimicrobial Surfaces

NIALL HALL

A thesis submitted in partial fulfilment of the
requirements of Manchester Metropolitan
University for the degree of Master of
Philosophy (MPhil)

Department of Engineering
Manchester Metropolitan University
In collaboration with the Manufacturing
Technology Centre

2023

Acknowledgements

Although there is only one name credited with the submission of this thesis, there are countless people that I would like to express my sincere thanks towards for helping contribute a wide range of help to finishing this work.

Firstly, I would like to extend my greatest appreciation and thanks to my supervisory team of Professor. Tomasz Liskiewicz, Professor. Peter Kelly, Professor. Kathryn Whitehead & Dr. Marina Ratova. They have been an inexhaustible source of knowledge and support that I could not have wished for a better team to help me through these three gruelling years. They have helped guide me from the first year where I had no idea what lay ahead of me, to my final third year, where I still have no idea what I'm doing!

I would also like to thank my parents; they have been the solid rock of support that I have needed whilst I haphazardly navigated my way through this MPhil degree. Their unwavering faith and their monetary support have been something that I could not have done this without. I will forever be in their debt for the years and years of support and love, whilst I have followed my academic ideas. Thanks, should also go to my brothers, who have had to listen to me complain incessantly about experiments and all the reports that I had to read and write. To my friends, who have mostly been going through the same trials and tribulations with their own research projects, you have all been massive helps with the various pub visits, where we all moaned and complained about our degrees, and the climbing sessions that helped us all get through the last years, I want to thank you all dearly.

Last, but certainly not the least, I would like to thank my girlfriend, Navkiran. Without her help, constant support and pushing me to do my work, I would most certainly have not carried on with this degree! She has been a constant boost to my confidence and her belief that this project would eventually be completed, consistently made me put in the effort to do my work.

Abstract

Titanium nitride and silver are a combination of materials that have been extensively used for production of antimicrobial coatings via physical vapour deposition (PVD), specifically the pulsed DC magnetron sputtering method. There are also widely reported textured samples, via an inexhaustive list of processes, this research project will focus on the laser induced periodic surface structures (LIPSS) method. Whilst there have been numerous studies that investigate the PVD & LIPSS processes individually, at the time of writing to the authors knowledge there were no studies that investigated the two processes combined.

*The main goal of this project was to investigate the possibility of synergy between the two well established processes of Physical Vapour Deposition and Laser Texturing, to determine if the combination of the two surface types provided an optimised antimicrobial surface that would be fit for purpose as a coating/texture for an external fixation device or would the two properties be antagonistic to each other. Titanium nitride, and silver were the deposited materials, with 316 stainless-steel chosen as the substrate. The bacteria that were chosen for investigation were *Staphylococcus aureus* and *Pseudomonas aeruginosa*, which are both common hospital-acquired infections (HAIs). The antimicrobial effect of titanium nitride and silver is demonstrated throughout, with increases in silver content producing increases in antimicrobial activity. The range of silver in the coatings, measured by atomic weight percentage (at%), was between 15 – 30 at%. Changes in number of retained bacterial cells is demonstrated throughout this thesis, with the texturing patterns having a substantial effect on the number of bacteria that were able to adhere to the substrates. These surface patterns were varied between linear grooves, and the randomly organised structures of LIPSS, which each had a different effect on the adherence of the two bacterial strains. Overall, the combination of the two processes reduced the antimicrobial efficacy and increased the number of bacteria cells adhered to the substrate. Utilising various analytical and microbiological tests, such as scanning electron microscope (SEM), energy dispersive x-ray diffraction (EDX), White Light Profilometry (WLP), X-Ray Diffraction Analysis (XRD), LIVE/DEAD staining, and retention assay the thin films produced were tested and analysed.*

Table of Contents

ACKNOWLEDGEMENTS	I
ABSTRACT	II
<i>Table of Contents</i>	<i>iii</i>
TABLE OF FIGURES	V
TABLE OF TABLES	VII
TABLE OF APPENDICES	VII
PART I	1
CHAPTER 1 – BACKGROUND	2
1.1 INTRODUCTION	2
1.2 BACKGROUND & MOTIVATIONS	2
1.3 RESEARCH AIMS & CONTRIBUTIONS	4
1.4 THESIS STRUCTURE	4
1.5 MICROBIOLOGICAL REVIEW	5
1.5.1 Definitions of Antimicrobial Surfaces.....	5
1.5.2 Stainless-Steel.....	6
1.5.3 Titanium Nitride & Silver	7
1.5.3.1 Background.....	7
1.5.3.2 Titanium.....	8
1.5.3.3 Titanium Nitride	9
1.5.3.4 Silver.....	9
1.5.3.5 Titanium Nitride & Silver	10
1.5.4 Textured Antimicrobial Surfaces.....	11
1.5.4.1 Introduction	11
1.5.4.2 Laser Texturing	11
1.5.5 Bacterial Strains	14
1.5.5.1 Staphylococcus aureus.....	14
1.5.5.2 Pseudomonas aeruginosa.....	15
1.6 DEPOSITION & TEXTURING REVIEW	16
1.6.1 Physical Vapour Deposition.....	16
1.6.1.1 DC Diode Sputtering	17
1.6.1.2 Magnetron Sputtering.....	17
1.6.1.2.1 Conventional Magnetron Sputtering.....	17

1.6.1.2.2 Unbalanced Magnetron Sputtering	19
1.6.1.3 Pulsed DC Magnetron Sputtering	19
1.6.1.4 Reactive Sputtering Deposition	20
1.6.1.5 High Power Impulse Magnetron Sputtering (HiPIMS)	21
1.6.2 <i>Surface Texturing Methods</i>	22
1.6.2.1 Laser Texturing	22
1.6.2.1.1 Laser Induced Periodic Surface Structures (LIPSS)	23
1.6.2.2 Biomimetic Surfaces	25
1.7 EXTERNAL FIXATION DEVICES	26
1.8 SUMMARY	27
1.8.1 <i>Summary & How it Affected Project</i>	27
PART II	29
CHAPTER 2 – METHODS	30
2.1 DEPOSITION TECHNIQUE	30
2.2 LASER TEXTURING TECHNIQUES	31
2.3 MICROBIOLOGICAL TECHNIQUES	33
2.3.1 <i>Microorganisms</i>	33
2.3.2 <i>Zones of Inhibition</i>	34
2.3.3 <i>Nitroblue Tetrazolium Test (NBT)</i>	35
2.3.4 <i>Retention Assay</i>	37
2.3.5 <i>LIVE/DEAD Stain</i>	40
2.3.6 <i>Statistical Analysis</i>	44
2.4 ANALYTICAL TECHNIQUES	44
2.4.1 <i>Overview</i>	44
2.4.2 <i>Scanning Electron Microscopy</i>	45
2.4.3 <i>Energy Dispersive X-Ray Spectroscopy</i>	46
2.4.4 <i>X-Ray Diffraction Spectroscopy</i>	47
2.4.5 <i>White Light Profilometry (WLP)</i>	47
2.5 SUMMARY	48
PART III	50
CHAPTER 3 – RESULTS	51
3.1 EDX RESULTS	51
3.2 XRD RESULTS	54

3.3 WLP RESULTS	58
3.4 SEM IMAGE RESULTS	60
3.5 ZONES OF INHIBITION (ZOI)	64
3.6 NITROBLUE TETRAZOLIUM TEST	64
3.7 RETENTION ASSAY	65
3.8 LIVE/DEAD ASSAY	70
PART IV	73
CHAPTER 4 – DISCUSSION & CONCLUSIONS	74
4.1 PERSPECTIVE	74
4.2 MAJOR FINDINGS	75
4.3 CONCLUSIONS & FUTURE WORK	79
4.3.1 <i>Conclusions Drawn</i>	79
4.3.2 <i>Future Work</i>	80
BIBLIOGRAPHY	I
APPENDICES	A

Table of Figures

FIGURE 1: SILVER USE THROUGHOUT THE YEARS (MOHLER ET AL., 2018)	6
FIGURE 2: TITANIUM NITRIDE COATED MEDICAL IMPLANT (GOTMAN AND GUTMANAS, 2014)	8
FIGURE 3: S. AUREUS INFECTED LIPSS STAINLESS-STEEL	13
FIGURE 4: RESULTS FOR DIFFERENT LASER TEXTURED STYLES ON BACTERIAL ADHESION (LUTEY ET AL., 2018)	14
FIGURE 5: STAPHYLOCOCCUS AUREUS BACTERIUM (CENTRE FOR DISEASE CONTROL & PREVENTION, 2018)	15
FIGURE 6: PSEUDOMONAS AERUGINOSA	16
FIGURE 7: TYPICAL PVD SPUTTERING PROCESS (BAPTISTA ET AL., 2018)	17
FIGURE 8: MAGNETRON SPUTTERING PROCESS (BCLUE, 2021)	18
FIGURE 9: SCHEMATIC FOR TARGET VOLTAGE WAVEFORM FOR PULSED DC POWER SUPPLY (KELLY AND ARNELL, 2000)	20
FIGURE 10: LIPSS TEXTURED STAINLESS-STEEL PRODUCED DURING RESEARCH PROJECT	24
FIGURE 11: SEM IMAGE OF SHARK SKIN (PU ET AL., 2016)	24
FIGURE 12: EXTERNAL FIXATION DEVICE (NEPHEW, 2012)	26

FIGURE 13: PLAN VIEW SCHEMATIC OF PVD RIG CONFIGURATION.	30
FIGURE 14: LIPSS TEXTURE ON STAINLESS-STEEL, POWER 36%, SCANNING SPEED 470MM/S, HATCHING 0.009MM, SEM IMAGE AT 4X MAGNIFICATION.....	32
FIGURE 15: ZONES OF INHIBITION TEST AGAINST STAPHYLOCOCCUS AUREUS USING 4 DIFFERENT ANTIMICROBIAL AGENTS (SPRINGER, 2018).....	35
FIGURE 16: NBT TEST ON STAINLESS-STEEL, BLUE DOTS REPRESENTING RESPIRING COLONIES	37
FIGURE 17: EPIFLUORESCENCE MICROSCOPY OF S. AUREUS ON LIPSS SAMPLE	39
FIGURE 18: FIJI SOFTWARE MACRO FOR RETENTION ASSAY CALCULATION.....	40
FIGURE 19: CODE FOR LIVE/DEAD FIJI CALCULATION	41
FIGURE 20: LIVE/DEAD STAIN OF P. AERUGINOSA ON TiN-AG 60W.....	42
FIGURE 21: LIVE/DEAD LIVE CELLS ON STAINLESS-STEEL.....	43
FIGURE 22: OVERLAY LIVE/DEAD STAIN FOR S. AUREUS ON TiN-AG 50W	44
FIGURE 23: SEM SCHEMATIC.....	46
FIGURE 24: EDX RESULTS FOR SECOND BATCH	53
FIGURE 25: EDX RESULTS FOR THIRD BATCH OF SAMPLES.....	54
FIGURE 26: XRD RESULTS COMPARISON OF DIFFERENT ANGLES OF INCIDENCE ON TiN.....	55
FIGURE 27: XRD RESULTS FOR TiN, TiN-AG 50 W, AND TiN-AG 60 W AT 3 DEGREES INCIDENT ANGLE	56
FIGURE 28: XRD RESULT FOR TiN-AG 70 W.....	56
FIGURE 29: XRD RESULTS FOR TiN-AG 80 W	56
FIGURE 30: XRD COMPARISON OF SUBSTRATE & COATING SIDE OF TiN.....	57
FIGURE 31: 3D SURFACE PROFIOMETRY MAP FROM TiN-AG 50W DEPOSITED ON STAINLESS STEEL.....	59
FIGURE 32: 3D SURFACE PROFIOMETRY MAP FOR LIPSS PATTERN TEXTURE ON STAINLESS-STEEL.....	59
FIGURE 33: LIPSS TEXTURED STAINLESS-STEEL	60
FIGURE 34: TiN-AG 50 W COATED STAINLESS-STEEL AT 10X MAGNIFICATION ON SEM	61
FIGURE 35: TiN-AG 60 W COATING ON STAINLESS-STEEL.....	61
FIGURE 36: STAINLESS-STEEL UNCOATED & UNTEXTURED, POLISHED BY EXTERNAL COMPANY.....	62
FIGURE 37: P. AERUGINOSA INOCULATED STAINLESS-STEEL LIPSS	63
FIGURE 38: LIPSS TEXTURED SS INOCULATED WITH S. AUREUS	64
FIGURE 39: NBT RESULTS FOR FINAL POWER VARIATIONS.....	65
FIGURE 40: RETAINED CELLS ON SAMPLES FOR S. AUREUS	66
FIGURE 41: RETAINED CELLS ON SAMPLES FOR P. AERUGINOSA	67
FIGURE 42: RETENTION ASSAY FOR D50 TEXTURE S. AUREUS	68
FIGURE 43: RETENTION ASSAY FOR LIPSS COATED S. AUREUS	69
FIGURE 44: RETENTION ASSAY FOR LIPSS P. AERUGINOSA	69
FIGURE 45: LIVE/DEAD RESULTS FOR P. AERUGINOSA	71

FIGURE 46: LIVE/DEAD RESULTS FOR S. AUREUS	72
--	----

Table of Tables

TABLE 1: MICROBIOLOGICAL METHODS SUMMARY	48
TABLE 2: ANALYTICAL METHOD SUMMARY	49
TABLE 3: EDX RESULTS FROM INITIAL SAMPLES	51
TABLE 4: EDX RESULTS SECOND BATCH	52
TABLE 5: EDX RESULTS THIRD BATCH	52
TABLE 6: WLP RESULTS FOR ALL SAMPLES	58

6

Table of Appendices

APPENDIX 1: TiN-Ag 50W DEPOSITED ON STAINLESS-STEEL	A
APPENDIX 2: TiN DEPOSITED ONTO STAINLESS-STEEL	B
APPENDIX 3: TiN-Ag 60W DEPOSITED ONTO STAINLESS-STEEL	C
APPENDIX 4: TiN-Ag 80W DEPOSITED ONTO STAINLESS-STEEL	D
APPENDIX 5: TiN-Ag 100W DEPOSITED ONTO STAINLESS-STEEL	E
APPENDIX 6: TiN-Ag 120W DEPOSITED ONTO STAINLESS-STEEL	F
APPENDIX 7: TiN-Ag 50W DEPOSITED ONTO STAINLESS-STEEL	G
APPENDIX 8: TiN-Ag 60W DEPOSITED ONTO STAINLESS-STEEL	H
APPENDIX 9: TiN-Ag 70W DEPOSITED ONTO STAINLESS-STEEL	I
APPENDIX 10: WLP 3D MAP OF STAINLESS-STEEL LASER TEXTURED D20 H5 PATTERN	J
APPENDIX 11: WLP 3D MAP OF D50 H5 LASER TEXTURE ON STAINLESS-STEEL	K
APPENDIX 12: WLP 3D MAP OF LIPSS PATTERN ON STAINLESS-STEEL	L
APPENDIX 13: WLP 3D MAP OF LIPSS PATTERN COATED WITH TiN-Ag 70W ON STAINLESS-STEEL	M
APPENDIX 14: WLP 3D MAP OF TiN COATED ON STAINLESS-STEEL	N
APPENDIX 15: WLP 3D MAP OF TiN-Ag 50W DEPOSITED ONTO STAINLESS-STEEL	O
APPENDIX 16: WLP 3D MAP OF TiN-Ag 60W DEPOSITED ONTO STAINLESS-STEEL	P
APPENDIX 17: WLP 3D MAP OF TiN-Ag 70W DEPOSITED ONTO STAINLESS-STEEL	Q
APPENDIX 18: WLP 3D MAP OF TiN-Ag 80W DEPOSITED ONTO STAINLESS-STEEL	R
APPENDIX 19: RAW DATA FOR LIVE/DEAD S. AUREUS.....	R
APPENDIX 20: RAW DATA FOR LIVE/DEAD P. AERUGINOSA.....	S
APPENDIX 21: RETENTION ASSAY FOR SAMPLES S. AUREUS.....	S
APPENDIX 22: RETENTION ASSAY FOR P. AERUGINOSA	T
APPENDIX 23: RAW DATA FOR T-TEST S. AUREUS	T

APPENDIX 24: ANALYSED DATA FOR T-TEST S. AUREUS	T
APPENDIX 25: RETENTION ASSAY RAW DATA T-TEST P. AERUGINOSA.....	U
APPENDIX 26: RETENTION ASSAY ANALYSED RESULTS T-TEST P. AERUGINOSA.....	U
APPENDIX 27: NBT RESULTS FOR SAMPLES	U

Part I

Background & Introduction

Chapter 1 – Background

1.1 Introduction

The primary goal of this research was to investigate the possible synergy between two well-established surface engineering methods, with the aim of producing an improved antimicrobial surface for external fixation devices. The chosen methods were Physical Vapour Deposition (PVD) and Laser Texturing (LT) for anti-adhesive properties. The influence of combining these methods will be discussed in multiple sections.

This following chapter contains an overview of all the work carried out, with the motivations and background also mentioned. The focus, the aims and the main research goals will also be highlighted, with the thesis layout also explained.

1.2 Background & Motivations

External fixation devices are common medical implants, which require an invasive operation to install, and are used for the reconstruction of a severely fractured bone, with many being compound fractures. Due their invasive nature, they create a permanent breach between the natural skin-air barrier. These implants can be very susceptible to bacterial infections, with the infection rates ranging from 19.6% up to 47.8% (Shah *et al.*, 2019). Should an implant become infected, the worst-case scenario is the implant must be removed. As once the bacteria have become sessile, they can begin to form a biofilm, and these can be difficult to remove. These removal surgeries not only place an increased cost on the hospitals, but it also places a further strain onto the patient, depending on the severity of the fracture, they may have to be anaesthetised. As there are countless bacteria that can cause infections, they are all brought under the umbrella term; hospital acquired infections (HAIs) (Campoccia *et al.*, 2006, Pietrocola *et al.*, 2022). Infections that are related to medical implants can make up to 25% of all recorded incidents of HAIs, and as many as 1 in 25 patients admitted to hospital can develop these infections. These infections can be classified as having a significant effect on the health-care industry (Zander and Becker, 2018).

The intended purpose of modifying medical devices with the two chosen engineering techniques was to investigate the possibility of reducing infection rates. There has also been an increase in the number of external fixator devices that are being reprocessed

and reused by hospitals, this is in an effort to reduce the costs of these usually single-use devices (Thamyongkit *et al.*, 2018). If the devices are to be re-used, then, they would have to be cleaned and free of any bacteria. It is known that most of these devices are manufactured from 316 medical grade stainless-steel, which has negligible inherent antimicrobial properties, which is derived from its molybdenum content, however it is not an effective agent. Bacterial infections on medical implants are generally characterise by biofilm formation on the surface of the device, and this formation can begin almost instantaneously once the bacteria has landed on the substrate. However, using the surface engineering techniques of physical vapour deposition, and laser texturing the surface of the stainless-steel can be manipulated to produce a surface that could be resistant to bacteria.

Magnetron sputtering is a branch of physical vapour deposition that can produce coatings that have high adhesion to their target substrate and have a high resistance to any external actions. These coatings, which can be produced from titanium nitride and silver, are classified as thin-film technologies, and are currently used in the fields of tool-coating and other hard-wearing applications. Depositing certain elements onto the substrate can provide the necessary antimicrobial activity, therefore titanium nitride and silver were chosen as the materials (Akhidime *et al.*, 2019, Kelly *et al.*, 2010, Kelly *et al.*, 2009, Whitehead *et al.*, 2010, Wickens *et al.*, 2012). Laser texturing is a method that can be utilised to alter the topographical features of a surface, with high levels of precision being attributed to it. Not only can the topographical features be altered, the surface hydrophobicity, and the surface chemistry can also be manipulated. As both processes can be used in commercial applications, there is potential that the following experimental procedures could be scaled up for commercial use.

This research project will focus on the combination of the two processes, to produce a thin-film coating that is either resistant to bacterial adhesion, or antimicrobial in application for coating external fixator devices. It will also investigate, should the combination of the processes not produce a viable surface, why it has failed in its application.

1.3 Research Aims & Contributions

This following section will be a summary of the various research goals and the objectives that had to be met to achieve the goals. The current research aim of this thesis is to investigate the potential synergy of magnetron sputtering titanium nitride and silver, and laser texturing to produce a viable antimicrobial surface. Hence, the thesis was divided into the following research directions.

1. Coating 316 medical-grade stainless-steel with titanium nitride and silver
2. Laser texturing of 316 medical-grade stainless-steel
3. Surface Characterisation analysis to determine what has been produced
4. Antimicrobial analysis to determine the efficacy of all produced variants of coatings and textures
5. Combination of the two processes, to produce an optimised coated & textured sample
6. Microbiological assays to determine antimicrobial efficacy & optimised coating/texture
7. Application of optimised texture/coating to stainless-steel

Application of this optimised coating/texture to the field of medical implants has a potentially large contribution to applying engineering techniques to the growing problem of bacterial infections of medical implants.

1.4 Thesis Structure

This thesis is a presentation of the work carried out to investigate the possibility of the synergy between thin-film coatings produced via magnetron sputtering and texturing made via laser texturing. The thesis is divided into four sections, which were divided into 9 sub-sections. Chapter I will contain the background information and the necessary literature research and review for the project. Chapter II will contain the descriptions of all the analytical techniques and experimental methods that have been used throughout the project. Chapter III is set out to contain an extensive review of all the results gained throughout the project, and the interpretation of these results regarding the application purpose. Chapter IV will contain the outcomes of this research project and will outline any possibility of future work being carried out.

- Chapter 1.** Provides the topic of study, the hypotheses to be investigated, layout of the project & the review of the literature
- Chapter 2.** Methods that were used throughout the project
- Chapter 3.** Results gained from the methods
- Chapter 4.** Discussion & Conclusions

1.5 Microbiological Review

This section will focus on antimicrobial surfaces, it will introduce what is meant by this term, it will not explore every antimicrobial surface currently available in detail but will highlight the ones that have been found to be relevant to this project. For example, surfaces that have been manufactured by either a surface deposition technique, or texturing process, e.g., titanium nitride and silver coatings. The chapter will introduce the multiple advantages/disadvantages of using titanium nitride and silver as an antimicrobial surface and will also touch on the topic of improvements to efficacy/efficiency that were investigated in this project.

1.5.1 Definitions of Antimicrobial Surfaces

The purpose of antimicrobial surfaces is to reduce, or prevent the formation of biofilms on their surface, biofilm formation can be a near irreversible process should it be allowed time to do so. Issues with biofilm formation spread across a wide range of modern industries, from food and water companies struggling to remove the bacteria that form in their water pipes, to cargo ships that have bacteria formation on their hulls and also to the medical industry (Epperlein *et al.*, 2017, Farkas *et al.*, 2020, Gonzalez *et al.*, 2021). Antimicrobial surfaces can generally be split into two different categories, one which is an anti-biofouling surface, and one that is antimicrobial surface. They are different in their approach towards bacterial infections of surfaces, in short, an anti-biofouling surface is one that attempts to resist bacteria from adhering to its surface without any bactericidal agents being present in its composition. Whereas an antimicrobial surface is one that has a bactericidal agent present in its composition, and once a bacteria has landed on its surface it will eradicate the bacteria via the mechanism of its agent (Zander and Becker, 2018). Antimicrobial surfaces can be manufactured from a broad spectrum of materials, with an equally broad spectrum of coating/texturing processes, there are certain metals that exhibit desirable properties for usage in antimicrobial surfaces. These include silver,

which has been used for over a millennium, the uses of silver ranged from storage of drinking water, needles for acupuncture and even wound treatment (Mohler *et al.*, 2018).

The use of silver inside the medical industry started to become better refined and more widely available during the 19th century, with some of the first commercially available products being produced (Taheri *et al.*, 2014). When considering a material for usage as an antimicrobial agent on a medical device, there are certain safety measurements that must be met. These are the measurements that have been put in place to ensure that there are no negative side-effects, or there are negligible side-effects, from using these materials in the industry. The materials must be biocompatible to begin with, meaning that they do not produce an inflammatory response from the host body, which can lead to more serious effects.

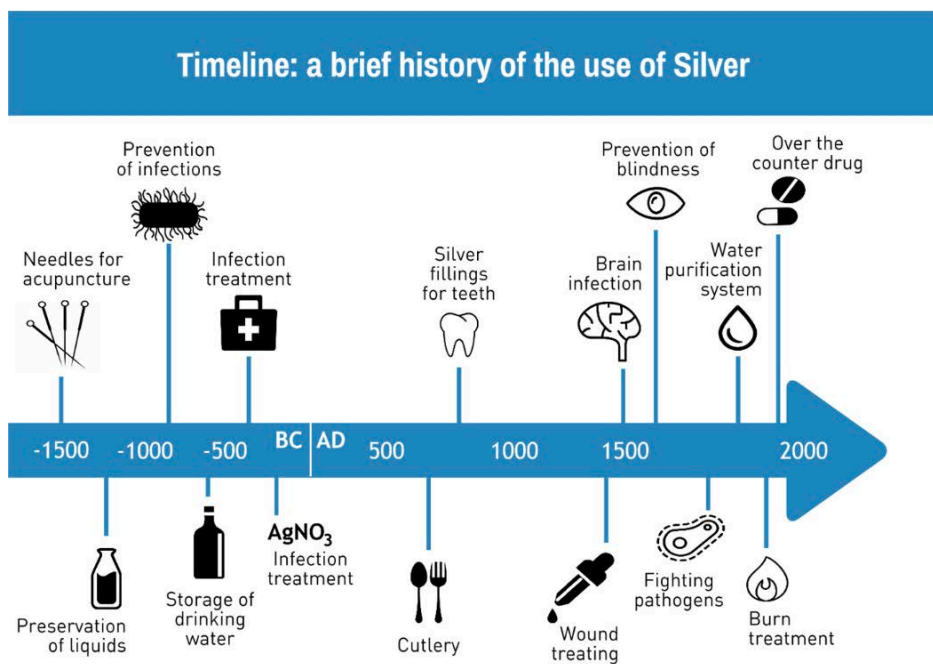


Figure 1: Silver Use Throughout the Years (Mohler *et al.*, 2018)

1.5.2 Stainless-Steel

Stainless steels are a diverse family of ferrous alloys that can be linked together by having specific amounts of constituting elements of chromium and iron. They are favoured across many different industries, such as the aerospace, food, and medical industry (Whitehead and Verran, 2007, Whitehead *et al.*, 2010, Kelly *et al.*, 2011, Wickens *et al.*, 2012, Kenar *et al.*, 2013, Skovager *et al.*, 2013, Wickens *et al.*, 2014, Epperlein *et al.*, 2017, Tetlow *et al.*, 2017). Their wide use can be traced to their excellent corrosion and

wear resistances, which has afforded them their ability to be used in numerous applications. There are countless numbers of different grades of stainless-steel, with some of them being favoured more in differing industries, for example 304 is used within the food industry and 316 is used within the medical industry (Whitehead and Verran, 2007, Slate *et al.*, 2018).

For this research project the 316 medical grade stainless-steel will be focused on, as there are innumerable grades that all have their own specific properties and applications. 316 stainless-steel is commonly found material that is used for external fixation devices, and it was chosen for this application due to its increased corrosion resistance, that is gained from the higher molybdenum content (Wickens *et al.*, 2012). However, as the stainless-steel has no inherent antimicrobial properties, it suffers from high rates of infections in this application, with reports ranging from 3 % to 30 % of all devices becoming infected.

1.5.3 Titanium Nitride & Silver

1.5.3.1 Background

When researching antimicrobial materials, there are few that are as widely reported within the literature as titanium nitride and silver, this combination of materials is used for a broad spectrum of applications. These can extend from tool coatings, which exploits the hard-wearing properties of the titanium nitride ceramic, and all the way to implantable medical devices. One of the methods for depositing this combination of materials is physical vapour deposition, and this is one of the most widely used methods for depositing this combination of materials. When using this method for coating, the resulting structure is expected to form a hard encapsulating titanium nitride matrix, with silver particles being trapped in the matrix (Kelly *et al.*, 2009, Kelly *et al.*, 2010, Whitehead *et al.*, 2010, Kelly *et al.*, 2011). This provides the beneficial properties of titanium nitride to the silver's antimicrobial properties, and the properties desired from titanium nitride is that it is hard wearing. If the coating was to be produced entirely of silver, then it would not be fit for the purpose of the coating, silver is a relatively soft metal, with a Vickers hardness rating of 75 VH. When compared to titanium nitrides hardness of 2100 – 2400 VH, it is clear to see that silver would not be suitable for a coating that has to be exposed to wear and loading (Gotman *et al.*, 2011). This also would be true for an entirely titanium nitride-based

coating, as it has no inherent antimicrobial properties, and thus would be unsuitable for application. Titanium nitride forms a gold-coloured coating, and when silver is added to a titanium nitride coating, the colour will begin to vary. This is entirely dependent on the amount of silver that can be found within the coating.



Figure 2: Titanium Nitride Coated Medical Implant (Gotman and Gutmanas, 2014)

1.5.3.2 Titanium

Titanium has been gaining popularity for usage in a wide variety of fields such as the medical industry, marine industry and even the aerospace industry. Its desirability across these different industries can be narrowed down to its versatile properties, such as the medical and the aerospace industry, its low specific weight is a desirable property, as this allows for reduction of the overall weight of their desired application. For medical implants having a lower specific weight is necessary for the comfort of the patient, and in the aerospace industry this can also be a benefit (Whitehead *et al.*, 2011, Gotman and Gutmanas, 2014). It also has the benefit of having a relatively low elastic modulus, with a value of 120 GPa, whilst 316 medical grade stainless steel has an elastic modulus value of 193 GPa and natural bone has an elastic modulus of around 15 GPa. This lower elastic modulus reduces the overall risk of stress-shielding, which is a phenomenon where the implanted material experiences more loading than the natural bone (Alexander *et al.*,

2021). Human bone remodels itself depending on the loading that it experiences, and if there is stress-shielding the bone will decrease in density (Ridzwan *et al.*, 2007).

Despite its desirable properties, titanium is not a perfect material for use on its own, for example its poor wear resistance can lead to it becoming fragmented and therefore creates titanium metal debris within the body (Alexander *et al.*, 2021).

1.5.3.3 Titanium Nitride

When considering the use of titanium nitride as the initial combination of materials, there are numerous benefits that can be exploited over the base titanium metal, one of which has been mentioned already and that is the increase in the hardness of the coatings produced. The addition of nitrogen to titanium, producing a ceramic coating overall, can lead to increases in the surface's wear and corrosion resistances (Raj *et al.*, 2022). Increasing these resistances can reduce the possibility of the material becoming fragmented. One problem that can be attributed to coated implants is the adhesive quality of the deposition process, meaning that during loading some methods can lead to delamination of the coating. If the coating is delaminated, it can cause complications due to metal poisoning, and any complications that arise from the material having to be removed from the patient.

Whilst stainless-steel is one of the most used materials for load-bearing orthopaedic implants, the use of titanium, including many of its alloys, has been growing in popularity. This usage is further increased via the addition of nitrogen, titanium nitride is a popular choice for use in cutting tools, and other high wear applications. Along with its increased corrosion resistance, it also has the benefit of being a biocompatible material (Moseke *et al.*, 2011). Titanium nitride is also used in orthodontic applications, this is attributed to its hard-wearing capabilities, however, when using certain deposition techniques, the surface is not entirely smooth. This was also found throughout this research project, as from the SEM imaging, there still appears to be roughness and even fragments of particles on the substrate surface (Zhang *et al.*, 2019).

1.5.3.4 Silver

As previously mentioned, silver is a well-established antimicrobial agent and this is thought to be due to its ability to inhibit DNA replication in most known strains of bacteria (Saubade *et al.*, 2019). However, the combination of all three materials can lead to some

detrimental properties being exhibited, such as the reduction in hardness of the materials. This has been documented in numerous research papers, with the effect being dependent on the amount of silver in the coatings, with reports suggesting that when 66% of the coating consists of silver the hardness can drop below 5.4 GPa, which is less than the hardness value of stainless steel, which in this paper was 420A stainless steel (Braceras *et al.*, 2021). This disadvantage of reduction in overall sample hardness can be circumvented by reducing the overall content of silver, with there being an optimum atomic weight percentage, which has the beneficial properties of all the elements used. It should be noted that silver as a bulk material has no antimicrobial activity and is inert. It requires being in contact with some form of fluid, bodily fluid or water, to become one of its oxidised ions (Slate *et al.*, 2018).

Being an inert bulk material, means that the silver ions must be able to leach from the substrate and begin to permeate into the bacterial cells. The mechanism by which silver exhibits its antimicrobial efficacy is dependent on the nature of the silver, meaning the state at which the silver is found within the material, it could be silver ions, nanoparticles or even in one of its salt forms. Silver nanoparticles are generally thought to be more effective when dealing with bacteria over its salt forms, and this is due to the larger surface area of the nanoparticles. The size and shape of the nanoparticles can also play an important role in how effective they will be at entering the bacterial cell and disrupting the respiratory chain (Rai *et al.*, 2009).

1.5.3.5 Titanium Nitride & Silver

Combining the two materials together can form a highly effective coating that can be deposited by numerous processes, such as physical vapour deposition, and chemical vapour deposition. When deposited via the PVD process, it tends to produce a nanocomposite structures of silver nanoparticles, encapsulated in a hard matrix of ceramic titanium nitride (Kelly *et al.*, 2009, Kelly *et al.*, 2010, Kelly *et al.*, 2011, Saubade *et al.*, 2019). These nanocomposite thin films are particularly resistant to corrosion, wear and possess the inherent antimicrobial activity attributed to the silver, if it is found in its nanoparticle form, as this will leach in its ion form. Adding this broad-spectrum antimicrobial agent to the already proven material, allows for the improved tribological properties to be enhanced with the silver doping. In studies already carried out within our

laboratories, the properties of titanium nitride and silver have been extensively researched, with the results being favourable in their eradication of different bacterial strains, both Gram-negative and Gram-positive bacteria (Kelly *et al.*, 2011, Whitehead *et al.*, 2011, Whitehead *et al.*, 2015, Slate *et al.*, 2018, Tetlow, 2018, Slate *et al.*, 2019). The difference between a Gram-negative and Gram-positive bacteria, is found within the cell wall composition. Gram-negative bacteria are surrounded by a thin peptidoglycan cell wall, which is then surrounded by an outer membrane comprised of lipopolysaccharide. Whereas, a Gram-positive bacteria lacks the outer membrane, but it is surrounded by multiple layers of peptidoglycan, making it thicker than the outer membrane of the negative.

1.5.4 Textured Antimicrobial Surfaces

1.5.4.1 Introduction

Textured antimicrobial surfaces can be constructed from numerous processes and materials, they can also be biomimetic. The term antimicrobial for these textured surfaces can be a contentious subject in some papers found within the literature, as some papers state their surface is antimicrobial, whilst presenting a surface that is antibiofouling. Antibiofouling, is a surfaces ability to resist the initial adhesion of bacteria/contaminants, and it can be manipulated by modifying the surface texture/chemistry (Zhu *et al.*, 2020). However, there can be certain surfaces that directly interfere with the bacteria, such as surfaces that have been developed to rupture the bacterial cell wall (Lutey *et al.*, 2018, Zander and Becker, 2018). Having a micro/nanostructure that has the capability of stretching out the bacterial cell wall, to the point that it begins to split is a theory that has been postulated in numerous papers (Jaggessar *et al.*, 2017).

1.5.4.2 Laser Texturing

Laser texturing presents itself as a promising method for producing surfaces that are antibiofouling and even could produce surfaces that are antimicrobial. By producing textures that have feature sizes that are of an order of magnitude smaller than the size of the bacteria, there could be a reduced adhesion rate as the bacteria will be unable to adhere (Lutey *et al.*, 2018). By using femtosecond pulsed lasers, it is possible to produce a surface nanotopography that has feature sizes smaller than that of the average bacterial cell. *S. aureus* has an average size of 1 micron. However, there is the issue that if you

produce a texture that is similar in size to the bacteria being tested against, the bacteria may 'hide' in the spacings between the features (Jäger *et al.*, 2017). By attempting to replicate the naturally occurring superhydrophobic surface of a lotus leaf, utilising femtosecond laser ablation on titanium surfaces, it was found that there was a reduction in the number of *Pseudomonas aeruginosa* cells. However, it was also found that there was no reduction in the number of *Staphylococcus aureus* cells, and this was hypothesised to be linked to the shape of the respective bacteria, *P. aeruginosa* is rod-shaped and *S. aureus* is spherical (Fadeeva *et al.*, 2011). This reduction in adhesion rates is not proof of an antimicrobial surface being produced by this method, as the cells have not been killed, but have simply been stopped from adhering, thus creating an antibiofouling surface.

Through laser texturing, it may be possible to enhance the properties of an already antimicrobial agent, such as a copper surface that has its surface area increased via the texturing. By producing simple 100 nanometre wide grooves on the surface of copper foil, it was found that there was a significant increase in the rate of death of cells when compared to untextured samples (Selvamani *et al.*, 2020). The efficacy of the copper was enhanced via the increase of surface area, thus increasing the contact between the surface and bacteria. In *Figure 3* below an inoculated laser textured, stainless-steel coupon can be seen. The small silver dots that are scattered across the surface, which have been highlighted by arrows, are the *S. aureus* cells that have successfully adhered to the surface. Where-as the texturing produced by Selvamani *et al.*, increased the efficacy of the copper, the following figure is an example of increased surface area, and thus increased contact between the bacteria and substrate, without an antimicrobial agent present.

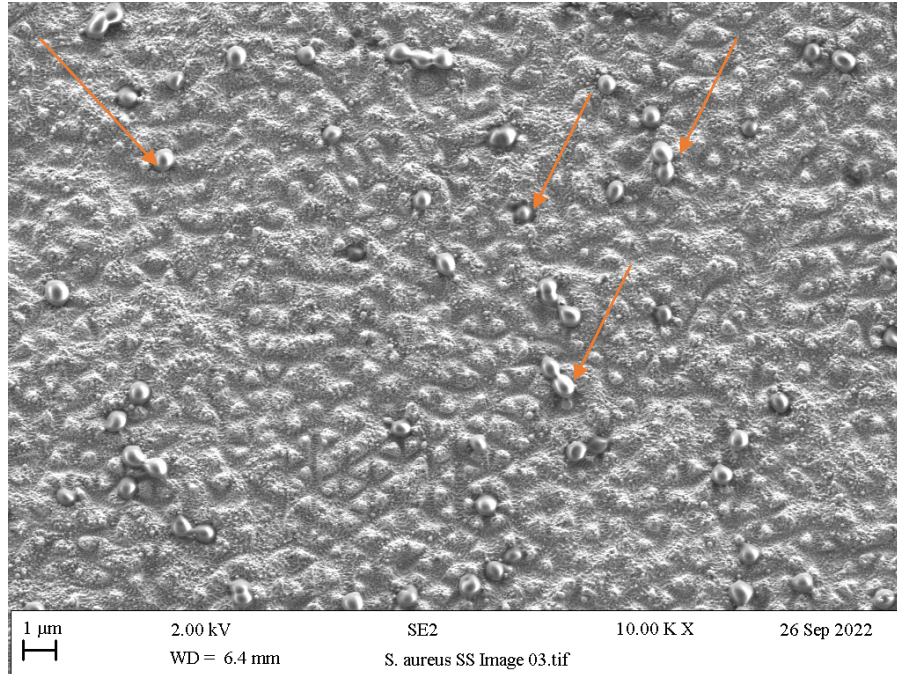


Figure 3: *S. aureus* Infected LIPSS Stainless-Steel

Laser texturing can also be utilised to produce surface topographical structures that can pierce the cell wall of bacteria, and therefore lead to cell death via rupture. However, this kind of treatment is very specific to the bacteria that is being treated, as all bacteria have different shapes and sizes. They also have their own specific ideal surface chemistry, meaning that what may reduce one bacterium, may increase another. As was found when testing *Escherichia coli* and *Staphylococcus aureus* against various designs. It was found that one design, specifically laser-induced spikes, increased the attachment

of *E. coli*, but conversely reduced the attachment of *S. aureus* (Lutey *et al.*, 2018). The results from their report can be seen below in *Figure 4*.

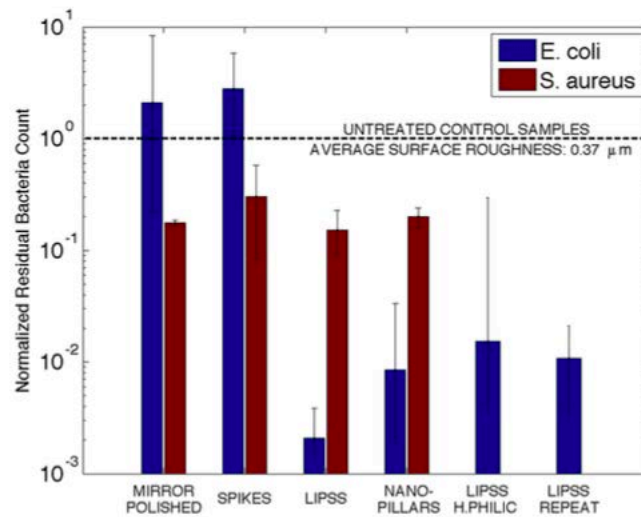


Figure 4: Results for Different Laser Textured Styles on Bacterial Adhesion (Lutey *et al.*, 2018)

1.5.5 Bacterial Strains

This sub-section will discuss some of the different bacterial strains that are commonly found within the procedure of installing an external fixation device and why they have been chosen will also be discussed. It will investigate *Staphylococcus aureus* and *Pseudomonas aeruginosa*.

1.5.5.1 *Staphylococcus aureus*

Staphylococcus aureus is a Gram-positive bacterium, which has an average diameter of 1 micron, and it is characterised by its spherical shape, and its trait to form in grape-like bunches, see below *Figure 5*. *Staph. aureus*, is one of the most common hospital acquired infections, and it can be found on the general population living on the host skin without causing any form of infection. This strain can be a community spread bacterium, with studies suggesting that anywhere from 50 % to 60 % of people can be infected with the bacteria in some respect (Kobayashi *et al.*, 2015). With such wide-spread colonisation of the population, and the fact that it is an opportunistic bacterium, meaning it will actively search for any abrasions or cuts to the skin that will allow it to breach the natural skin barrier. It is not surprising that it is the most prevalent pin-site infections, pin-site is where an external fixation device pin has been placed into the skin to hold the fragmented bone together, and these sites are the perfect location for the bacteria to proliferate and form

biofilms (Dong *et al.*, 2017). However, the infection rate of external fixation devices with this strain are difficult to standardise, as there is limited data on the standard cleaning procedures that are put in place for these procedures (Tetlow, 2018). After a surgical procedure, for implanting a medical device for example, there is a critical period where bacterial colonisation of the wound-site is most likely, and it is roughly the first 6 hours after. Whilst in this stage the bacteria are metabolically active, and more susceptible to the host immune system. However, should the bacteria be successful in adhering to the surface of the wound, or implant, they can form biofilms and prove difficult to remove (Kao *et al.*, 2017).

1.5.5.2 *Pseudomonas aeruginosa*

Pseudomonas aeruginosa is a Gram-negative bacterium, which can be characterised by being rod-shaped and having an average size measuring 0.8 microns by 3 microns, see *Figure 6* below. Whilst not as prevalent as Gram-positive bacterium in infection rates on medical implants, Gram-negative bacterium are still responsible for several infections in hospitals. It is also an opportunistic bacterium, which if left untreated can cause serious

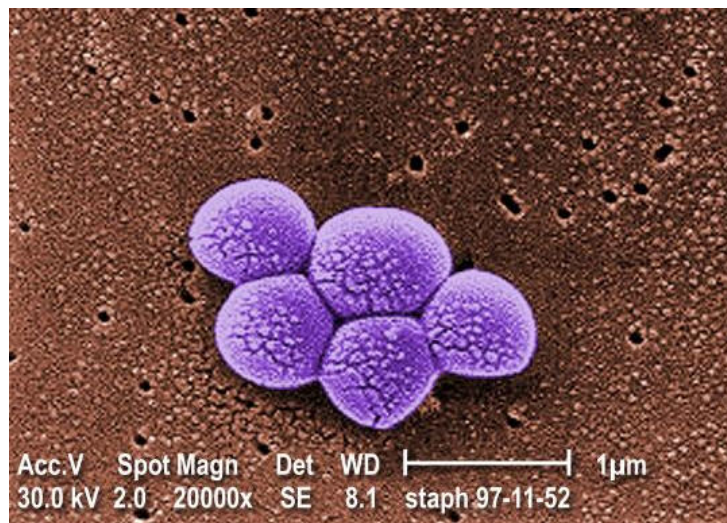


Figure 5: Staphylococcus aureus Bacterium (Centre for Disease Control & Prevention, 2018)

medical complications, such as pneumonia and other blood borne problems (Flores *et al.*, 2010).

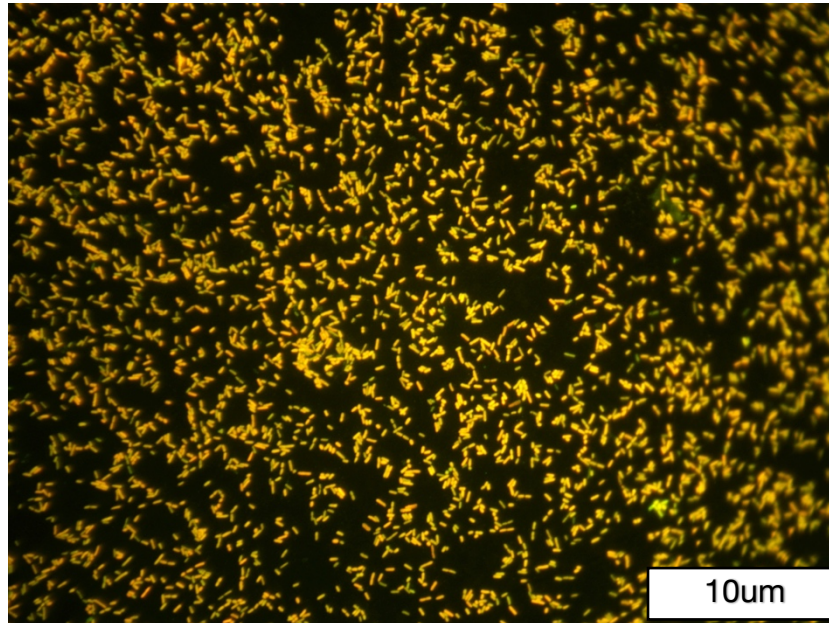


Figure 6: *Pseudomonas aeruginosa*

1.6 Deposition & Texturing Review

This following section will be focused on the various deposition/texturing processes that are currently available within the literature, the focus will be on the LIPSS texturing and Physical Vapour Deposition techniques. It will be split into sub-sections named 3.1 Physical Vapour Deposition, & 3.2 Laser Texturing. Each of these sub-sections will be divided into smaller sections that will contain information about other processes that can be used.

1.6.1 Physical Vapour Deposition

Physical vapour deposition is a deposition process that can be dated back to the 19th century, its first iteration was most likely vacuum evaporation deposition and it was originally used to produce mirrors (Dearnley and Dearnley, 2017). It has since grown to be one of the most versatile and reliable surface deposition techniques. PVD is an umbrella term for a variety of processes, each of which can be defined by the production of thin films via the condensation of a vaporised form of solid material onto a substrate surface. It can be used to produce coatings that can range from a few nanometres, up to several microns in thickness. Using this method, a wide variety of materials can be deposited onto a broad spectrum of substrates.

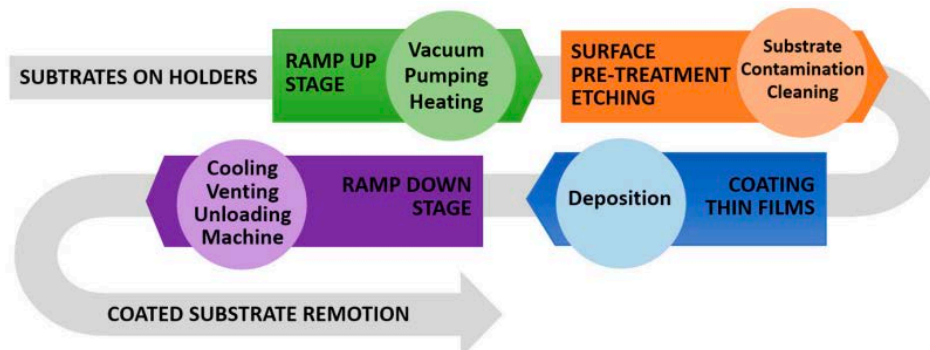


Figure 7: Typical PVD Sputtering Process (Baptista et al., 2018)

1.6.1.1 DC Diode Sputtering

Considered to be the most basic iteration of the sputtering branch of physical vapour deposition, DC diode sputtering is composed of two planar electrodes within a vacuum, an anode, and a cathode. The target is usually placed on the side of the cathode, which faces towards the plasma and generally it will have a water coolant system in place. To initiate the discharge, and therefore begin the sputtering process, argon gas is introduced into the chamber and a potential difference is then applied across the two electrodes. This example of sputtering deposition does not benefit from the introduction of magnetrons to the system, and because of this it has lower deposition rates (Waite et al., 2007).

1.6.1.2 Magnetron Sputtering

1.6.1.2.1 Conventional Magnetron Sputtering

Physical sputtering is classed as a line-of-sight deposition technique, which means that to coat a 3D substrate entirely, the sample will have to be rotated to gain an even coating. Most forms of physical sputtering methods have a relatively low deposition rates when they are compared to methods such as evaporation deposition. However, the deposition rates can be improved when utilising magnetron sputtering. Magnetron sputtering is considered one of the most effective and powerful sputtering techniques that PVD has to offer, it can be used at low operating temperatures, which extends the already broad range of substrates that can be deposited onto. It can also be used for large deposition areas, which makes it quite suitable for commercial coating levels (Lévy, 2016). This specific method can be used in a variety of configurations, with one being the method that was implemented into this research project. This configuration involves co-sputtering from two separate targets in an argon (Ar) and nitrogen (N₂) environment, with a constantly rotating substrate holder, resulting in a nanocomposite coating being deposited across the substrate.

Magnetron sputtering is based on the vaporisation of a target material (cathode) via bombardment of positive inert gas ions, usually it is argon that is the inert gas chosen, in a glow discharge plasma. This results in atoms from the target material being ejected from the surface, and they travel across the chamber in which the plasma is being created and land onto the substrate, producing a thin film, see *Figure 8* below.

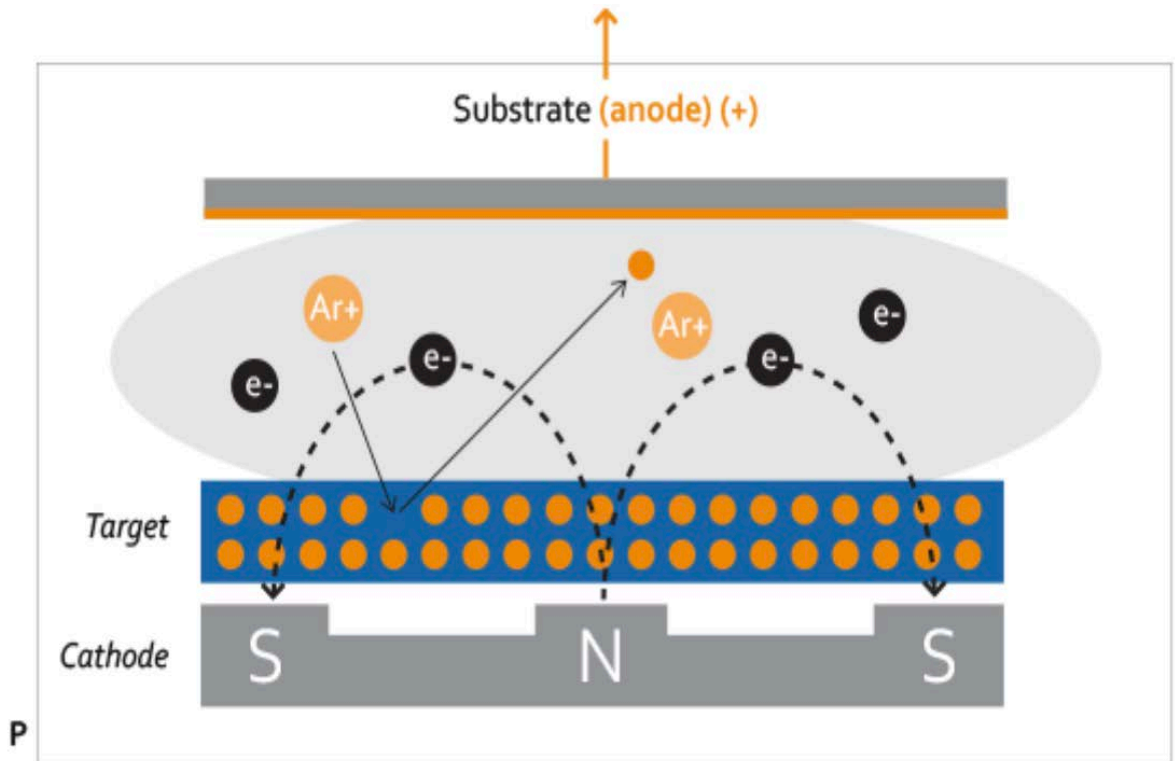


Figure 8: Magnetron Sputtering Process (BCLUE, 2021)

Taking advantage of the addition of magnetrons to the basic sputtering process allows for the exploitation of the magnetic field that is generated. The magnetic field, that is in parallel to the target, can constrain secondary electron motion towards the target, and in doing substantially increases the possibility of an ionising electron-atom collision happening. By improving the possibility of these collisions happening within the chamber also leads to a denser plasma around the target region, which results in improved deposition rates over basic sputtering (Kelly and Arnell, 2000). In addition to the improved deposition rates, the addition of magnetic field allows for the discharge required to be maintained at a lower operating pressure.

1.6.1.2.2 Unbalanced Magnetron Sputtering

A further modification to magnetron sputtering, is the unbalanced magnetron sputtering, and although there are only small changes to the overall design, there are significant differences between the two processes. The small change to the design leads to variations in the performance, for example in conventional magnetron sputtering there is a region of dense plasma that can be found close to the target surface and is confined there. Any substrates positioned away from the target area will be in areas of low plasma density, which can be circumvented by increasing the negative bias across the substrate. However, doing this can lead to defects forming in the coating and increased film stress and thus is not preferential for consistent film production on complex, or larger components (J. Musil *et al.*, 1990). Thus, the concept of unbalanced magnetron sputtering was designed to improve on the conventional magnetron sputtering's shortcomings.

To create this unbalanced magnetron sputtering configuration, the outer ring of magnets is strengthened relative to the central pole, and by doing this the field lines are not all closed between the central and outer poles of the magnetron. Some of the field lines are redirected towards the substrate, allowing for some secondary electrons to follow along these and therefore the plasma generated is not as strongly confined to the target region, allowing for high ion currents to be extracted without a need for the negative bias increase (Kelly and Arnell, 2000).

1.6.1.3 Pulsed DC Magnetron Sputtering

Pulsed DC Magnetron Sputtering is a method that is run within reactive sputtering mode, and it can be considered an improvement on the base mode. Developed in the early 1990s, with the intention of producing a method that had a reliable deposition rate for insulating materials, which is not possible in conventional reactive sputtering due to the poisoning of the target with the insulating material (Musil *et al.*, 2001). With the ability to reduce the accumulation of charge on film surfaces, by also reducing the arcing event, this method has an advantage over radio-frequency magnetron sputtering, which has unreliable deposition rates (Yeh *et al.*, 2008). The three parameters that are reported to affect the structure and properties of any magnetron sputtered coating are the homologous temperature, ratio of the fluxes of bombarding ions and depositing atoms, and the energy of the bombarding ions. The introduction of the pulsed power across the

target can have an effect on these three parameters, causing the surface properties to be altered (Arnell *et al.*, 2004). This method can be highly effective for depositing material combinations such as titanium nitride, as it has been reported to present coatings that have a more desirable compressive strength than coatings produced through continuous DC mode. When using dual magnetrons in this method, there is a promising effect of the magnetrons alternating between being the cathode and anode, which in turn allows for the charge to be effectively dissipated across them. This dual bipolar magnetron arrangement also removes the possibility of the disappearing anode phenomenon taking place, which means that the anode has been coated with an insulating material, rendering it unusable in future runs. By limiting the 'pulse-on' time, the charging of the poisoned regions does not reach the point of breakdown and begin to arc, the charge that is built up is then dissipated through the plasma during the 'pulse-off' time, by switching the target voltage to a more positive value (Kelly and Arnell, 2000). A schematic of the target voltage waveform during pulsed mode can be seen below in *Figure 9*.

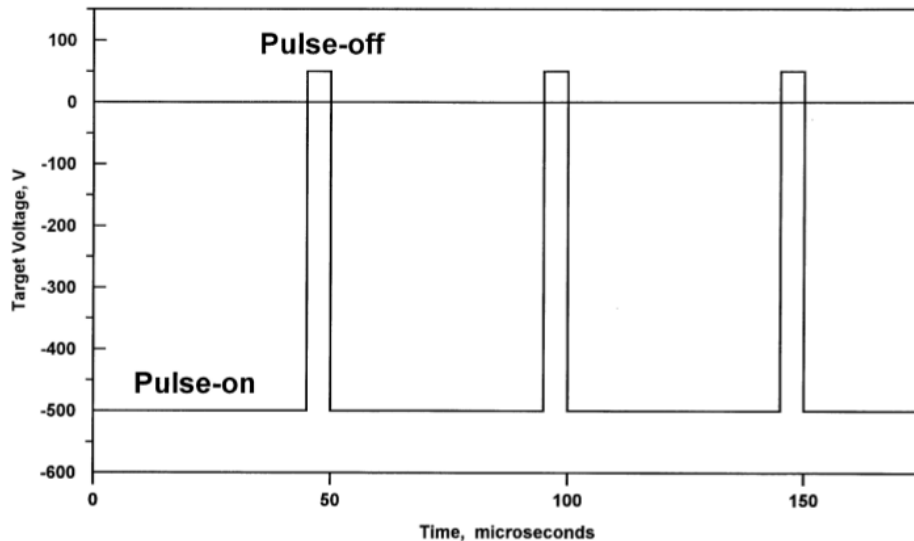


Figure 9: Schematic for Target Voltage Waveform for Pulsed DC Power Supply (Kelly and Arnell, 2000)

1.6.1.4 Reactive Sputtering Deposition

Reactive Sputtering is a well-established method for producing coatings consisting of insulating and dielectric films, such as oxides and even nitrides (Waite *et al.*, 2007). It can be used to produce a wide range of thin-film compounds, on an equally wide number of substrate materials. Reactive sputtering works on the principle of introducing a reactive

gas that reacts with the sputtered material and can be a relatively temperamental and hard to control process. Whilst based on a simple principle of a reaction between the gas and sputtered material, controlling the range at which this is an efficient process can become difficult, as too low pressure of the gas can cause high metallic sputtering, and too high pressure can cause the target material to become poisoned (Berg and Nyberg, 2005). By introducing the reactive gas into the chamber, it is possible to form more complex combinations of materials, such as oxides, borides, and nitrides (Springer, 2008).

1.6.1.5 High Power Impulse Magnetron Sputtering (HiPIMS)

A variation on the conventional magnetron sputtering is called high power impulse magnetron sputtering and is one of the most recent advances to come out of the physical vapour deposition family of techniques. One of the most significant differences between this and conventional magnetron sputtering is found within the modes of operation, more specifically it lies in how power is applied across the target. The power is supplied to the magnetron in unipolar pulses at a low duty factor, generally below 10% and at a much lower frequency than conventional, around 11 kHz. This results in peak target power densities, but also keeps the magnetron from overheating and melting (Lundin and Sarakinos, 2012). HiPIMS was first suggested for use in 1999 by Kouznetsov *et al.*, and was initially designed to be a method that could circumvent the current restrictions of how much power can be applied across the magnetron target (Kouznetsov *et al.*, 1999). It can circumvent these restrictions due to the pulsed nature of the process; these pulses are kept below 1 millisecond in duration and only happened at intervals of 10 milliseconds to 1000 milliseconds (Kouznetsov, 2001). These pulses result in the peak power being increased up to 100-fold that it usually is with conventional sputtering, but allows for the average power to be kept within the same range (Waite *et al.*, 2007).

When depositing thin films via HiPIMS compared to conventional sputtering, it is possible to produce thin film densities that range between 10% and 30% greater depending on the study that is being referenced (DeKoven *et al.*, 2003, Konstantinidis *et al.*, 2007). This increase in density is achieved via the ability to produce higher density plasmas within the chamber, and this in turn enables a greater level of control over the sputtering direction and flux which can also increase the adhesion of the film (Samuelsson

et al., 2010). With this greater level of control over the direction, there is an increase in the uniformity of the coatings produced, and most rigs can be converted with relative ease, as all is required to change over is a power supply that can produce the high-power pulses. Due to the long pulse off periods of using HiPIMS, the total heat load across the substrate is significantly lowered, and this can expand the broad range of substrates that can be deposited onto. With there being a reported reduction in thermal power density by between 5 and 10 times when compared to using conventional sputtering methods (West *et al.*, 2009).

1.6.2 Surface Texturing Methods

There are countless available methods for producing a textured substrate, they can vary from processes that remove material to texture and to processes that involve coating the surface with a material that produces a desired topography. Whilst some are biomimetic, meaning they are based on a structure that is found within nature, others are entirely a man-made invention and design. For this thesis, laser textured surfaces will be the primary method for texturing samples.

Surface texturing has been gaining a lot of interest within the literature in recent years, and this is due to the myriad of different techniques that can be implemented, such as laser texturing, chemical etching, lithography, and ion beam texturing (Mohd Mahayuddin *et al.*, 2020).

1.6.2.1 Laser Texturing

Laser texturing has been gaining popularity as an effective method for texturing a wide range of materials, largely due to its relative ease of use and its ability to create complex texturing patterns. With recent studies investigating the use of femtosecond pulsed laser ablation over nanosecond pulsed, stating that the benefits include the reduction in heat affected zones and therefore reducing the build-up of molten material at the textured site (Tsukamoto *et al.*, 2006). Applications for laser textured surfaces can range from medical implants, with studies citing the improvement of osseointegration, which means an improvement of bone integration of the implant, to the microelectronics industry texturing of silicon (Oliveira *et al.*, 2009, Fasasi *et al.*, 2009, Jeong *et al.*, 2011, Fadeeva *et al.*, 2011, Schlie *et al.*, 2011, Kenar *et al.*, 2013, Vorobyev and Guo, 2013, Ahmmed *et al.*, 2014, Li *et al.*, 2016, Kuczyńska *et al.*, 2016, Müller *et al.*, 2016, Rosenkranz *et al.*, 2016,

Epperlein *et al.*, 2017, Chan *et al.*, 2017, Shaikh *et al.*, 2019, Chen *et al.*, 2020). The increased use of lasers in these industries can be attributed to the ease of use, as many of the materials that can be textured this way can be done whilst in ambient air, meaning that there is little no extra processes that have to be considered, and primarily they can be done outside of a vacuum environment (Jeong *et al.*, 2011, Li *et al.*, 2016).

1.6.2.1.1 Laser Induced Periodic Surface Structures (LIPSS)

Laser induced periodic surface structures, or LIPSS for short, are the result of the universal phenomena that affects all surfaces during exposure to linearly polarised femtosecond pulsed laser radiation. The result of this phenomena is generally categorised as ripples across the surface, whose shape are wholly dependent on the parameters of the laser that has irradiated the surface. There has been an increase in the number of papers that exploit this method in recent years, and this can be correlated to the increased commercial availability of femtosecond pulsed lasers. LIPSS can be split into two sub-sections low-spatial frequency LIPSS (LSFL), and high-spatial frequency LIPSS (HSFL). The difference is the energy distribution of the laser beam. LSFL patterns are formed when there is a higher local fluence that is close to the ablation threshold of the material, and HSFL patterns are formed when the local fluence is relatively lower than that required for LSFL (Liu *et al.*, 2020).

LIPSS has gained status as an invaluable method for creating a diverse range of surfaces, this is primarily due to its ability for the surfaces to be produced in ambient air and in a single step process (Bonse, 2020). LIPSS can be used to create patterns that have been inspired by naturally occurring surfaces, which have all been evolved over millennia for specific purposes and advantages for the flora/fauna that have implemented them. These bio-inspired surfaces can be based on some of the more well-documented phenomena, such as shark skin, which has evolved to become incredibly effective at reducing the fouling that can occur, or the lotus leaf effect, which has evolved to have such a high surface hydrophobicity that it has become self-cleaning once a water droplet has landed on the leaves. The *Figure 10* below exemplifies the surface pattern that can be created via the laser texturing process, that was exploited throughout the research.

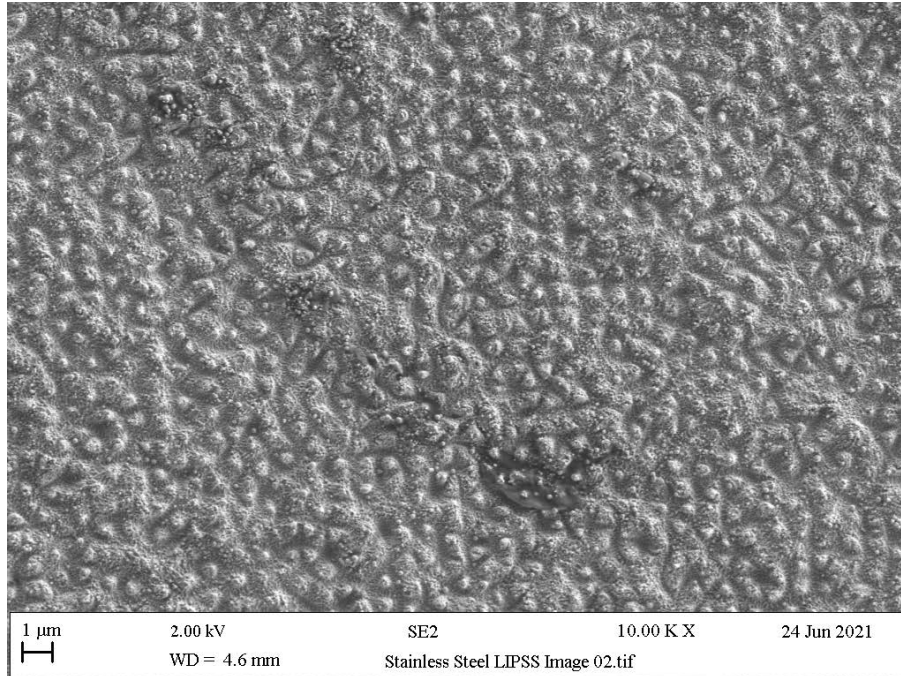


Figure 10: LIPSS Textured Stainless-Steel Produced During Research Project

This patterning was found to bear a striking resemblance to the natural anti-biofouling surface pattern of shark skin & the comparison image can be below in Figure 11.

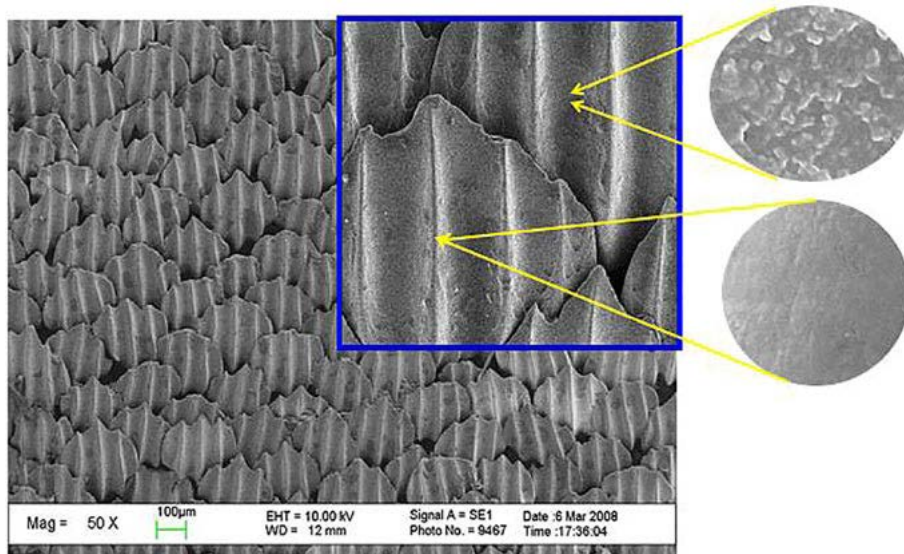


Figure 11: SEM Image of Shark Skin (Pu et al., 2016)

Through laser texturing, and producing laser induced periodic surface structures, it is possible to manipulate a surface's wettability, which has been a topic gaining much

interest in recent years. More specifically, the production of extreme surface wettability has been gaining traction, whether that be a surface that is superhydrophobic, meaning its contact angle is 150° or higher, or a surface that is superhydrophilic, which means its water contact angle is around 0° (Li *et al.*, 2016). The thought process behind producing these surfaces via laser texturing, is to recreate the effect that happens when a droplet of water lands on the surface of a lotus leaf. This naturally occurring phenomenon can be described as a self-cleaning act, as when the droplet lands on the surface, which is superhydrophobic, it begins to roll off the surface and during this movement it collects all of the debris and dirt that C - which can be seen below in Figure 11. There are generally three points of

has also landed on the surface (Fadeeva *et al.*, 2011).

1.6.2.2 Biomimetic Surfaces

As stated, biomimetic surfaces are man-made surfaces that have been engineered to copy surfaces that have been found to occur naturally, whether that be the skin of a shark, which is antibiofouling, or the lotus leaf, which causes water droplets to roll off the surface and self-clean the leaf. To the naked eye a lotus leaf would appear to have a smooth surface, with no recognisable surface features, however, under microscopic analysis there are clearer defined features. It is from these features that the lotus-leaf effect is derived, the surface is dense with micro- and nano-scale papillae that are encased in a hydrophobic wax (Gomes *et al.*, 2022). These biomimetic surfaces that can be produced usually attempt to recreate one property that is generally exhibited by the surfaces found in nature, and this is the super-hydrophobicity of the naturally occurring surfaces (Saubade *et al.*, 2021). The applications for biomimetic surfaces can be the medical industry, or the food industry, which has recently been gaining more popularity due to the restrictions that are placed onto the usage of materials around food sources. In particular, the use of laser texturing for producing surfaces that are resistant to the fouling that occur within the dairy industry are of interest, as there are reports that suggest that via the texturing there can be a reduction in the fouling of the surfaces (Whitehead *et al.*, 2022).

1.7 External Fixation Devices

In the respect of producing a viable coating for an external fixation device, it first must be learnt what the ideal external fixation device consists of. Meaning, what is the function of the device, what is the device usually made of (dependent on the model that has been chosen) and what does each part do. For the scope of this project, the theoretical model for the device has been based around the multi-planar model, which can be seen below in *Figure 12*. There are generally three points of contact between the fixator and the bone. This can vary depending on the severity of the fracture that has been sustained, as this can influence the number of pins that have to be drilled into the bones to reconstruct the fractured bone. Whilst there are numerous designs for the external fixator device, each with their own specific application depending on the style of fracture, this design was chosen as it was found to be the most used design for fractures.

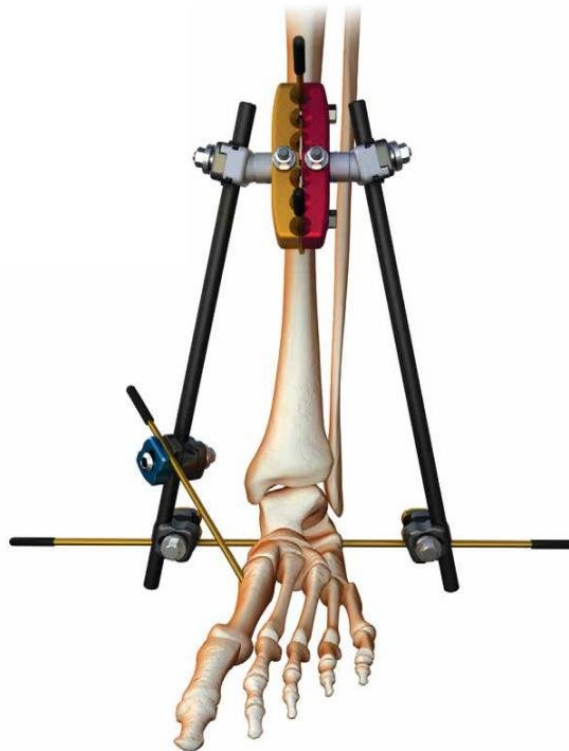


Figure 12: External Fixation Device (Nephew, 2012)

The areas that are at most risk of being infected are the sites at which the pins are placed into the patient's limbs, these create open-wound sites that provide favourable areas for bacterial infection.

1.8 Summary

This section will provide a summary of all the information that has been gathered from the review of the literature, and how this information further affects the hypothesis. The main takeaways from the information will be highlighted and how these have been considered regarding the way this research project was carried out and planned.

1.8.1 Summary & How it Affected Project

Reviewing the literature that surrounded the topic of antimicrobial surfaces, whether they be from deposition processes, texturing processes, and some naturally occurring surfaces, has led to the conclusion of choosing the materials and processes that have been used in this research project. By investigating the assorted studies that surround the numerous antimicrobial agents that have been tested, the review allowed for the informed decision of using silver as the agent. This was chosen due to its proven broad-spectrum antimicrobial activity, it was chosen over other materials, such as copper, as it was found that it has relatively low cytotoxicity when placed in-vitro. In combination with the review of which bacteria are most found when placing external fixation devices, there were numerous studies that relate to using *Staphylococcus aureus* as the strain. There are also studies that explore the risk that the Gram-negative bacterial strains pose to modern medicine, even though there are less reported cases of infections due to these strains, its pertinent that they should also be tested against. Therefore, the chosen strain for the Gram-negative species was decided to be *Pseudomonas aeruginosa*, as this was another potentially community-spread infection. These specific strains have been studied by the Manchester Metropolitan University in numerous studies, and therefore the scaffolding was already there for this research project to be built off (Kelly *et al.*, 2011, Whitehead *et al.*, 2015, Tetlow, 2018, Saubade *et al.*, 2021).

It was found that, especially from reviewing the texturing processes, that whilst man-made designs can be effective against the growth of some bacterial strains, they were found to be inferior in their design in comparison to the naturally occurring surfaces that flora and fauna have developed over millennia. This is due to the surfaces found in nature do not serve just a singular purpose, they have been designed through evolution to have more than a singular beneficial property, where man-made processes are unable to develop. The various deposition techniques that can be classed under physical vapour

deposition, all had their own specific advantages and disadvantages. It was found that depending on what materials were going to be deposit, there were certain deposition methods that were better suited. However, it was found that the best method for these combinations of materials that the best process would be to produce the coatings via pulsed DC dual magnetron sputtering. This was chosen because of several papers that suggest it is more suitable for producing coatings that have better compressive strength. There has also been a plethora of studies carried out at the Manchester Metropolitan University, which have all used the same process for creating similar coatings (Kelly *et al.*, 2009, Kelly *et al.*, 2010, Whitehead *et al.*, 2010, Kelly *et al.*, 2011, Whitehead *et al.*, 2011, Wickens *et al.*, 2012, Kelly *et al.*, 2014, Saubade *et al.*, 2019).

As it was found that there was a significant gap within the literature, regarding there not being, at the time of writing, any papers that suggested the combination of the physical vapour deposition & laser texturing processes, this research project was defined to produce new contributions to the literature.

Part II

Analytical & Experimental Methods

Chapter 2 – Methods

This chapter will focus on the methods that were used throughout the research project, and it will be divided into sub-sections that will follow the structure 2.1 Deposition Techniques, 2.2 Texturing Process, 2.3 Microbiological Techniques, and finally 2.4 Analytical Techniques. These were further divided into sections that will contain information regarding their specific title.

2.1 Deposition Technique

Throughout this project there was one main deposition technique used, and that is physical vapour deposition via pulsed DC magnetron sputtering.

The titanium nitride and silver coatings were produced in a Teer UDP450 (Teer Coatings, United Kingdom) using two vertically opposed type II unbalanced planar magnetrons, which both measured 300 x 100 mm, and were installed into the reaction chamber in a closed field configuration. A schematic of the configuration can be visualised below in *Figure 13*.

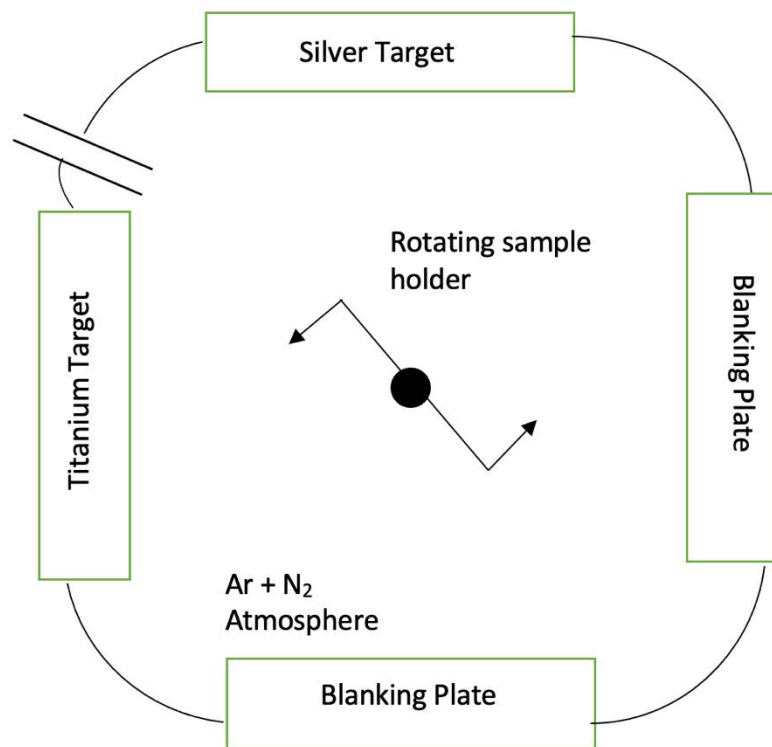


Figure 13: Plan view Schematic of PVD Rig Configuration.

The titanium target, which was directly cooled and 99.5% purity, was placed onto one of the magnetrons, with the silver target, that was mounted onto a copper backing plate and of 99.5% purity, was mounted onto the other. Utilising a combination of rotary and combination pumps, the rig was evacuated to achieve the internal pressure of 2.0×10^{-5} mbar or below. The two targets were then driven in pulsed DC mode, via a dual channel Advanced Energy Pinnacle Plus power supply, at a pulse frequency of 100 kHz, and at a duty of 50% (synchronous mode), and these parameters were utilised for all the deposition runs. The power across the two targets was set at various levels, with the titanium target being supplied with a constant 1500W for all the runs, and the silver target was supplied with a varying power level, between 50 – 80 W. By varying the power across the silver target the atomic weight percentage (at%) could be manipulated, and this allowed for the investigation of the effect of lower/higher silver content on the antimicrobial efficacy.

The sputtering process was carried out in a mixed atmosphere of nitrogen and argon, with the gas flow being controlled via mass flow controllers. The flow was set at 19 sccm for the argon gas, and 10 sccm for nitrogen gas for all deposition runs. The stainless-steel-coupons that were used as the substrate, were attached to the rotating substrate holder, which was rotated at 5 rpm for all runs, using polyimide adhesive tape. The distance between the substrate holder and the targets was kept at a constant distance of 10 cm and all substrates were initially RF-bias cleaned before deposition. RF-bias cleaning was used to clean the substrate prior to deposition, it was done by applying a bias in the presence of a partial pressure of gas, which created a localised plasma at the surface of the substrate. This process was carried out to remove any potential contaminants on the surface of the substrate, these can include oxides, hydrocarbons and water molecules, which can all reduce the adhesion of the coating deposited.

2.2 Laser Texturing Techniques

To manufacture the textures that were tested throughout this process the lasers based at the Manufacturing Technology Centre (MTC) were used, which was a GF Machining Solutions Laser P400U system (Coventry, United Kingdom). This laser system utilises an ytterbium pulsed fibre laser, capable of an average power of 30 W, at a wavelength of

1064 nm, with a pulse duration of up to 200 nanoseconds and with a pulse energy of 1 mJ at 200 nanoseconds.

This laser system was used to produce a variety of texturing designs, with the primary designs configured as grooves across the surface of the stainless-steel substrates, these grooves were initially designed to have a depth of 5 microns, a groove density that was varied at 20%, 50% and 80%, which affected the distance between the grooves. There was a limitation on the current system, which restricted the width of the grooves to the size of the laser beam spot size, and this was 50 microns. To circumvent these technical limitations, the texturing method was altered from being regular features to more irregular features. This is where the samples would no longer be regular grooves across the surface, but would follow along LIPSS, laser induced periodic surface structures. These LIPSS patterns follow a pattern that would be more of a wavy structure across the surface, and this can be seen in *Figure 14* below. The benefits of producing textures via the LIPSS process, is that they can be made to an order of magnitude smaller than the previous method of regular grooves. The wavy structure that was produced on the surface of the stainless-steel was produced by the interference of the incident/refracted laser light, with the scattered/diffracted light found at the surface. Whilst these patterns are named randomly organised, they are controlled by the parameters of the laser that was used.

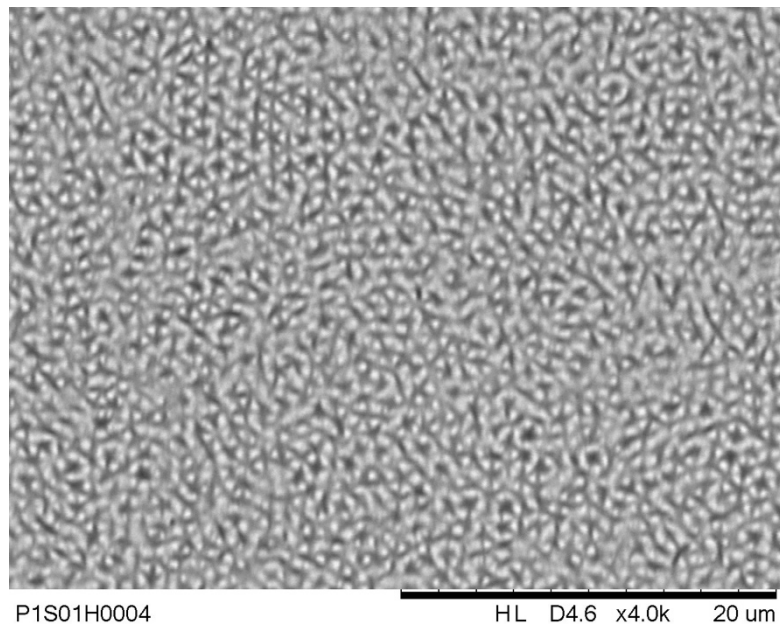


Figure 14: LIPSS Texture on Stainless-Steel, Power 36%, Scanning Speed 470mm/s, Hatching 0.009mm, SEM Image at 4x Magnification.

These samples were produced using the LIPSS process, and as can be seen the surface features produced are randomised peaks and troughs. These samples have been previously investigated by the Manufacturing Technology Centre, and were found to be super-hydrophobic materials, meaning they have a contact angle that exceeds 150°. The parameters for producing these textures were as follows; the power level was kept at 36%, scanning speed set at 470 mm/s, frequency of 500 kHz, and beam spot size of 50 µm. Initially these parameters were used for a single pass over the substrate surface, but a second batch of samples were produced using the exact parameters, with an extra pass of the laser at a 90-degree angle to the original texture. This second pass could potentially lead to more surface oxidization, which in turn could cause a different surface chemistry to be formed on the substrate. However, these properties were not fully explored and analysed.

2.3 Microbiological Techniques

2.3.1 Microorganisms

During this project there were two different strains of bacteria analysed, which are both prevalent within hospital environments. *Staphylococcus aureus* and *Pseudomonas aeruginosa* are a Gram-positive and Gram-negative bacteria respectively, which means that they have different cell wall compositions and were chosen for this property to determine if the chosen antimicrobial agents would be effective against both. The difference between a Gram-positive and Gram-negative bacterium cell wall is the structuring of their cell wall, or membrane, Gram-negative bacteria are surrounded by an outer membrane containing lipopolysaccharide. Whereas a Gram-positive bacterium does not have this outer membrane and is instead surrounded by very thick layers of peptidoglycan, which are many times thicker than those found in Gram-negative. These bacteria are both different shapes, with the *S. aureus* being a coccus, which is one that is mostly spherical, and measures roughly 1 µm in diameter. Whereas the *P. aeruginosa* is a rod-shaped bacteria, that measures 1 µm x 3 µm with flagellum, both bacteria are commonly found within any man-made structures, with *S. aureus* being one of the most prevalent pathogens found within hospitals.

Staphylococcus aureus (NCTC 6571) and *Pseudomonas aeruginosa* (NCTC 10332), which were both harvested from the Manchester Metropolitan University's stock cultures,

were inoculated onto plates of nutrient agar (Oxoid, Basingstoke, Hampshire, England) overnight at 37°C. These plates provided the stock bacterial plates for both the strains and were stored in the fridge at 4°C, which allowed for them to be used for up to 4 weeks at a time. After 4 weeks these plates were disposed of, and the process was repeated, to keep viable samples for testing, this was repeated numerous times throughout the project. Single colonies taken from the stock plates were then incubated in 10ml of nutrient broth (Oxoid, Basingstoke, Hampshire, England) for 18hrs with shaking (150rpm) at 37°C. To determine the number of colony forming units per ml (CFU/mL), which means the number of *S. aureus* or *P. aeruginosa* colonies that can be found within the mixture, the inoculated broth was centrifuged at 3000g for 10 minutes, the supernatant was carefully disposed of, under aseptic conditions. The pellet of cells was then washed with 10mL of sterile water and centrifuged at 3000g again, with the supernatant being removed again and cells re-suspended with 10mL of sterile water to an OD, which is optical density and is a measurement of the amount of light scattered through a culture, of 1.0 ± 0.1 at 540 nm on the spectrometer. Once an OD of 1.0 ± 0.1 is gained, a serial dilution is carried out, which involves diluting down the bacteria to 10^{-8} at 10^{-1} increments. For each dilution 100 μ L of the mixture was spread onto nutrient agar plates, the plates were then incubated overnight at 37°C and the number of separate colonies were counted, with any dilution that provided over 300 colonies being regarded as too numerous to count (TNTC). The number of colonies determined the CFU/mL for the respective bacteria. For *S. aureus* the CFU/mL was determined to be $5.2 \pm 0.6 \times 10^8$ CFU/mL and for *P. aeruginosa* was found to be $2.59 \pm 0.88 \times 10^8$ CFU/mL.

2.3.2 Zones of Inhibition

During this project there were four main microbiological techniques used, and each of these methods test a specific property of the thin-film samples manufactured. For the samples manufactured to be considered effective antimicrobial surfaces, they must either be able to resist the adhesion of bacteria onto the surface or be able to destroy any bacteria once adhered. One of the tests for analysing the samples efficacy against the bacteria was to use a zone of inhibition, which follows this procedure: An overnight culture of each bacterium was obtained at an OD of 1.0 ± 0.1 CFU/mL, and to sterile agar plates

100 mL of the solution was spread across and allowed to dry within a microbiological class-2 laminar flow cabinet. To prepare the coupons for analysis, they were firstly cleaned with 70% ethanol for 10 minutes, this removed any organic contaminants that may have been present on the surface of the coupons, once they were washed with ethanol, they were rinsed with sterile water to remove any ethanol that may have been present on the coupons. Once rinsed they were dried in a microbiological class-2 laminar flow cabinet, once the coupons had dried, they were placed aseptically onto the inoculated agar plates. This was done via sterilising metal forceps, done via dipping in ethanol and placing them into the flame of a Bunsen burner. For each different variation of the coating and texture design, 3 plates of agar had 3 coupons, coating/texturing side down, spread in a triangle formation across the surface and then incubated overnight at 37°C. The distance around the edge of the coupon surface and the bacterial growth surrounding the coupon was measured using callipers and this gave the created zone of inhibition.

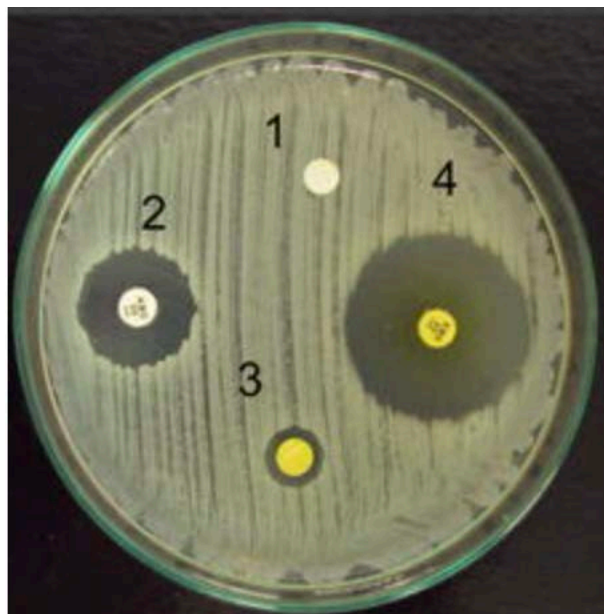


Figure 15: Zones of Inhibition Test Against Staphylococcus aureus using 4 Different Antimicrobial Agents (Springer, 2018)

2.3.3 Nitroblue Tetrazolium Test (NBT)

The second microbiological test that was carried out during this project was the nitroblue tetrazolium test. Which investigates similar properties to the zones of inhibition test, but in a different manner. Whereas the ZOI testing investigates the antimicrobial

agent's ability to leach and kill/prevent bacteria from growing in a wide area, the NBT test investigates the agent's ability to kill any bacteria following an incubation period. This was done via the NBT redox dye staining any respiring bacterial colonies blue, and the number of respiring colonies is then measured.

For this method, a singular colony was taken from the stock plates of *S. aureus* and *P. aeruginosa* and inoculated into 10ml of nutrient broth (Oxoid, Basingstoke, Hampshire, England) and incubated overnight at 37°C. Nutrient agar (Oxoid, Basingstoke, Hampshire, England) was prepared on the day of testing, and this was sterilised via autoclaving the mixture at 121°C for 20 minutes, and resting in a water bath at 50°C to keep it from solidifying. The inoculated broths were centrifuged at 3000g for 10 minutes and the resulting supernatant was carefully disposed of. The bacterial cells were washed with sterile water and centrifuged again, with the supernatant being removed under aseptic conditions. Once washed, the cells were suspended into 10mL of sterile water and diluted to an optical density (OD) of 1.0 ± 0.1 at 540nm. Once diluted to the required optical density, the bacteria are then diluted to gain 1×10^6 CFU/mL, CFU/mL. The metal coupons are prepared as they would be for the ZOI testing, and once they have completely airdried, 20 mL of the bacterial solution is pipetted onto the coating side of the coupons and left to dry again in a microbiological class-2 laminar flow cabinet. After the bacteria has been dried onto the surface of the coupons, 25 mL of the prepared nutrient agar is poured onto sterile Petri dishes and the substrata are completely covered and allowed to set at room temperature. The plates are then incubated overnight at 37°C, without shaking, once incubated the surfaces of the plates are flooded with 2 mL of 1 gL^{-1} of the NBT solution, which is made up of distilled water. Once flooded, the plates were left to incubate at room temperature for a minimum of 6 hours, and once this is done the respiring colonies were highlighted blue and counted. With this method for measuring the active respiring colonies, it was a clear indication of how effective the coatings are at leaching the antimicrobial agent, which in this case would be silver ions and disrupting the bacteria's processes.

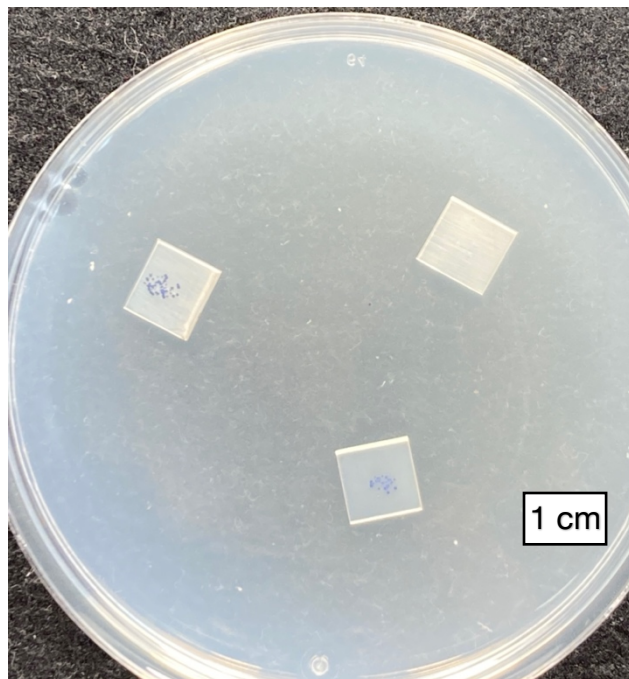


Figure 16: NBT Test on Stainless-Steel, Blue Dots Representing Respiring Colonies

2.3.4 Retention Assay

To understand how effective the designed substrata are at resisting the retention of bacteria, multiple retention assays were carried out, and this allowed insight into which pattern design/coating was most effective. Surface topographies and properties can play a role in the adhesion rates of different bacteria, and thus it is important to understand how changing any one of these parameters can impact the retention rates. The retention rate can be displayed as the percentage coverage of the substrata, with the aim to be a reduced coverage. The assays were carried out via the following procedure.

The samples were prepared for testing via the same procedures as described above, with them being ethanol washed and air-dried. Overnight cell cultures were washed and re-suspended to an OD of 1.0 ± 0.1 CFU/mL, within sterile plastic 6-well plates 3 of each variation of substrata were aseptically placed and 5 mL of the standardised cell suspension was poured over them. These plates were then incubated at 37°C without shaking for an hour, once incubated the cell suspension is carefully removed via pipette and the substrata are washed with 5 mL of sterile distilled water at a 45° angle. The

samples with any retained bacteria were then air-dried in a class-2 laminar flow hood for 1 hour, to allow visualisation of the retained bacteria via epifluorescence microscopy, the samples are stained with 0.03% acridine orange (Sigma, USA) diluted in 2% glacial acetic acid (BDH, UK) for 2 minutes and rinsed in sterile water and allowed to dry in the dark inside a laminar flow cupboard. Once dried, the samples are imaged immediately in the epifluorescence microscope, and visualised at 502-526 nm wavelength. This wavelength is used, as this is the excitation wavelength range of the acridine orange stain. Acridine orange binds to any RNA that has managed to adhere to the surface of the substrata, and when visualised at this wavelength range it turns the bacteria into a bright red cell. Once visualised the results are processed through Fiji image processing, which is a version of ImageJ that is more suited to scientific processing, with the number of bacteria adhered being used rather than surface coverage, this was decided upon as the two bacterium that have been chosen for this project are different in size and shape. Thus, it would not be a viable method for analysing the area covered by their cells.

Whilst this type of assay is generally only for the visualisation of adhered bacteria, whether they have been killed or not, it can be a very useful tool for viewing the substrata's ability to resist the initial adhesion of the bacteria. Further analysis can be done on these samples using a similar process to retention assays, which will be discussed in a later sub-section of this thesis. By calculating the number of bacteria that have been able to adhere, we can begin to extrapolate which coating/texture would be most beneficial for use and therefore can decide which coating/texture we would combine for further investigation. Images gained from this assay can be seen in the below *Figure 17* which highlights what is to be expected from the epifluorescence microscope. In the figure below every green dot that is present on the coupon is a bacteria cell that has managed to

adhere itself to the surface, and by using the Fiji image processing it can be determined how many bacteria are on each image.

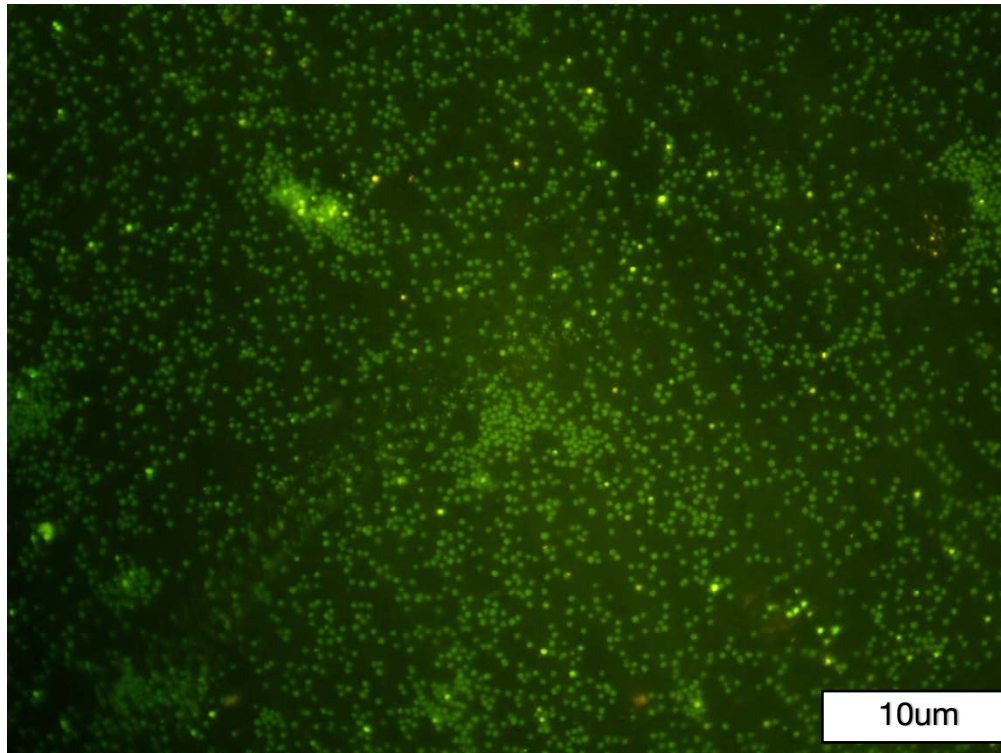


Figure 17: Epifluorescence Microscopy of S. aureus on LIPSS Sample

This was done via several different processes that are available for use on the software and using these processes a macro was written inside the software that allowed for batch processing of all images created in the assay. The macro can be seen below in *Figure 18*, this macro was used for analysing all the images produced. To determine the number of bacteria that were retained in a centimetre squared area, which is the area of the substrates used in this project, a scale bar was first produced on the ToupView software (ToupTek Photonics, Hangzhou, P. R. China) and this was set at 10 microns. Once the image was then uploaded to the Fiji software a global scale bar was determined using the stock photo, and it was determined that 17.2 pixels was equal to 1 micron on the software. Using this an area of each image was calculated and used to determine the total area imaged and finally a ratio of cells to this area was found.

```

filename = getTitle();
run("8-bit");
run("Median...", "radius=2");
run("Subtract Background...", "rolling=50");
setAutoThreshold("Default dark no-reset");
//run("Threshold...");
//setThreshold(20, 255);
setOption("BlackBackground", true);
run("Convert to Mask");
run("Analyze Particles...", "size=0-10000 pixel display clear include add", "display summarize");
selectWindow("Results");
saveAS("Results", "/Volumes/NIALL USB/PhD Work/Epifluorescent/Results/Results.tsv")

```

Figure 18: Fiji Software Macro for Retention Assay Calculation.

2.3.5 LIVE/DEAD Stain

To further investigate the effectiveness of the coatings produced through this project, the substrata are exposed to a LIVE/DEAD staining process. This process follows a similar procedure to the retention assays, as it is effectively the same assay, with a different stain being used for the epifluorescence microscopy. Where the retention assay used acridine orange stain, this assay will utilise LIVE/DEAD *BacLight* Bacterial Viability Kit (ThermoFisher Scientific). This kit contains SYTO 9 nucleic acid stain and propidium iodide, which are both dissolved within dimethyl sulfoxide (DMSO), at concentrations of 3.34 mM and 20 mM respectively. The procedure for this assay is as follows and has been adapted from (Slate *et al.*, 2018).

Overnight cell cultures were prepared, with them being washed and re-suspended in distilled water to an OD of 1.0 ± 0.1 at 540 nm. All tested substrata are washed with ethanol for 10 minutes to remove organic contaminants, then rinsed with distilled water and finally placed within a microbiological class-2 laminar flow cupboard to air dry. Once the substrata are dry, they are placed into sterile plastic 6-well plates and 5 mL of the cell suspension is poured over them, completely submerging them and plates are then incubated at 37°C for 1 hour without agitation. Whilst the samples are incubating the stain mixture is prepared, as the stains from the kit are already dissolved within DMSO they do not need to be dissolved again and can be mixed with sterile water at a 1:10 ratio. Once incubated, the samples are drained of the cell suspension via pipettes and rinsed with 5 mL of sterile water and again excess is pipetted out, once rinsed they are placed into a class-2 laminar flow cupboard to air-dry for a minimum of 45 minutes. After drying 2.5 mL of the SYTO 9/propidium iodide mixture is added to each substrate and left to dry for 15 minutes in a dark class-2 laminar flow cupboard, once dried they are visualised

immediately via epifluorescence microscopy at 502-526 nm wavelength range. With this staining kit any bacteria that are adhered will either be stained green, which could indicate that they have intact cell membranes and can be classed as live cells. Or they could be stained red, which indicated compromised cell membranes and can be classed as dead. After visualisation the images are processed through Fiji, this is done by splitting the image into its 3 colour channels of red, blue, and green. As there are no bacteria stained blue, this channel can be ignored, whilst the red and green channels are important. Once the colour channels have been split into the green and red channels, the images are processed by several filters that allow for all the individual cells to be highlighted. These processes include the removal of the background, which negates the background interference, then using the process of watershed, the cells are individually divided from their blocks depending on the size used. Once these processes, which can be seen in code form below in *Figure 19*, have been applied the number of live/dead cells can be calculated. The control for these processes was carried out by counting the number of bacteria by hand, making use of the Fiji software's built-in marker option. The scale was pre-set to 17.2 pixels = 1 micron, and this was used for the calculation of the number of cells found across the surface.

```
run("Median...", "radius=2");
run("Subtract Background...", "rolling=50");
setAutoThreshold("Default dark");
//run("Threshold...");
//setThreshold(55, 255);
setOption("BlackBackground", true);
run("Convert to Mask");
run("Watershed");
run("Analyze Particles...", "size= 17.2-10000 pixel display clear include add");
```

Figure 19: Code for LIVE/DEAD Fiji Calculation

By knowing whether the substrata have been able to kill the adhered bacteria it is easy to identify which composition would be most effective in this application. An example of the image that is produced via this method can be seen below in *Figure 19*, and this is what is seen through the microscope, an analysed image can then be seen in *Figure 20*.

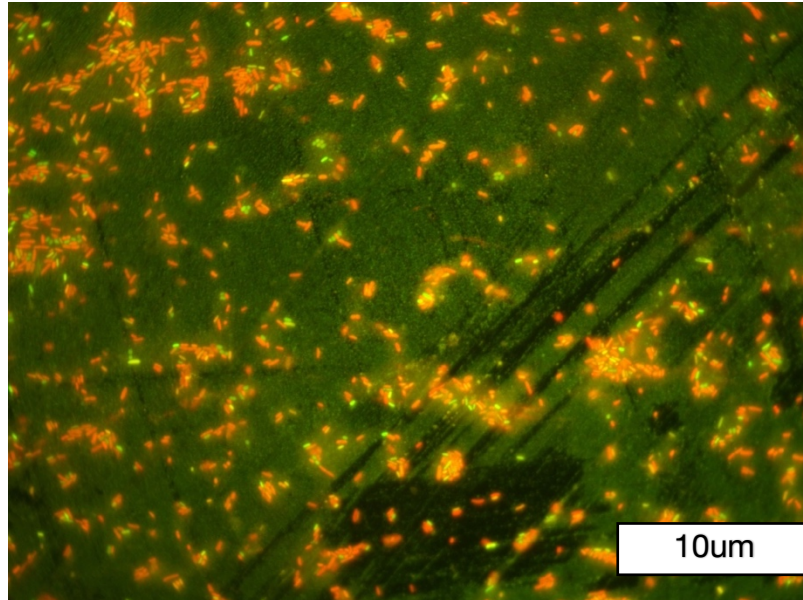


Figure 20: LIVE/DEAD Stain of P. aeruginosa on TiN-Ag 60W

In the figure below the cells that have been highlighted as green are classed as still being alive, as they are respiring. All the cells that are stained red/orange, are dead cells and by counting the number of each and gaining the percentage of this compared to all cells found, the % efficacy of the substrate can be calculated.

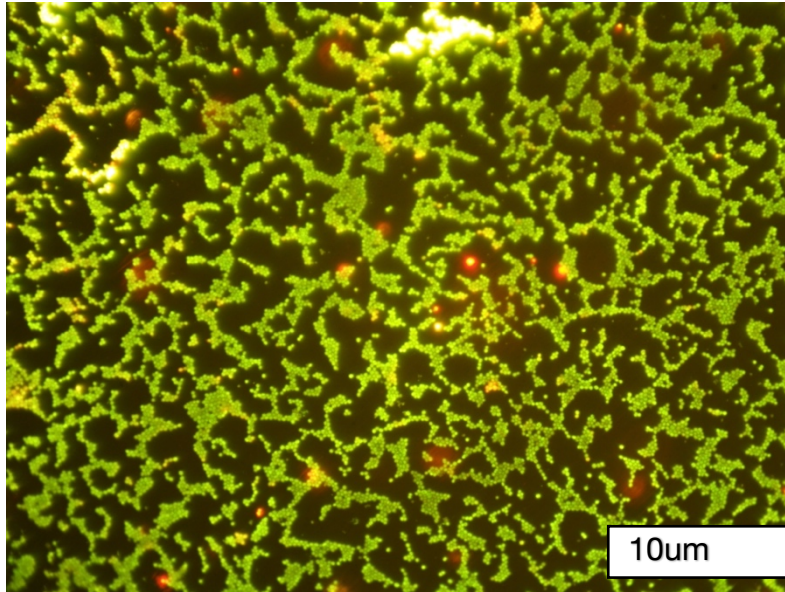


Figure 21: LIVE/DEAD Live Cells on Stainless-Steel

In the *Figure 22* below, the analysed image can be seen, this shows the overlay of the process that involves splitting the image into its red and green channels. This allows for only the corresponding bacteria to be visualised, and once they have been individually counted the image is overlayed to count all bacteria.

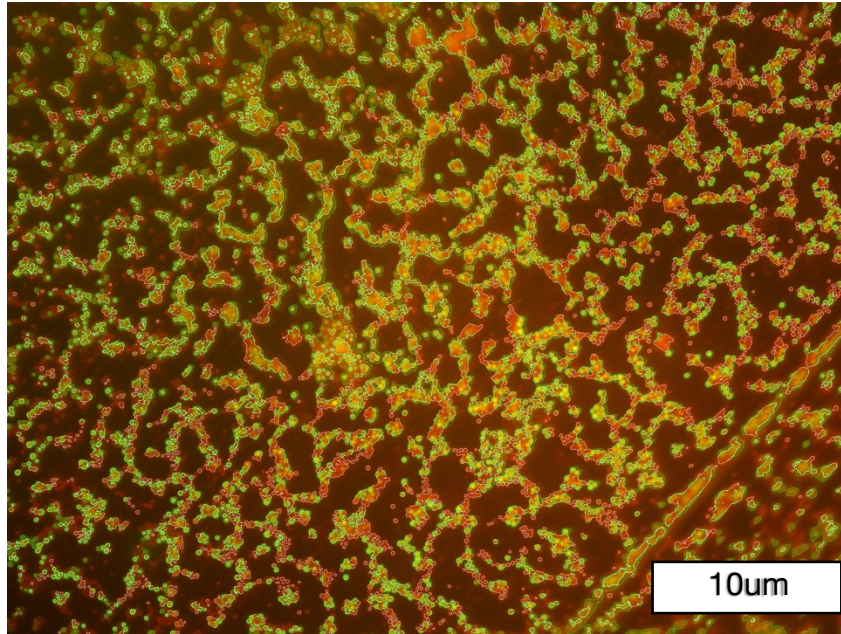


Figure 22: Overlay LIVE/DEAD Stain for *S. aureus* on TiN-Ag 50W

2.3.6 Statistical Analysis

Replicated samples were either tested in duplicate, or in triplicate, and all repeated experiments mean values were recorded and plotted, the raw data can be seen in the appendices (see [Appendices](#)). Error bars on the graphs represents the standard deviation of the results, and all data was statistically analysed for significance, with t-tests and with a confidence interval considered significant when $p < 0.05$.

2.4 Analytical Techniques

2.4.1 Overview

A range of analytical techniques were utilised throughout this project, with each being required to analyse a specific property of the thin films that have been produced. For example, the scanning electron microscopy allows for a high magnification image of the surface of the samples to be produced, allowing for the surface topography to be visualised. By understanding the properties that these analytical techniques provide, we can begin to understand how changing the composition of the coating or changing the texture design can affect the surface chemistry, or the surface topography. It will also provide the ability to differentiate between the properties of the base substrate, 316 stainless-steel, and why this is a less preferential material for use in the application.

2.4.2 Scanning Electron Microscopy

Scanning electron microscopy, or SEM, is a type of electron microscopy that can produce high magnification images of surfaces by scanning them with an electron beam. It allows for highly detailed images to be captured, and thus the nanoscale topography of the surface of materials can be visualised, allowing for the orientation of the comprising components to be seen. There is also the possibility of placing substrata that have been inoculated with bacterial strains to be imaged, which would provide an image detailing the orientation of the bacteria on the substrata. This is a crucial piece of information for this application, as it will provide the necessary information for understanding how the texturing process has affected the adherence ability of the bacteria. SEM is a non-destructive analytical technique and will allow for samples to be repeatedly tested.

To analyse the surfaces of the samples, they are placed into the chamber and then the chamber is evacuated of all air to create the vacuum that is required for the microscope to function, 1.31×10^{-9} bar is the working pressure inside the vacuum. After 5 minutes the samples can begin to be imaged using the electron beam, depending on the sample the working distance between the lens and sample will have to be adjusted to allow for an in-focus image to be taken. This can vary if the sample is coated or textured and can be dependent on whether there are any bacteria adhered that are being imaged.

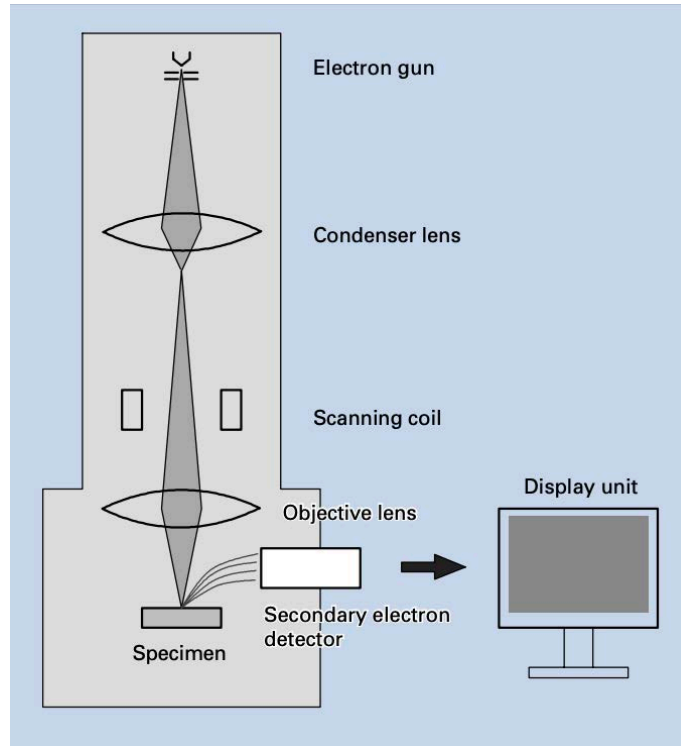


Figure 23: SEM Schematic

2.4.3 Energy Dispersive X-Ray Spectroscopy

Energy dispersive x-ray spectroscopy, or EDX, is a microanalysis technique that can be used in parallel with SEM and provides the elemental composition of the tested material. This method utilises the x-ray spectrum of a solid substrate that has been bombarded by a focused beam of electrons.

To analyse the solid substrates, they are placed within the scanning electron microscope and then they are bombarded by the focused beam of electrons. To maximise the accuracy of the gathered measurements, the surfaces of the samples would ideally be well polished, as this method is only capable of shallow penetration depths. This electron beam excites characteristic x-rays, which can be analysed to provide the chemical composition of the sample, this is done either via energy or wavelength x-ray detectors. During this analysis an incident high energy electron creates a hole in the inner shell of the atom, that ejects the core electron of the specimen. This hole is then filled by an electron that moves from the outer shell down to the inner shell, the energy that is emitted by this transfer is emitted as a characteristic x-ray. This x-ray is specific for each atomic number of the specimen.

As each element has its own characteristic energy line position, EDX is a method that can provide the ability to detect each of every element that has an energy that is greater than 1 keV (as any with an energy less than this is adsorbed by the beryllium window that separates the spectrometer and microscope). The qualitative data is processed via identifying all the characteristic peaks, for the quantitative data calibration samples of each element are used to measure and compare the line intensities of the gained results.

2.4.4 X-Ray Diffraction Spectroscopy

X-Ray diffraction is a very useful analytical technique that can be used for the identification of the crystal phases that are present in the materials used. In addition to the crystal phases, it can be used to identify the phase composition, the grain size etc. This method is also categorised as a non-destructive method, as it does not damage the coatings of any samples that have been analysed, this is due to it not requiring a vacuum for analysis.

This method is based upon the scattered intensity of an X-Ray beam hitting the sample as a function of incident and scattered angle, along with the polarisation and wavelength of the energy. Depending on the incident angle of the X-Ray beam, it can penetrate the surface of the sample and be diffracted throughout via the various planes of the crystalline solid. Using the Braggs law equation gives the calculation of the value for the crystal lattice spacing d by measuring the angle of the diffracted beam:

$$n\lambda = 2d \times \sin\theta \quad (1)$$

Where n is an integer, λ is the wavelength of the incident X-Ray, d is the crystal lattice spacing and θ is the diffraction angle.

2.4.5 White Light Profilometry (WLP)

White Light Profilometry, or WLP, is a specialised non-contact interferometric based method of characterising the surface topography of a substrate material, and it can provide this in both 2D and 3D images, it can provide this along with all the surface roughness values. WLP works by using a white light source that is filtered through an optical component that is directed towards the substrate surface. This light source is capable of being separated into its component wavelengths by a dispersive lens, which are attributed to a different z -coordinate in the optical axis. Thus, the visible light will be

encoded with z-coordinates as a function of the focal distance of the lens from the end of the lens.

White light profilometry can be used on a diverse range of samples and can be used to get the surface roughness values, and the thickness of a coating. It can also be used to identify the highest peaks and deepest valleys of a textured sample. This is particularly useful for analysing the thickness of the coatings that have been produced, which can be calculated by coating a stainless-steel coupon partially with the desired power variations. Once the sample is partially coated, it is analysed using WLP and the difference in the height across the visible coated and un-coated sections can be calculated as the thickness of the coating.

2.5 Summary

To provide clarity on which methods were used on which material, including the microbiological methods, the following table was constructed to provide a reference point.

Table 1: Microbiological Methods Summary

Sample Name	Microbiological Methods			
	Zones of Inhibition	Nitroblue Tetrazolium Test	Retention Assay	LIVE/DEAD Stain
316 Stainless-Steel	✓	✓	✓	✓
TiN	✓	✓	✓	✓
TiN-Ag 50W	✓	✓	✓	✓
TiN-Ag 60W	✓	✓	✓	✓
TiN-Ag 70W	✓	✓	✓	✓
TiN-Ag 75W				
TiN-Ag 80W	✓	✓	✓	✓
TiN-Ag 100W				
TiN-Ag 150W				
LIPSS SS			✓	
LIPSS Coated		✓	✓	✓
D20		✓	✓	✓
D50		✓	✓	✓

Table 2: Analytical Method Summary

Sample Name	Analytical Methods		
	Scanning Electron Microscope	Energy Dispersive X-Ray Diffraction	White Light Profilometry
316 Stainless-Steel	✓	✓	✓
TiN	✓	✓	✓
TiN-Ag 50W	✓	✓	✓
TiN-Ag 60W	✓	✓	✓
TiN-Ag 70W	✓	✓	✓
TiN-Ag 75W		✓	
TiN-Ag 80W	✓	✓	✓
TiN-Ag 100W		✓	
TiN-Ag 150W		✓	
LIPSS SS	✓	✓	✓
LIPSS Coated	✓	✓	✓
D20		✓	✓
D50		✓	✓

Part III

Experimental Results

Chapter 3 – Results

This chapter will provide the interpreted results that have been gained through the methods that were listed in the previous chapter, it is divided into sub-sections that will follow the structure 3.1 EDX Results, 3.2 XRD Results, 3.3 WLP Results, 3.4 SEM Results, 3.5 Zones of Inhibition, 3.6 Nitroblue Tetrazolium Test, 3.7 Retention Assay & finally 3.8 LIVE/DEAD Assay

3.1 EDX Results

To produce all the coatings throughout this project, as mentioned previously, the substrates were placed into a Teer UDP450 sputtering rig and to determine the atomic weight percentages of all the composing elements EDX was utilised. During this project the power level across the silver target was varied to gain different levels of silver in the atomic weight composition, to begin with there was a broader range that was between 50 and 150 watts, at 25 W intervals and then a 50 W interval between 100 and 150 W. However, the first batch of samples that were produced had atomic weight percentages that were not in line with previous work done at Manchester Metropolitan University, or that were found within the literature. This was believed to have been caused by the samples not being bias cleaned initially before deposition of the target materials, and therefore the procedure was modified to allow for this first step. By not bias cleaning the samples before deposition it was found that there were problems with delamination of the surfaces after basic ethanol cleaning.

Table 3: EDX Results from Initial Samples

Element	Average Atomic Weight (at%)			
	TiN-Ag 50W	TiN-Ag 75W	TiN-Ag 100W	TiN-Ag 150W
N	39.32	35.05	28.36	28.04
Ti	57.87	53.18	40.55	39.43
Ag	2.81	11.19	31.09	32.53

These results, seen above in *Table 1* were not representative of the results that would have been expected from the power variations that were applied across the silver target, as the silver content should scale with the power level across the target, with the 50 & 75 W variation having their silver atomic weight too low and the 100 & 150 W being too high (Kelly *et al.*, 2010, Kelly *et al.*, 2011, Akhidime *et al.*, 2019, Skovager *et al.*, 2013). This

was rectified by the previously mentioned method of bias cleaning the samples, and this allowed for a better adhesion between the substrate and target material. However, it should be noted that using EDX for measuring nitrogen content is not the most accurate method for this and thus it causes some discrepancies between the content of nitrogen and titanium.

When the coating procedure was repeated the results from the EDX method were the more expected range of results, when compared to the literature and previous studies carried out. For the following coating produced the power variations across the silver target was reduced to a smaller range, this was to investigate the lowest quantity of silver that could be deposited, whilst still providing the required antimicrobial activity. There was also the consideration that increasing the silver content of a coating can begin to reduce its wear resistance, as previously mentioned.

Table 4: EDX Results Second Batch

	Average Atomic Weight (at%)		
Element	TiN-Ag 60W	TiN-Ag 70W	TiN-Ag 80W
N	36.48	33.99	33.19
Ti	42.51	40.09	39.12
Ag	21.01	25.92	27.69

As can be seen from the above *Table 2* the atomic weight distribution of silver is different to the initial batch, and this was found to be more in-line with studies within the literature, and from studies carried out at the Manchester Metropolitan University. The samples manufactured in this run of coating were utilised throughout the microbiological testing methods explained in the previous section, and these results will be displayed in a later section of this thesis. From the findings of these tests the power range was again modified to allow for a lower concentration of silver to be implemented into the testing parameters, the explanation of these results will be discussed in a later section.

Table 5: EDX Results Third Batch

	Average Atomic Weight (at%)			
Element	TiN-Ag 50W	TiN-Ag 60W	TiN-Ag 70W	TiN-Ag 80W
N	39.06	36.06	34.00	32.39
Ti	45.41	43.81	44.75	40.33
Ag	15.53	20.13	21.26	27.28

This variation of power levels across the silver target was the final range that was used throughout the project, as it was found during the microbiological testing to present the most efficient antimicrobial properties, whilst also keeping the silver atomic weight percentage relatively low. As can be seen in the above *Table 4* the at% of silver is within a more concise range than the previous samples.

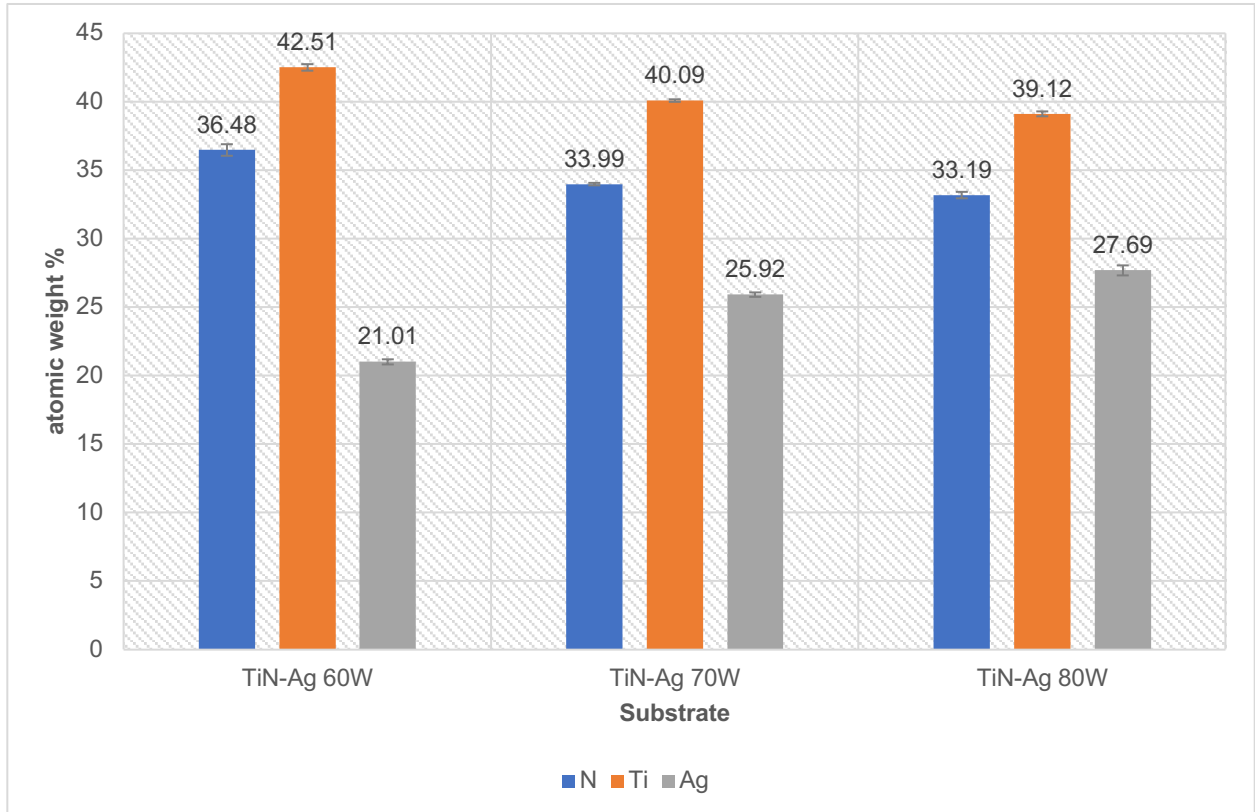


Figure 24: EDX Results for Second Batch

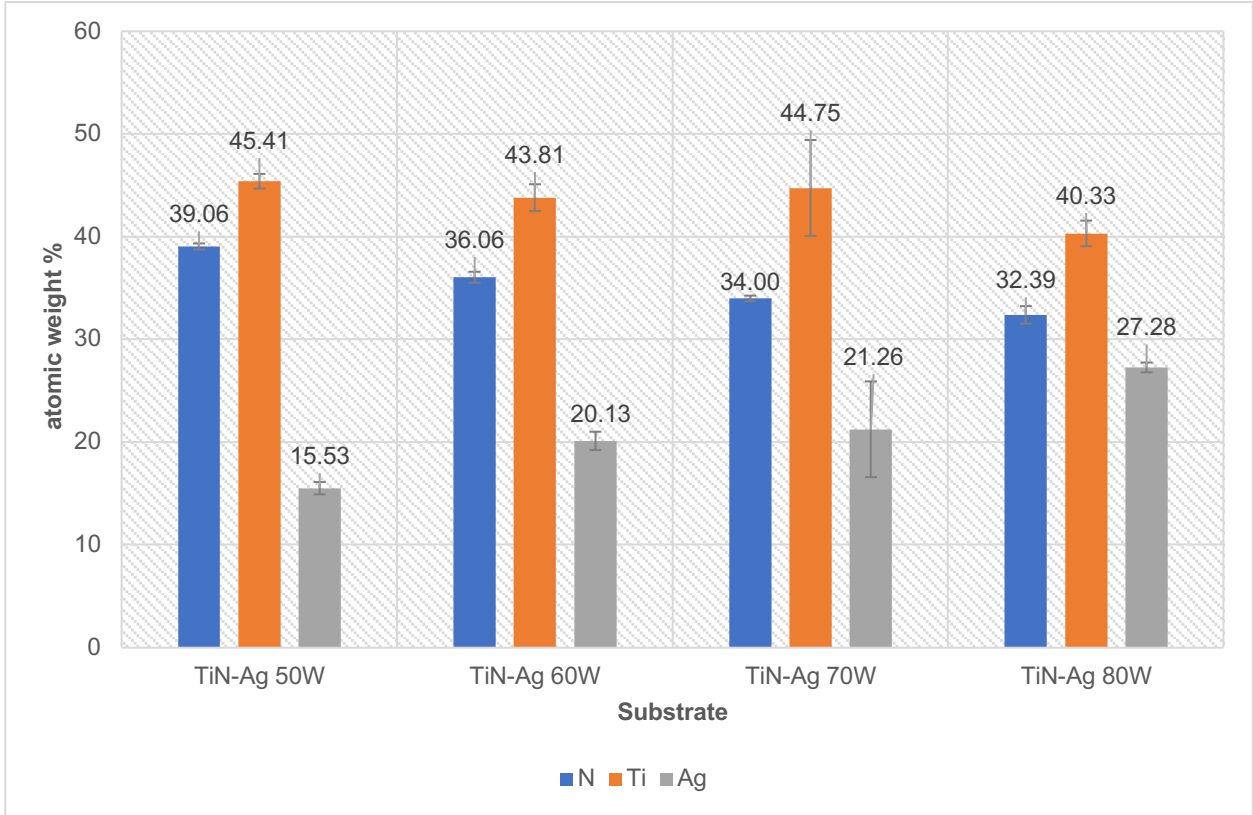


Figure 25: EDX Results for Third Batch of Samples

3.2 XRD Results

To understand how the crystallinity of the coatings produced would affect the antimicrobial efficacy and thus their suitability for application, the samples were analysed using XRD. There were complications with analysing these samples using this method, as the samples coatings produced were less than a micron in thickness, this was calculated using white light profilometry. This caused an issue as the characteristic peaks were found to be in different locations than they should be, which could be due to the crystallinity of the sample, as they can be entirely absent in the analysis.

The below *Figure 26* is a comparison of three different angles of incidence that have been used to scan titanium nitride coated stainless-steel. The calculated penetration depth of the three different beams into cubic titanium nitride are 1.628 microns for 3°, 1.086 microns for 2° and 0.543 microns at 1°. From these results it was decided that for following tests the angle chosen would be 3°, as they presented the best intensity for the tests. This is the glancing angle of XRD, which is a method of analysing a coating that is

very thin, and it is implemented if the results gained from higher angles are presenting the substrate material more than the coated sample, as was found in this project.

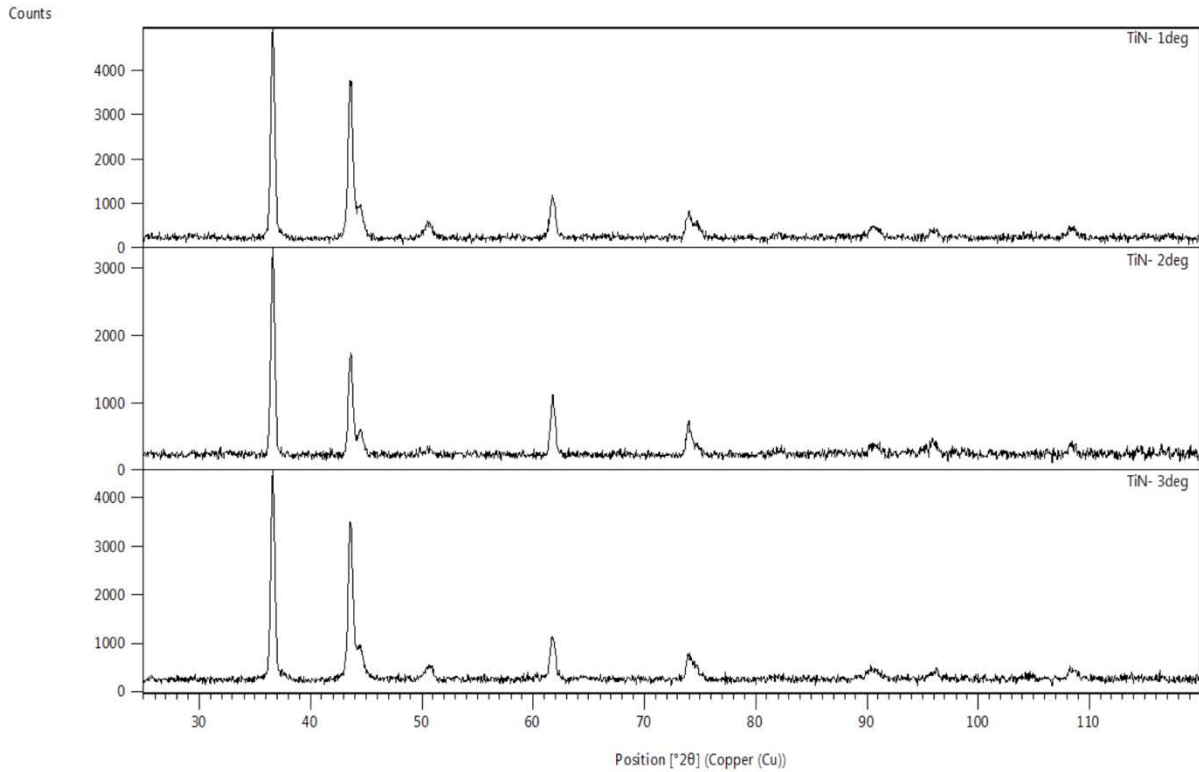


Figure 26: XRD Results Comparison of Different Angles of Incidence on TiN

In the Figure 27 below, the results for the TiN, TiN-Ag 50 W and TiN-Ag 60 W samples can be visualised, these samples were put back through the XRD process at lower incident angles than previously used. This was done to investigate if it was an issue with the samples, or the equipment, and there was still not any silver detected from the coated samples.

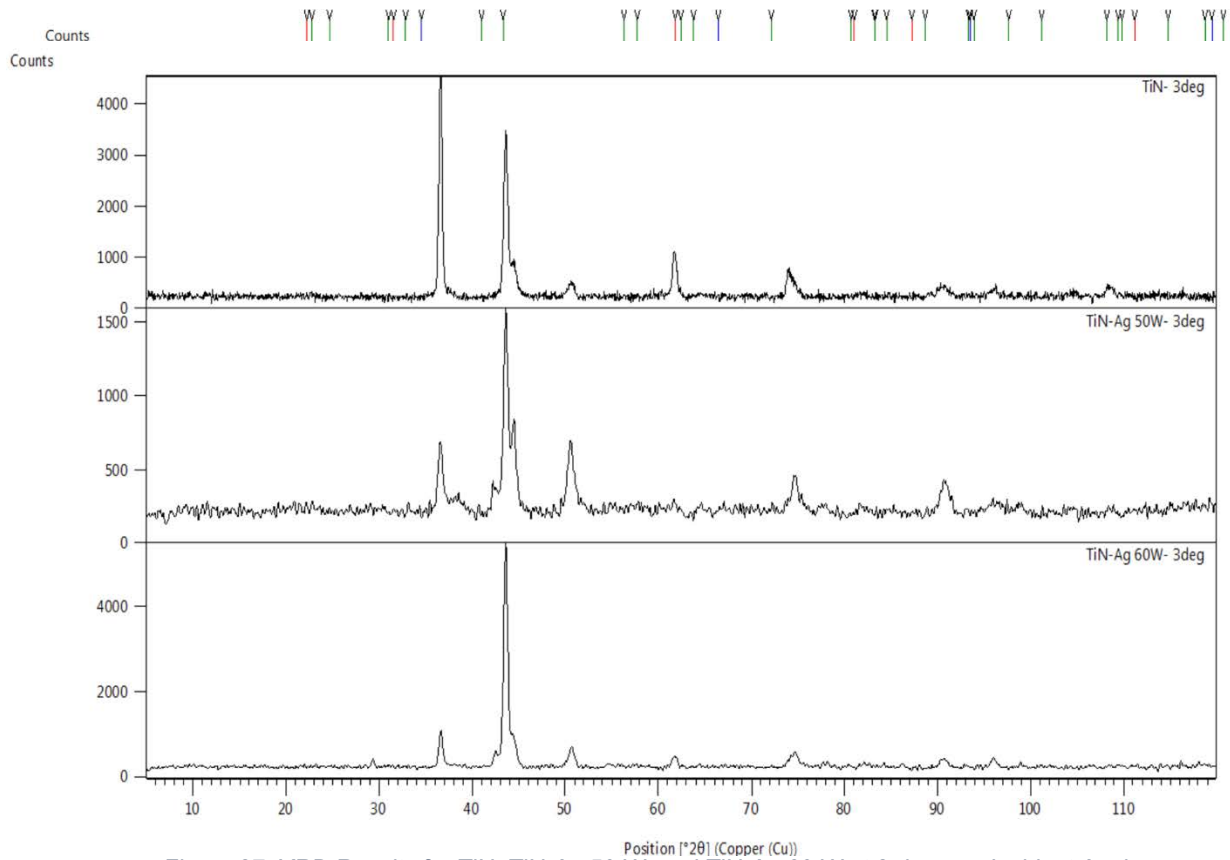


Figure 27: XRD Results for TiN, TiN-Ag 50 W, and TiN-Ag 60 W at 3 degrees Incident Angle

Throughout the project, there has not been any silver detected via the XRD process, and this could be due to other elements blocking the characteristic peak, or due to the coating being relatively thin it not being picked up.

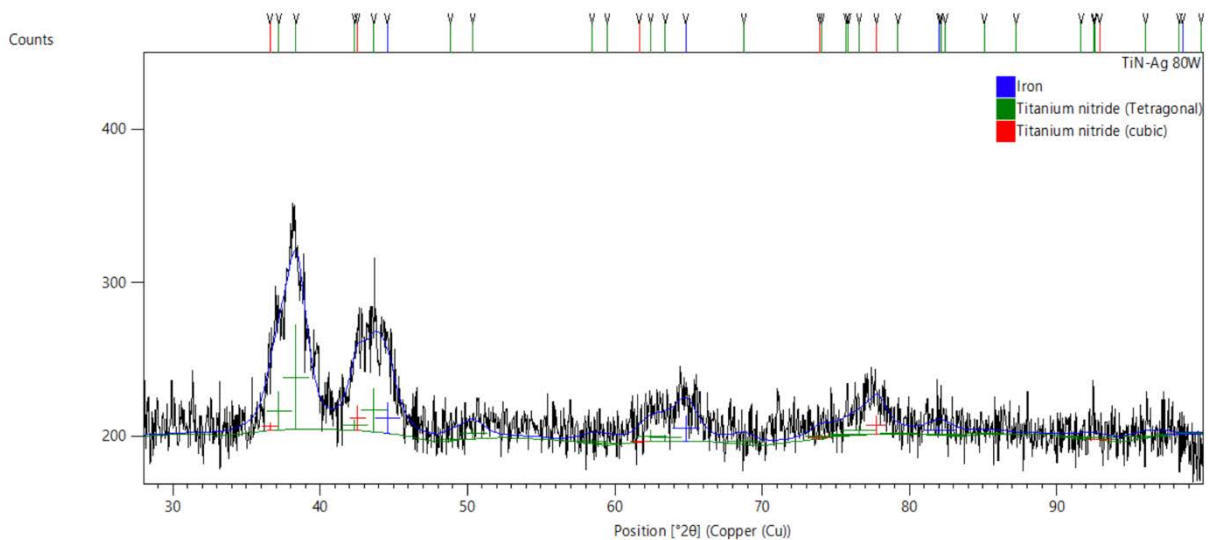


Figure 29: XRD Results for TiN-Ag 80 W

The results gained from the XRD analysis for the titanium nitride coating were not particularly conclusive, and the main results for the 3-degree angle were found to have a diffraction pattern broadly consistent with the cubic (Fm-3m) phase of TiN but one of the main peaks- the one at $43.568^\circ 2\theta$ - isn't where it was expected to be for TiN. This should be around $41.786^\circ 2\theta$ if it's the TiN (020) peak. Diffraction peaks can shift from their expected positions due to strain and can be more or less intense than expected (or absent entirely) due to the crystallites adopting a common orientation on the substrate. There are also several different phases of TiN with varying Ti:N ratios that have peaks in different positions.

One of the complications that arose from these results was the location of the nickel (111) peak, which should be located at $43.468^\circ 2\theta$, was not found and once the samples had been analysed from both the substrate side and coating side of the TiN the resulting peaks did not match up, which can be seen below in *Figure 29*. The most intense peak found on these samples, the one that was found at $50^\circ 2\theta$, is also visible from the coating side, however this could be due to the 1Ti : 3N phase that has a peak at this location.

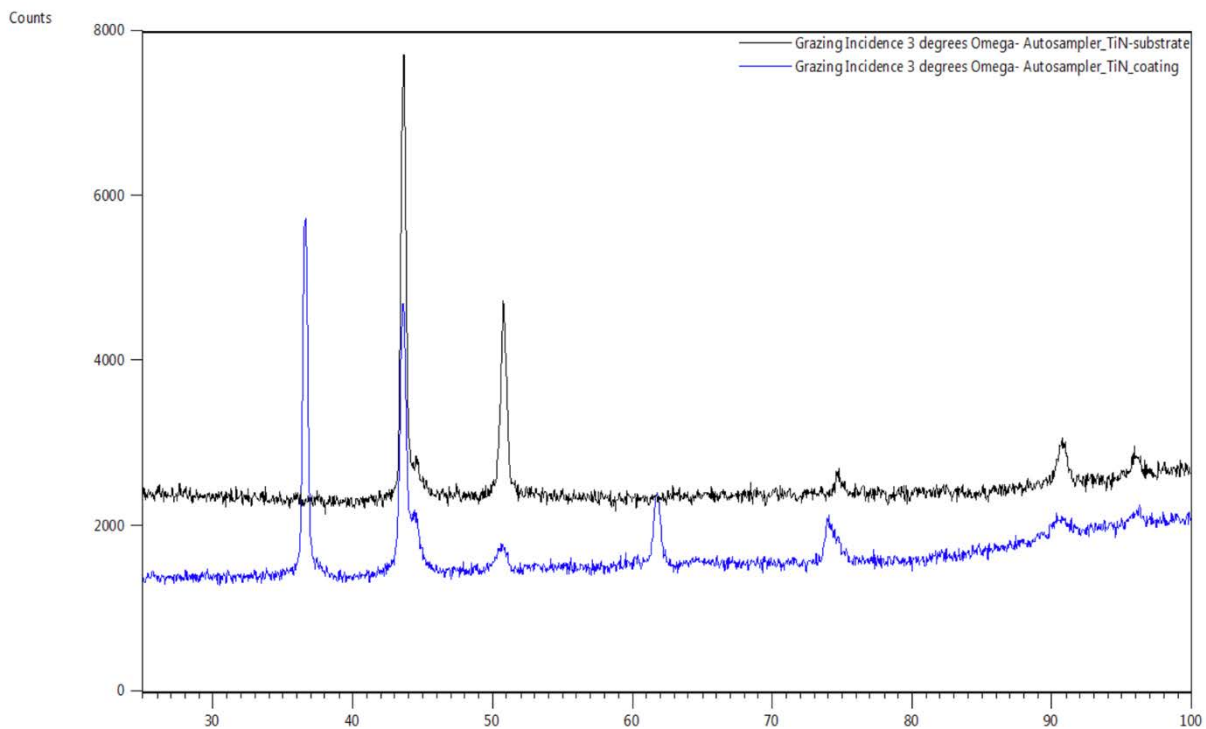


Figure 30: XRD Comparison of Substrate & Coating Side of TiN

3.3 WLP Results

As the samples that have been produced throughout this project are either a coated/textured, or a combination of the two procedure they modify the surface texture or morphology of original stainless-steel substrate. To understand the effect that this has on the properties the method of white light profilometry was implemented, and this allowed an insight into the surface roughness, and the actual structure of the surface topography. The information for the surface roughness of the coatings produced is described in *Table 6*, which includes the uncoated and untextured base sample stainless-steel.

Table 6: WLP Results for all Samples

Sample	Spv (μm)	Sa (μm)	Sq (μm)	Rpv (μm)	Rq (μm)	Ra (μm)
Stainless-Steel	0.00992 \pm 0.05	0.0563 \pm 0.04	0.0152 \pm 0.01	0.0878 \pm 0.23	0.0309 \pm 0.06	0.0510 \pm 0.04
TiN	1.26 \pm 0.79	0.152 \pm 0.24	0.129 \pm 0.21	0.400 \pm 0.61	0.908 \pm 0.14	0.0293 \pm 0.44
TiN-Ag 50W	2.96 \pm 1.56	0.325 \pm 0.28	0.266 \pm 0.24	0.880 \pm 0.74	0.216 \pm 0.20	0.172 \pm 0.17
TiN-Ag 60W	3.64 \pm 2.64	0.221 \pm 0.19	0.162 \pm 0.16	0.945 \pm 0.70	0.181 \pm 0.19	0.180 \pm 0.20
TiN-Ag 70W	2.19 \pm 1.83	0.123 \pm 0.10	0.0944 \pm 0.08	0.261 \pm 0.23	0.0647 \pm 0.06	0.0466 \pm 0.05
TiN-Ag 80W	5.16 \pm 8.13	0.269 \pm 0.23	0.210 \pm 0.19	0.524 \pm 0.52	0.121 \pm 0.13	0.0994 \pm 0.10
LIPSS 2	4.27 \pm 0.90	0.389 \pm 0.03	0.468 \pm 0.04	1.06 \pm 0.25	0.193 \pm 0.04	0.15 \pm 0.02
LIPSS 2 Coated	3.55 \pm 0.62	0.155 \pm .02	0.203 \pm .03	0.366 \pm 0.17	0.0396 \pm 0.01	0.0309 \pm 0.01
D20	8.52 \pm 0.57	1.62 \pm 0.06	1.85 \pm 0.04	2.72 \pm 1.18	0.570 \pm 0.37	0.480 \pm 0.33
D50	5.44 \pm 0.46	0.570 \pm 0.05	0.694 \pm 0.07	1.59 \pm 0.54	0.339 \pm 0.22	0.289 \pm 0.2

From the above table the values for all the coated samples are within a small range of values. This is thought to be because all the samples are being coated with similar content of silver, and as there has been no texturing work carried out on the samples then there should be relatively similar surface topography produced. The D20 & D50 results are attributed to the groove density percentage for the linear groove pattern that was produced, with D20 being 20% line density and D50 being 50% line density.

An example of the 3D surface maps that can be produced via the WLP method can also be seen in the below *Figure 31* this 3D map can provide a visual aid to understanding what is meant by the values listed in the table above.

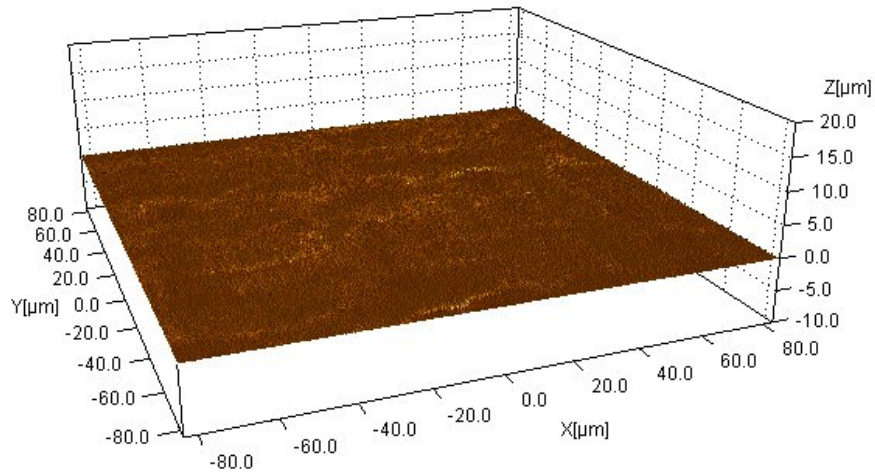


Figure 31: 3D Surface Profilometry Map from TiN-Ag 50W Deposited on Stainless Steel

The above figure shows the 3D map for the coated and untextured samples, and therefore it is relatively smooth across the surface. An example for the textured surfaces can be seen below in *Figure 32* and this is vastly different to the untextured samples. The roughness that is visualised in the surface map highlights how the texturing pattern affects the polished stainless-steel surface, and the difference between coated & untextured to textured.

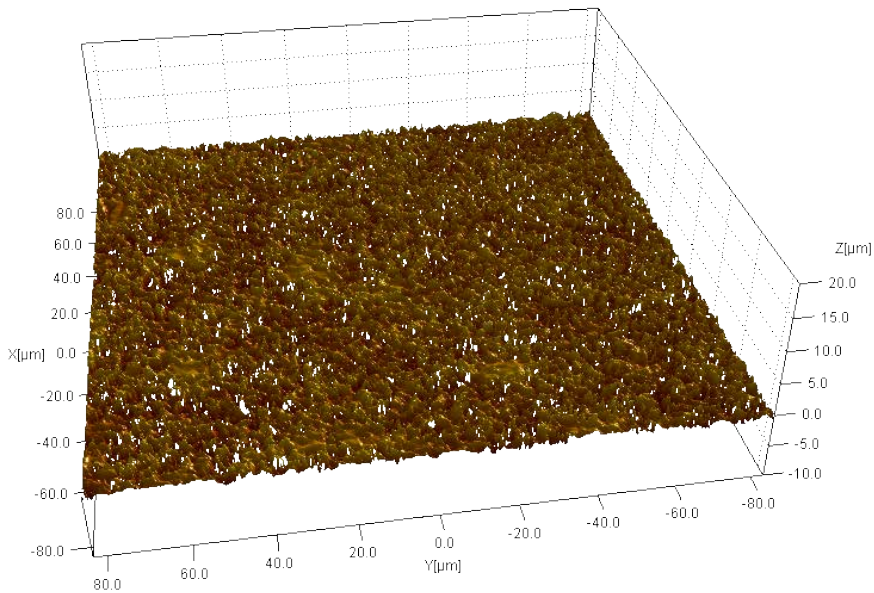


Figure 32: 3D Surface Profilometry Map for LIPSS Pattern Texture on Stainless-Steel

3.4 SEM Image Results

To visualise the changes to the surface topography of the substrates after coating and texturing, they were imaged using the SEM method described previously (see 2.4.2 Scanning Electron Microscopy). By looking at the surface topography we gained an understanding of how these substrates were affected throughout the project, there was also images taken of the LIPSS samples after they had been inoculated with bacteria. This allowed us to see how the bacteria was organised across the surface, and even allowed for insight to see where they prefer to adhere to and what structures they would be more likely to adhere to. As there are numerous images for all the coatings that have been produced, the majority will be in the appendices towards the end of this thesis.

As can be seen in the below *Figure 33*, the texturing process resulted in the self-organised laser induced periodic surface structures, and these are presented as the ripples that can be seen across the substrate surface. In comparison to the untextured coating the surface topography has been significantly modified and altered.

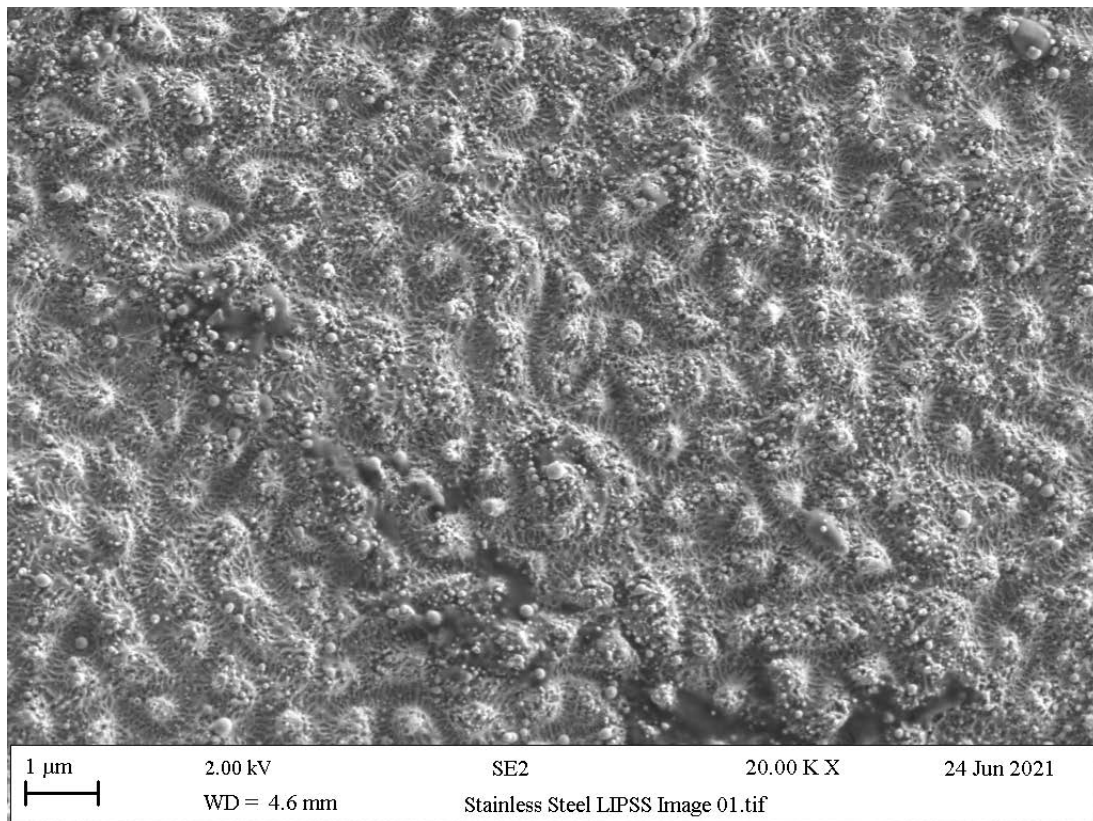


Figure 33: LIPSS Textured Stainless-Steel

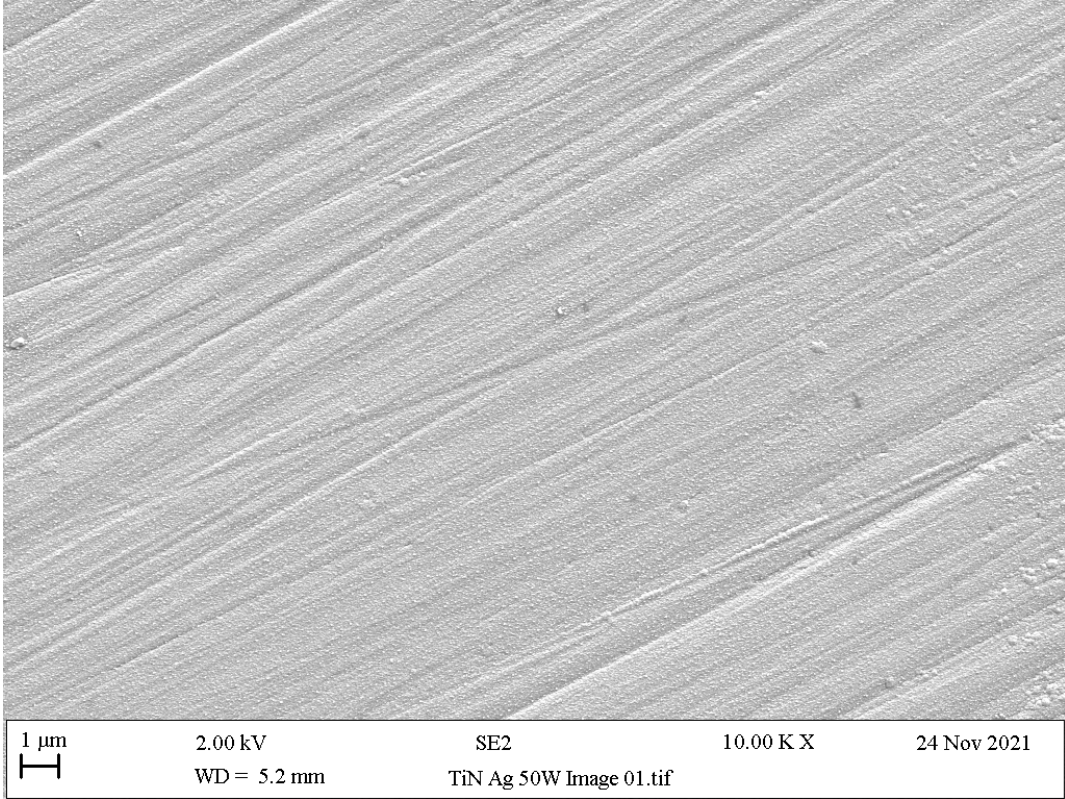


Figure 34: TiN-Ag 50 W Coated Stainless-Steel at 10x Magnification on SEM

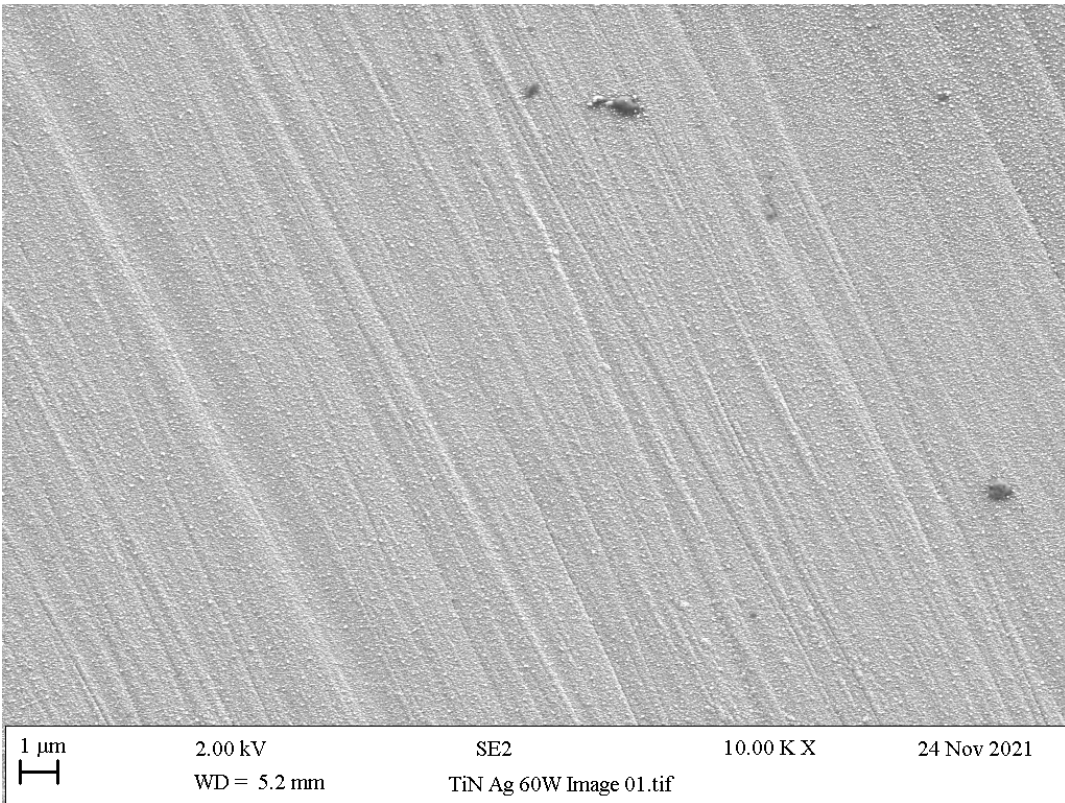


Figure 35: TiN-Ag 60 W Coating on Stainless-Steel

As the coatings are predominantly all similar in the image gathered from the SEM, the rest of the photos will be placed into the appendices.

The following images will be of the textured stainless-steel before and after it has been inoculated with the bacterial strains *P. aeruginosa* and *S. aureus*.

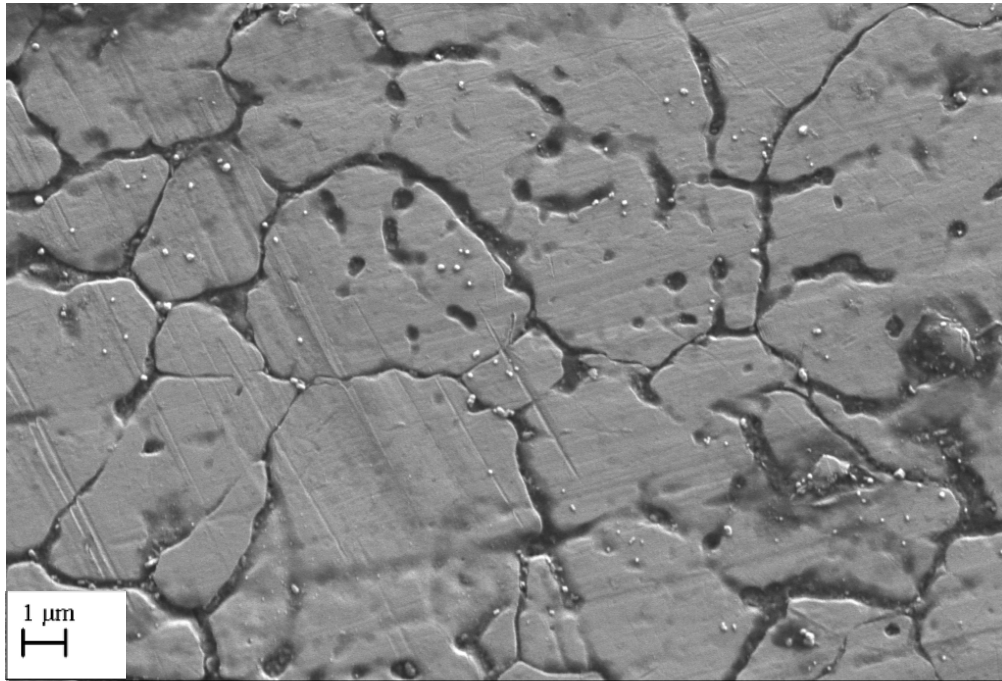


Figure 36: Stainless-Steel Uncoated & Untextured, polished by external company.

In the below figures, see *Figures 36 & 37*, the samples had been inoculated with the two strains of bacteria that have been tested against throughout this research project. This was done so it could be visualised how the bacteria would adhere to the surface of the texture pattern, this visualisation allowed for better understanding of the difference the size and shape of each cell made to the adherence. When compared with the results that had been gained from the retention testing, there appears to be more of the *S. aureus* bacterial strain adhered to the surface of the LIPSS pattern when compared to the *P. aeruginosa* bacterial strain cells. The arrows on both figures indicate where the bacterial cell is located on the substrate.

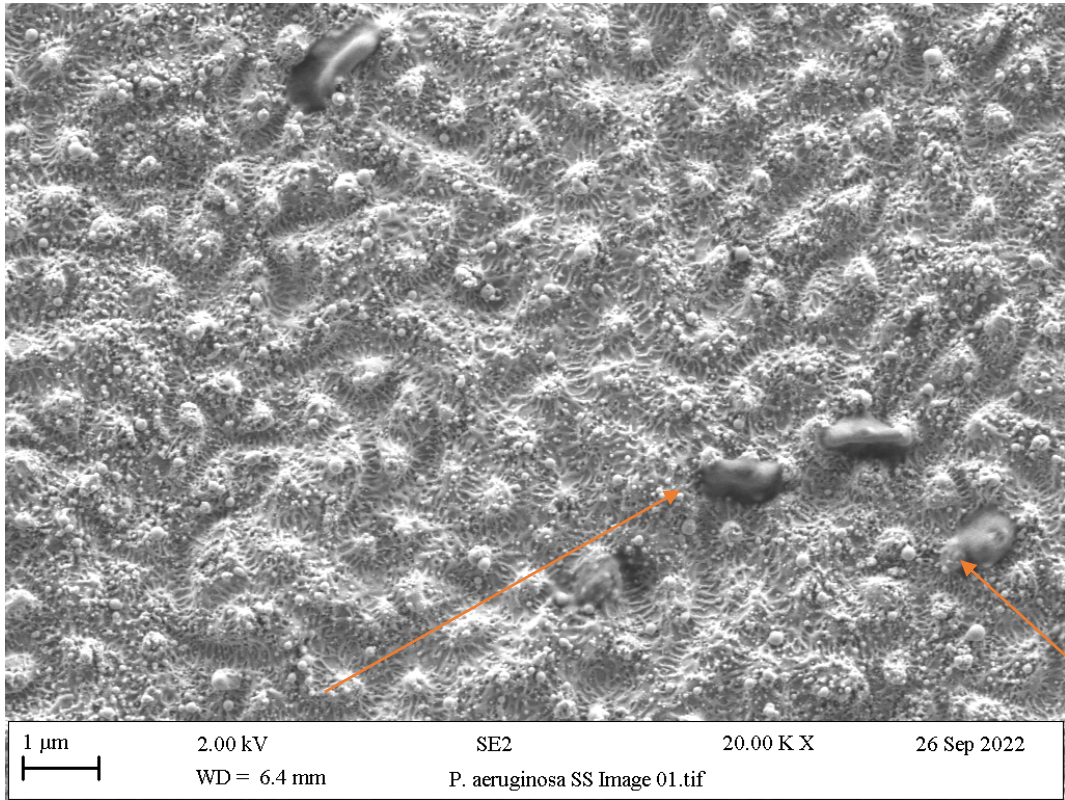


Figure 37: *P. aeruginosa* Inoculated Stainless-Steel LIPSS

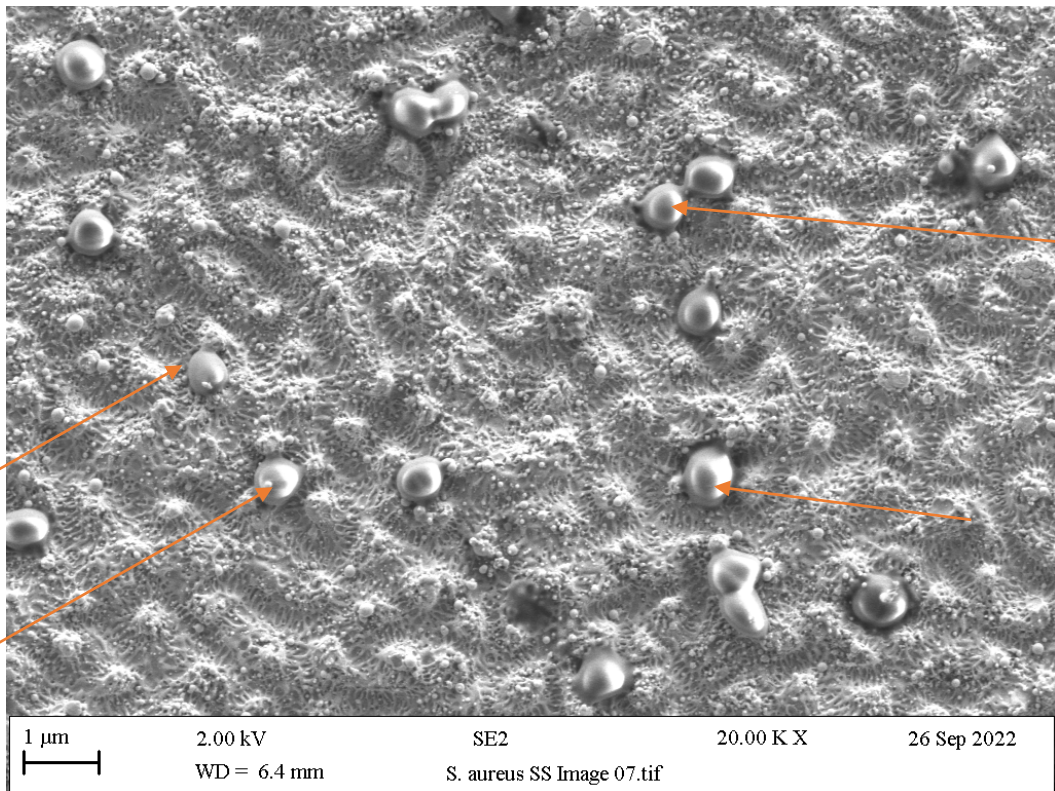


Figure 38: LIPSS Textured SS Inoculated with *S. aureus*

3.5 Zones of Inhibition (ZOI)

Determining the leaching capabilities of the silver particles within the titanium nitride matrix was the initial test carried out in the microbiological side of this project, and with this it could also be determined the efficacy of the coatings produced. This testing method was inconclusive, as the samples did not produce any zone of inhibition, it was found that most of the samples that had been produced throughout the project did not create a zone around the sample. This was concluded to be due to the silver in the sample not being able to leach far enough from the sample, this did not mean that the sample had no leaching, to be an antimicrobial agent the silver must leach partially. As there were no zones of inhibition produced, it was assumed that the silver was too encapsulated within the titanium nitride matrix, inhibiting the silver from leaching.

3.6 Nitroblue Tetrazolium Test

Similar to the previous testing, the nitroblue tetrazolium test (NBT) investigates the coating's ability to leach its antimicrobial agent, but on a smaller scale. This is because

this procedure only investigates the ability to leach from the surface to affect any microbes that have been incubated onto the surface of the coating. The results from this testing were much easier to understand and quantify the actual bacteria found on the surface of the material.

In the below *Figure 39*, the results for the above table can be seen in graph form, the increase in the number of bacterial colonies on the surface of the materials on the titanium nitride material can be seen. These results were from the coated, and untextured samples, and were used in the final decision for choosing the optimum power variant for the silver content.

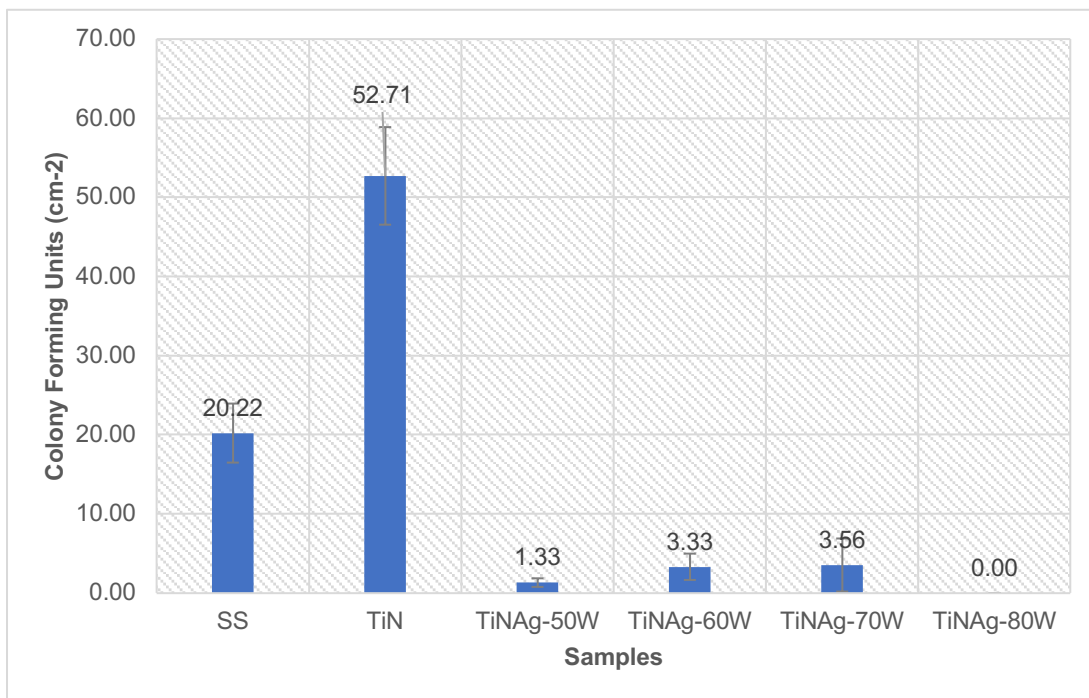


Figure 39: NBT Results for Final Power Variations

3.7 Retention Assay

By using the previously mentioned method of retention assay, which was described in detail (see 2.3.4 Retention Assay), the number of retained bacteria on each substrate created throughout this project was determined. The following *Figure 39* highlights the cells that were found to have been able to adhere to the surface of the tested substrates,

as can be seen there was a decrease in the number of cells that were able to adhere to the coated samples.

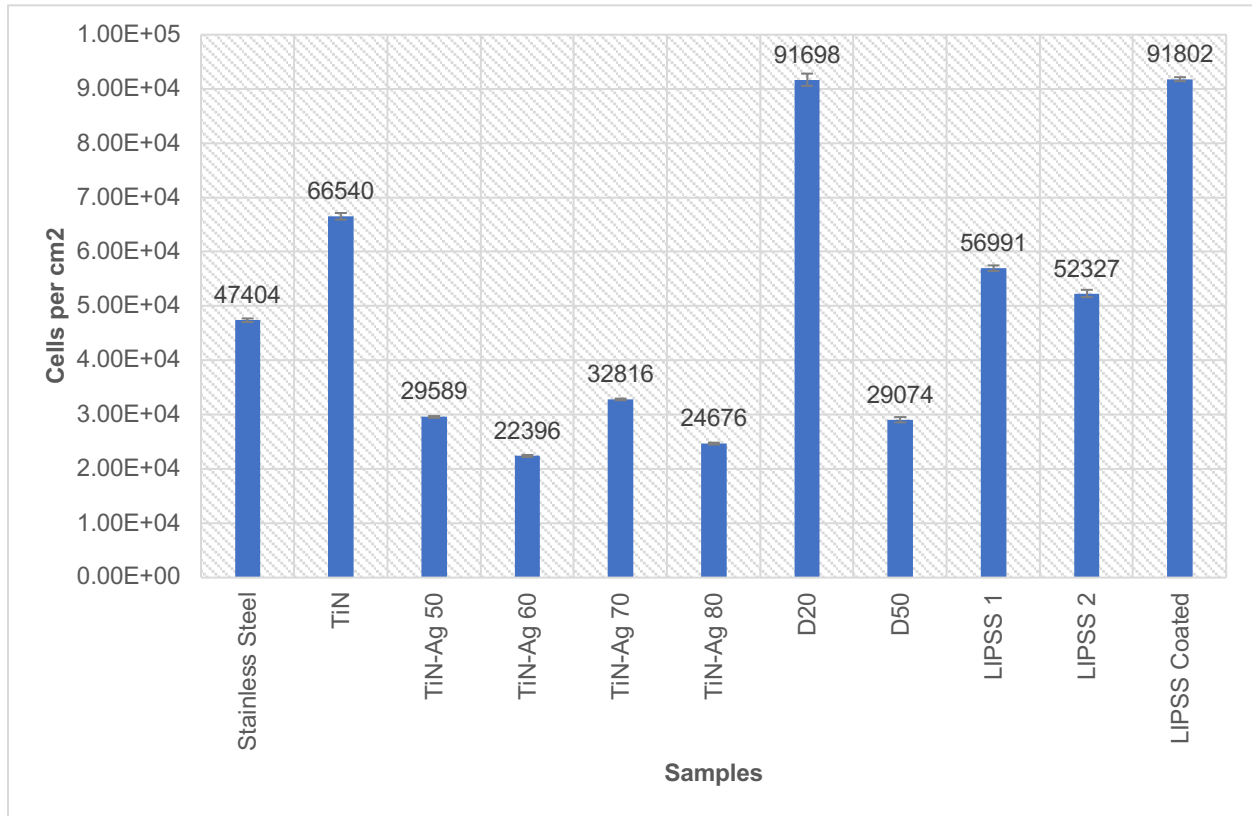


Figure 40: Retained Cells on Samples for *S. aureus*

As mentioned in the statistical analysis, all the samples were analysed for statistical significance to determine if there was a difference that could be determined with confidence. When compared to the control substrate 316 medical-grade stainless-steel some of the samples showed a significant difference in the number of *Staphylococcus aureus* cells retained on the substrate surface ($p < 0.05$), this was true for all the coated samples that have been produced, there was a reduction in the number of retained cells found on the substrate surface. However, there was no significant difference in the number of cells that had been retained on the LIPSS textured samples, when compared to the untextured stainless-steel ($p > 0.05$). There was also a significant difference found between the pure titanium nitride coating, and all the coated samples with silver in their

composition ($p < 0.05$). For the raw data that was gathered from the statistical analysis, refer to the appendix of this research project, see [Appendices](#).

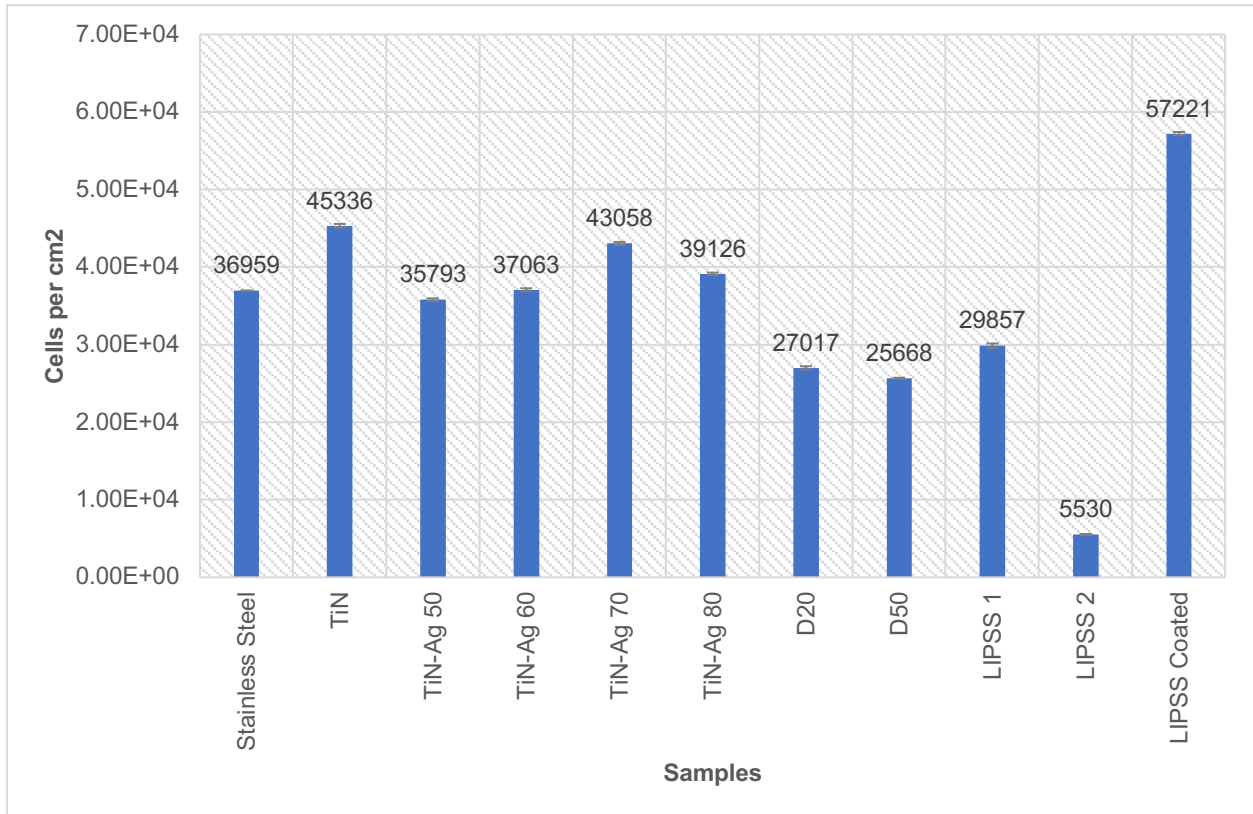


Figure 41: Retained Cells on Samples for *P. aeruginosa*

For the *Pseudomonas aeruginosa* bacterium, it was found that there was a general increase in the number of bacterial cells that had adhered to the surface of the substrate, when compared to the number of *S. aureus* cells that had been able to adhere. As for the *Staphylococcus aureus* results, the results for *Pseudomonas aeruginosa* were also statistically analysed to understand if there were any significant differences between the results. For the coated samples there was only one coating that had no significant difference between the number of cells that were retained, with the comparison between titanium nitride and titanium nitride and silver 70 W having $p = 0.33$. There was a significant difference between the LIPSS textured samples and the coated samples, this was found to be a decrease in the number of cells that were retained ($p < 0.05$).

For further analysis, the results gained from both bacterial strains were also statistically analysed for significant differences between the two. This allowed for there to be checks between if there will be a difference between how many bacteria are adhered

to the same surface, gaining insight into what kind of surface the two prefer. There was a significant difference between the number of *S. aureus* and *P. aeruginosa* cells adhered to the surfaces, with $p = < 0.05$, except for the comparison between the D50 texture pattern, $p = 0.37$. As there was a large amount of raw data that was analysed and put into tables, they have been placed into the appendices section of this thesis, the results gathered can be difficult to determine the differences between how many cells had been retained across the surfaces.

For this assay, images were captured that were subsequently analysed to calculate the number of cells retained, and examples of these images can be seen below. There are many more images that were captured and analysed, and due to the large volume of images being effectively a reproduction of the previous image produced they were omitted from this thesis. The design of the D50 texture provided some of the more useful visualisations of how the bacteria was retained across the surface, as can be seen in the below *Figure 41*, the area that was shown to have the greatest affinity to retaining bacteria was in the grooves created.

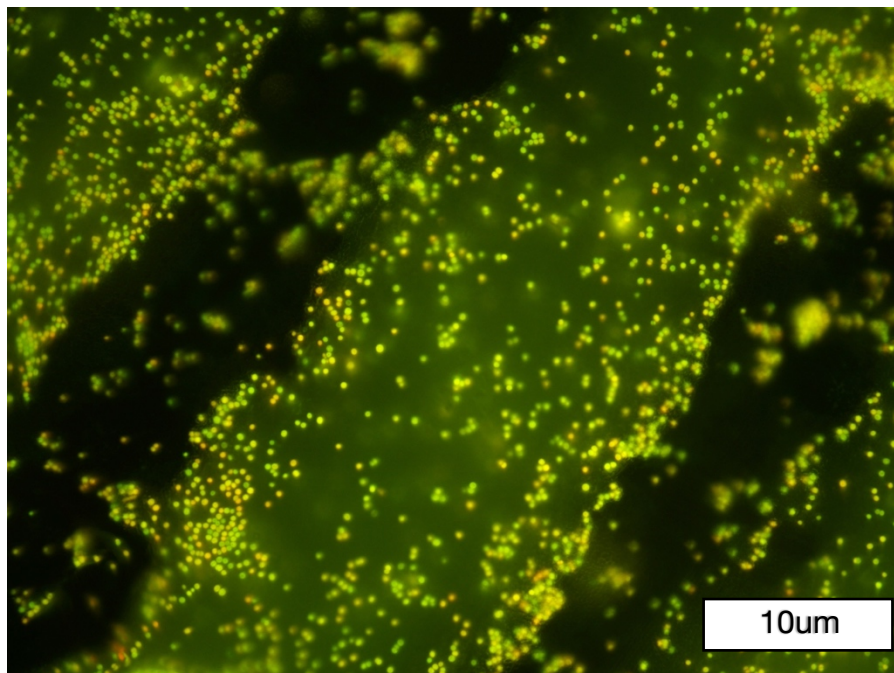


Figure 42: Retention Assay for D50 Texture S. aureus

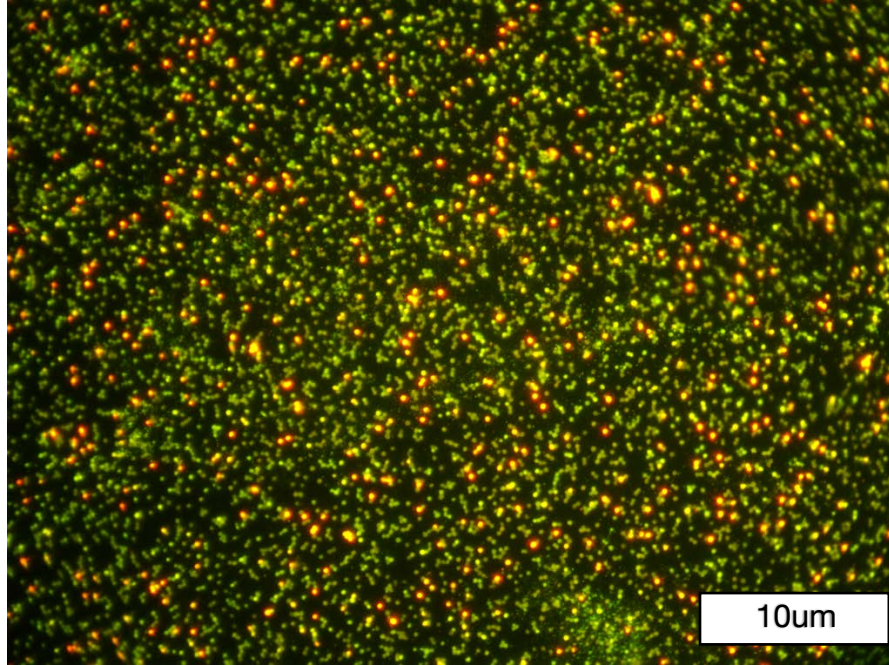


Figure 43: Retention Assay for LIPSS Coated S. aureus

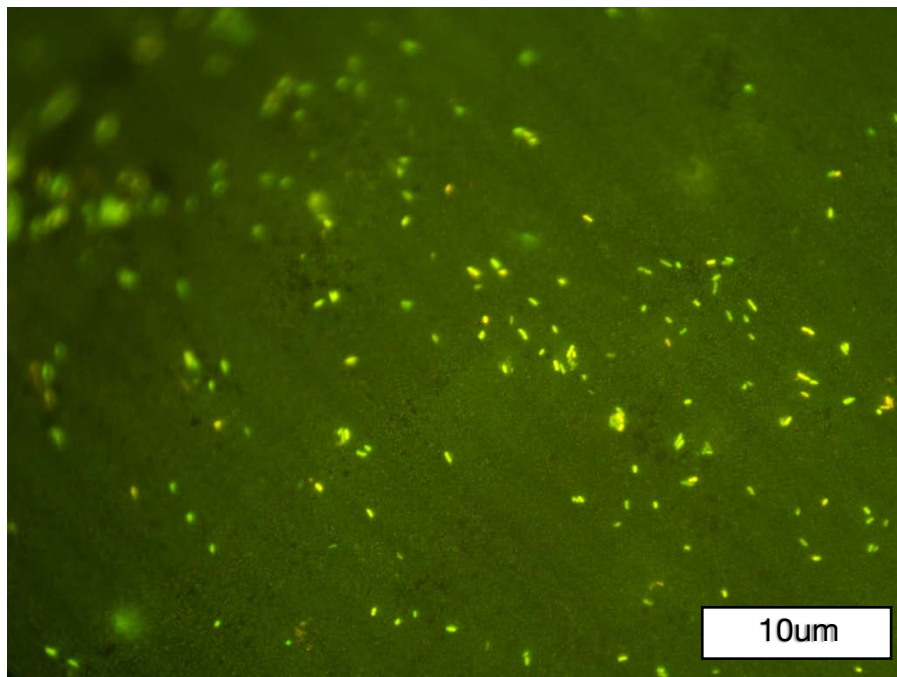


Figure 44: Retention Assay for LIPSS P. aeruginosa

3.8 LIVE/DEAD Assay

The tool for determining antimicrobial efficacy is the LIVE/DEAD staining kit, and this was implemented to understand how each coating variation would interact with the bacteria and to determine the most effective coating. It should be noted that the most effective coating variation was then chosen to be deposited onto the textured patterns, this was to optimise any synergy that could be found between the two techniques. Therefore, we tested all the samples that were made throughout this project with the same procedure as described in previous section, see 2.3.5 LIVE/DEAD Stain.

The results gained from this testing can be visualised in the following figures, they have been calculated in their logarithmic scale, as there is a large volume of cells that have been analysed. From the below *Figure 45* there is a general decrease in the number of cells that can be found alive across the surface of the coated samples, but there was also a decrease in the antimicrobial efficacy of the coating deposited onto the LIPSS textured sample. The LIPSS coated sample is the control stainless-steel substrate after it has been textured and coated with the combination of TiN-Ag 70 W variant.

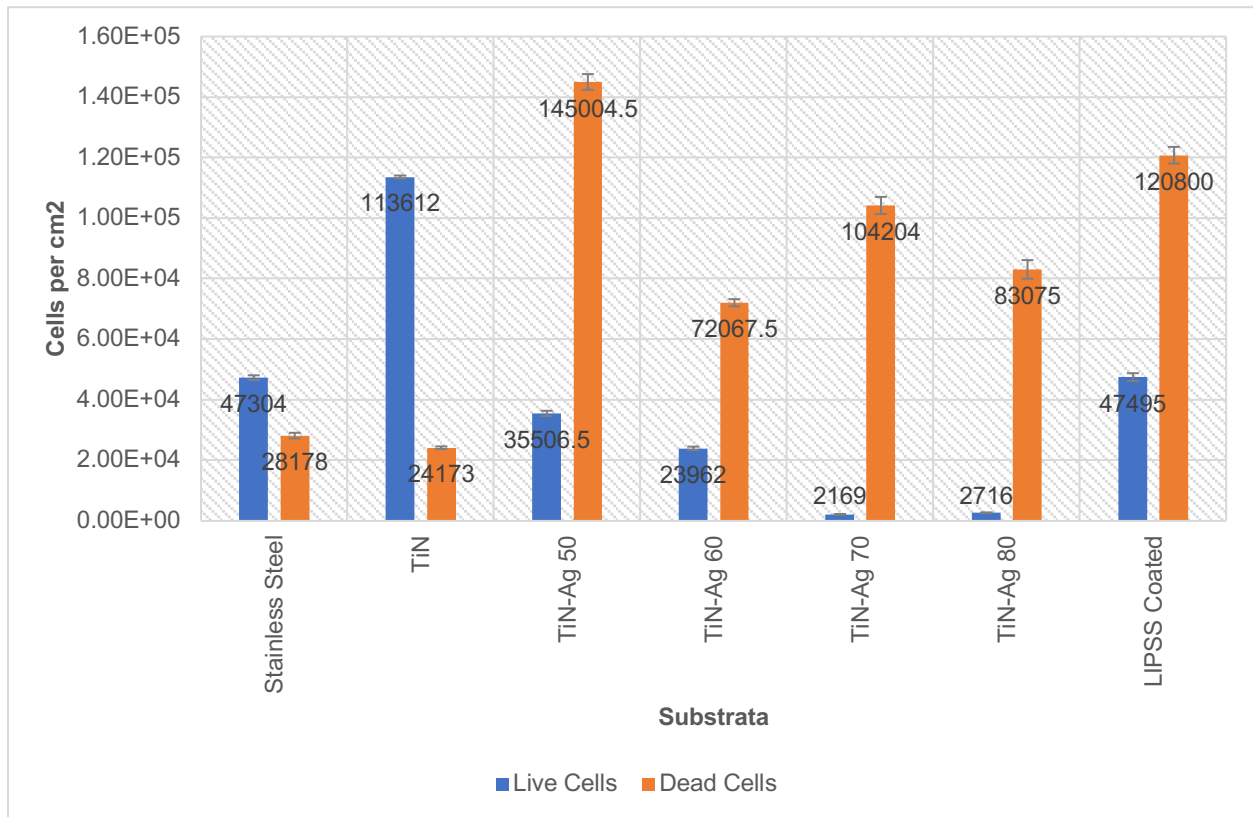


Figure 45: LIVE/DEAD Results for *P. aeruginosa*

Again, from the below *Figure 45* there is a clear trend of relative increases in the number of dead cells found across the sample surface, and this can be concluded to be that there is an increase in antimicrobial efficacy. However, this will be further analysed in the discussion section following, see Chapter 4 – Discussion & Conclusions. All the raw data that was gathered throughout this project, and put into tables, can be found in the appendices, as the raw data can be difficult to understand and see where the difference in number of cells is, see [Appendices](#).

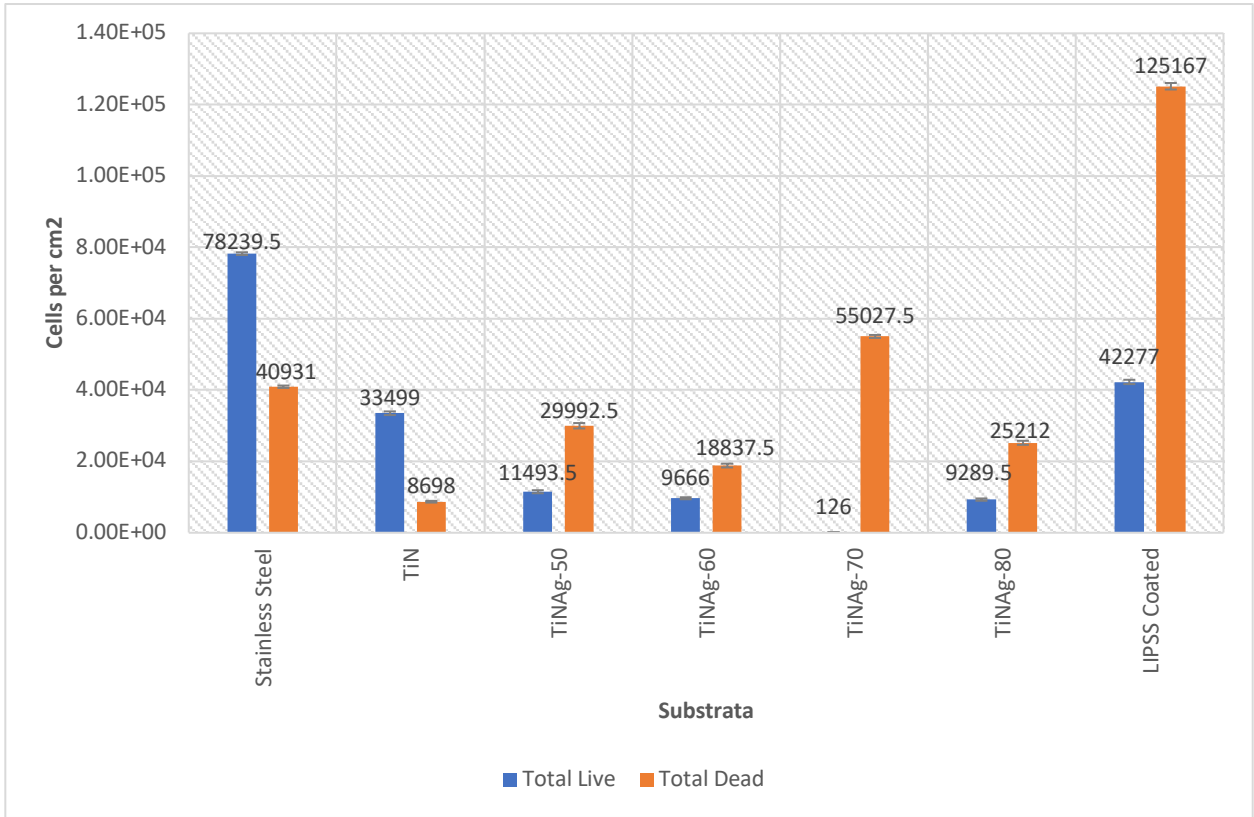


Figure 46: LIVE/DEAD Results for *S. aureus*

Part IV

Discussion & Conclusion

Chapter 4 – Discussion & Conclusions

The following chapter will discuss all the results that have been presented in the previous sections, it will aim to explain what these results can be interpreted as meaning. It will be split up into multiple sub-sections, that will be structure as follows: 4.1 Discussion, 4.1 Perspective, 4.2 Major Findings, 4.3 Conclusions & Future Work

4.1 Perspective

The outcomes of this research project have provided insight into the potential synergy of two engineering processes of Physical Vapour Deposition (PVD) and Laser Texturing (LT) for producing an effective antimicrobial surface with the intention of coating an external fixation device. However, these results should be interpreted with caution, due to the limitations of the study. This following chapter provides reflection on the study and results gained there-in, the limitations and potential consequences of the studies design will be discussed, and the chapter will be rounded out with recommendations for further study.

The importance of designing such a surface can be highlighted in the papers that state the current state of affairs regarding the high volume of infected implants, and the costs that can be attributed to them (Wu *et al.*, 2011, Moseke *et al.*, 2011, Vargas-Reus *et al.*, 2012, Gotman and Gutmanas, 2014, Riool *et al.*, 2014, Sáenz de Viteri *et al.*, 2016, Chan *et al.*, 2017, Chouirfa *et al.*, 2019, Pietrocola *et al.*, 2022). Implants that are at greater risk of infection from bacteria, are external fixation device pins, these medical devices that are designed to aid in the returning of normal function to a broken bone, penetrate the natural skin-air interface and are then connected to an external frame. These open-wound sites pose a risk of tracking infection from any skin-borne bacteria into the limb, and the treatment of these infected implants is proposed to reach over \$1.6 billion per annum in 2020, in the US alone (Haddad *et al.*, 2017). However, the choice of material for replacing the current standard of producing these implants must take into consideration the functionality of these implants and therefore the chosen materials must be carefully selected to uphold these roles. The production of a coating/texturing that can aid in reducing the infection rates of external fixation device implants, could not only improve

public health from reduction of infections, but could also aid in reducing the economic burden of treating infected implants.

Previous studies and assessments have focused on the production of either a coating or texturing that could provide a solution to the problems stated, and have often overlooked the potential for combining the two together and exploiting any potential synergy (Wickens *et al.*, 2012, Goodman *et al.*, 2013, Kazmers *et al.*, 2016, Dong *et al.*, 2017, Slate *et al.*, 2018). The aim of this study was to investigate the potential bridging of the two processes and test them against pathogens of relevance to the infecting of medical implants. This study attempted to present the findings of untextured, but coated materials capabilities, textured and uncoated materials and finally textured and coated materials.

4.2 Major Findings

Through assessment of the surface roughness parameters of the produced coating/texture designs effect on the retention of bacteria, it was found that there was a significant change on the number of retained bacteria dependent on the patterning that was placed onto the substrate. There was a significant decrease in the number of *Pseudomonas aeruginosa* cells on the LIPSS textured sample, and despite this sample having a lower surface roughness value (R_a) than the D20 sample, it proved to have significantly less bacteria retained across its surface. It is hypothesised that whilst the surface roughness parameters can play a crucial role in the retention of bacteria, they are not the sole cause of reduction, or increased retention, there are other parameters that must be considered. However, the retention of *Staphylococcus aureus* cells did appear to increase with the increased surface roughness, although there was also a significant increase in the number of cells retained on the LIPSS coated sample, which exhibited a reduced surface roughness value, again contributing to the hypothesis that surface roughness is not the sole parameter for bacterial retention. This work is comparable to the study conducted by (Whitehead *et al.*, 2015), in which there was a trend of *S. aureus* retention and surface roughness parameters. It also correlates to the results that were gained by (Fadeeva *et al.*, 2011), whom found that there was an increase in the number of *S. aureus* cells retained on laser textured titanium and also a decrease in the number of retained *P. aeruginosa* cells after texturing.

By texturing the substrate, the surface topography was altered, and through the analysis of these surfaces it can be hypothesised that the effect of changing the surface topography can cause changes in the number of retained bacterial cells. This was found to be true when considering the results gained that examined the number of retained cells between the LIPSS textured and un-coated sample and the LIPSS textured & coated samples, there was a significant increase in retention of both *S. aureus* & *P. aeruginosa* cells on the coated LIPSS sample in comparison to the un-coated. However, the effects of changing the surface topography are a highly contentious point within the literature, there are many different conclusions that have been drawn from results and many of them are contradictory to each other. In line with the results gained during this project, there are reports that will agree that the alteration of the surface topography does indeed play a role in the retention of bacteria (Whitehead *et al.*, 2011, Skovager *et al.*, 2013, Huang *et al.*, 2014, Tetlow, 2018). However, due to the limitation of this study not carrying out more specific surface topography analysis there cannot be a concise answer drawn from this and there are also studies that state that there was no effect found when altering the surface topography (Whitehead *et al.*, 2005). There is also the predicament that once you have added a texture to surface, the coating quality will be diminished. Cavities can exist within a material, that cannot normally be accessed without removing some material, for example after exposing the surface to a laser.

Results produced through coating the substrate with the known antimicrobial agent silver was found to influence the number of retained bacterial cells, this is evident from the results that show the significant reduction of *S. aureus* cells and an increase in the number of retained *P. aeruginosa* cells. These results are consistent with studies that were found within the literature, with the studies carried out by (Kelly *et al.*, 2011, Whitehead *et al.*, 2011, Akhidime *et al.*, 2019, Saubade *et al.*, 2019, Slate *et al.*, 2019). The effect of crystallinity was assessed also, however the results that were gained from this research project proved to be inconclusive of any theory, there were issues regarding the detection of silver through the XRD analysis. The results that were gained were not what would have been expected from studying the literature, the peaks that would normally correlate to the characteristic peaks for the elements were in different locations,

and although this can be common with coated samples, it did result in the reliability of the results to be questioned.

It should be noted that the studies provided are not testing the same materials, using the same processes and therefore there could be different variables that lead to the preferential retention of bacteria. Therefore, the lack of consensus within this study to the effect of surface roughness and topography on the retention of bacteria could be due to the lack of standardisation between the studies, as each study has its own procedures for analysis bacterial retention and the use of different deposition/texturing techniques can further lead to there being less correlation between all studies. There is also the limitation that this study did not carry out any surface chemistry analysis, and thus this is another variable that could be affecting the retention across the different studies. A further limitation of this study, or any study that involves biochemistry, or biomolecules, such as cells, is that it takes thousands of repeat procedures to produce any form of statistically sound result.

Assessment of the manufactured samples potential antimicrobial efficacy revealed that only the samples with silver in their composition produced any antimicrobial activity. Comparatively the most effective coating, which was demonstrated through the LIVE/DEAD staining, that was produced through this research project was the coating of TiN-Ag 70 W coating, which averaged 21.26 at% of silver in its composition. Assessment of the antimicrobial action was demonstrated against both bacterial strains, with all silver containing samples exhibiting antimicrobial properties when in contact with the bacteria. However, assessments of the potential leaching capability of the coatings produced were found to not exhibit leaching into the surroundings. This was analysed through the zones of inhibition testing, within which there were no zones created around the samples after testing, leading to the hypothesis that there is limited leaching from the samples. As the silver must leach from the surface to produce any antimicrobial action, this hypothesis does hold, as there were positive results gained from the later tests carried out. Thus, it is suggested from these results that the TiN matrix, in-which the silver is encapsulated, was altering the activity of the antimicrobial ions. However, due to the limitation of the microbiological testing and no tribological testing being conducted through this study, it was not possible to determine if this hypothesis would be proven.

These results were concurrent with the results gained in other studies, with the limited leaching capability of silver when deposited being exhibited (Kelly *et al.*, 2010, Kelly *et al.*, 2011, Wickens *et al.*, 2012, Tetlow *et al.*, 2017). Whilst there were no zones of inhibition displayed during this research project, there were results gained from the other microbiological tests that presented results that suggested the silver containing samples exhibited antimicrobial action. This was found through the NBT and LIVE/DEAD assays, during which there was significant increases in antimicrobial action as the content of silver was increased within the samples. The antimicrobial action was demonstrated against both strains of bacteria that were tested against, which was found to be in-line with the literature, which also reported that as the silver content is increased, the antimicrobial efficacy is also increased (Ewald *et al.*, 2006, Kelly *et al.*, 2009, Rai *et al.*, 2009, Kelly *et al.*, 2010, Whitehead *et al.*, 2010, Kelly *et al.*, 2011, Whitehead *et al.*, 2011, Wickens *et al.*, 2012, Vargas-Reus *et al.*, 2012, Sáenz de Viteri *et al.*, 2016, Slate *et al.*, 2018, Saubade *et al.*, 2019, Mohamed *et al.*, 2020, Braceras *et al.*, 2021, Raj *et al.*, 2022). However, due to the limitation of this research project not investigating the longevity of the antimicrobial activity of silver when co-deposited with titanium nitride, it cannot be said that this coating will provide the required antimicrobial activity for the period that an external fixation device would be placed. There is also the limitation that these samples were not tribologically tested, and therefore the risk of delamination and wear could prove to reduce the efficacy of the coatings and whether they would be fit for purpose in a high-wear application.

Following from these results, which were initially carried out on un-textured samples, the TiN/Ag-21.26 at% was chosen to be deposited onto the texturing patterns that were produced via the laser texturing. This proved to reduce the antimicrobial action of the coating, and this was determined through the LIVE/DEAD staining test, which produced results in which there were more live/respiring bacteria found on the textured & coated substrate surface than were found on the non-textured sample. Through assessment of retention of bacterial cells to the LIPSS coated samples, it was found that for both bacterial strains, there was a significant increase in the number of cells that were retained on the surface. Which suggests that for *P. aeruginosa*, the surface topography/features that initially reduced the number of retained cells, were diminished in its ability to prevent

cells from being retained. This could be related to the overall decrease in the surface roughness values, which could be a result of the deposition process coating the sample in a layer of material that filled the features of the texture, thus smoothing out and removing the texture.

The most significant result that was gained from this research project was the results that suggested that the combination of these two processes diminished the individual benefits gained from the processes, and this is displayed in the reduction of the antimicrobial activity and the increase in the number of cells that were retained on the surface.

As this research project and thesis, at the time of writing and to the authors knowledge, is unique in its combination of LIPSS and PVD coating, there were no studies that directly related to the results gained here-in. However, there is the hypothesis that after coating the textured samples, there was not complete coverage of the surface from the deposition process, and therefore the reduction in antimicrobial activity can be traced to this reduction in the coverage producing a less effective antimicrobial surface.

4.3 Conclusions & Future Work

4.3.1 Conclusions Drawn

In conclusion, whilst the two engineering processes can produce effective methods of producing antimicrobial surfaces, the combination of the two diminished the beneficial properties of each individual process. The results produced during these works highlights the limited synergy between physical vapour deposition and laser texturing, the antagonistic behaviour of reduced antimicrobial activity and increased bacterial cell retention across the samples surface leads to the conclusion that the combining of the two processes would be detrimental in application.

Assessment of the laser texturing phenomenon of producing laser induced periodic surface structures is important, as the significant reduction of bacterial cell retention could provide the required surface patterning for the temporary external fixation devices. Through all the assessments carried out during, the most important coating parameters produced, and thus the one of greatest interest to produce a surface for use in an external fixation device, was the TiN/Ag-21.26 at% coating. This is due to its nearly complete eradication of any bacterial cells after exposure, and thus it could provide the solution to

the increasing infection rates. As an external fixation device is a temporary fixture, the unknown longevity of the coating's efficacy could be negated by its reduced period of usage.

However, as stated the combination of the two engineering processes did not result in an optimised surface being produced, the two processes were antagonistic to each other, and it is because of this that the recommendation from this study is that their combination be limited for the application stated.

4.3.2 Future Work

Future work surrounding this topic should be carried out to investigate whether different texture patterns could provide the solution to the antagonistic nature of the LIPSS pattern and PVD process. Analysis should be conducted further on the longevity of the produced antimicrobial agents, this could be done by measuring their efficacy at extended time periods, and not just for one assay. As there were only two bacterial strains tested against, further work could be conducted to investigate the effectiveness against an extended range of bacterial strains, as the number of strains responsible for infections on implants is broad and diverse. Tribological studies would also be benefitted from for the development of an effective surface, as this study did not research the corrosion and wear capabilities of the samples. Therefore, the risk of delamination of the coating was not investigated, nor was the fragmentation of the texture investigated. Analysis of how the produced surfaces would react during cleaning protocols could also be studied, as the implants would undergo some cleaning procedure, and there could be problems arising from this.

Given the opportunity to carry out the research project again, the main research goals would be modified to further analyse the antimicrobial efficacy under more environmental conditions. There would also be a greater focus upon the microbiological testing being carried out over an extended period. Rather than being carried out over a 24-hour period, the samples would be exposed continuously to the bacteria, to model how they would react in a simulated scenario.

Bibliography

- AHMMED, K., GRAMBOW, C. & KIETZIG, A.-M. 2014. Fabrication of Micro/Nano Structures on Metals by Femtosecond Laser Micromachining. *Micromachines*, 5, 1219-1253.
- AKHIDIME, I. D., SAUBADE, F., BENSON, P. S., BUTLER, J. A., OLIVIER, S., KELLY, P., VERRAN, J. & WHITEHEAD, K. A. 2019. The antimicrobial effect of metal substrates on food pathogens. *Food and Bioproducts Processing*, 113, 68-76.
- ALEXANDER, J., DONG, H., BOSE, D., HASSAN, A. A., SOO, S. L., ZHANG, Z., TAO, X., KUEHNE, S., LI, X. & DONG, H. 2021. Novel Catalytic Ceramic Conversion Treatment of Ti6Al4V for Improved Tribological and Antibacterial Properties for Biomedical Applications. *Materials (Basel)*, 14.
- ARNELL, R. D., KELLY, P. J. & BRADLEY, J. W. 2004. Recent developments in pulsed magnetron sputtering. *Surface and Coatings Technology*, 188-189, 158-163.
- BAPTISTA, A., SILVA, F., PORTEIRO, J., MÍGUEZ, J. & PINTO, G. 2018. Sputtering Physical Vapour Deposition (PVD) Coatings: A Critical Review on Process Improvement and Market Trend Demands. *Coatings*, 8.
- BCLUE 2021. Magnetron Sputtering. <https://www.bcluae.com/upload/product/magnetron-sputtering1.png>.
- BERG, S. & NYBERG, T. 2005. Fundamental understanding and modeling of reactive sputtering processes. *Thin Solid Films*, 476, 215-230.
- BONSE, J. 2020. Quo Vadis LIPSS?-Recent and Future Trends on Laser-Induced Periodic Surface Structures. *Nanomaterials (Basel)*, 10.
- BRACERAS, I., BRIZUELA, M., ÁLVAREZ, N., MARTÍNEZ VAN GEETERUYEN, M. & AZKONA, I. 2021. TiN-Ag as an antimicrobial and wear resistant coating. *Biotribology*, 28, 2-9.
- CAMPOCCIA, D., MONTANARO, L. & ARCIOLA, C. R. 2006. The significance of infection related to orthopedic devices and issues of antibiotic resistance. *Biomaterials*, 27, 2331-2339.
- CENTRE FOR DISEASE CONTROL & PREVENTION, C. 2018. Staphylococcus aureus. Online.
- CHAN, C. W., CARSON, L., SMITH, G. C., MORELLI, A. & LEE, S. 2017. Enhancing the antibacterial performance of orthopaedic implant materials by fibre laser surface engineering. *Applied Surface Science*, 404, 67-81.
- CHEN, C., ENRICO, A., PETTERSSON, T., EK, M., HERLAND, A., NIKLAUS, F., STEMME, G. & WÄGGER, L. 2020. Bactericidal surfaces prepared by femtosecond laser patterning and layer-by-layer polyelectrolyte coating. *Journal of Colloid and Interface Science*, 575, 286-297.
- CHOUIRFA, H., BOULOUSA, H., MIGONNEY, V. & FALENTIN-DAUDRÉ, C. 2019. Review of titanium surface modification techniques and coatings for antibacterial applications. *Acta Biomaterialia*, 83, 37-54.
- DEARNLEY, P. A. & DEARNLEY, P. A. 2017. *Surface Engineering with Deposition Technologies*.
- DEKOVEN, B. M., P.R. WARD, R.E. WEISS, D.J. CHRISTIE, R.A. SCHOLL, W.D. SPROUL, F. TOMASEL & ANDERS, A. 46th Annual Technical Conference Proceedings of the Society of Vacuum Coaters. 46th Annual Technical Conference Proceedings of the Society of Vacuum Coaters, 2003 San Francisco, CA, USA. 158.
- DONG, H., MUKINAY, T., LI, M., HOOD, R., SOO, S. L., COCKSHOTT, S., SAMMONS, R. & LI, X. 2017. Improving tribological and anti-bacterial properties of titanium external fixation pins through surface ceramic conversion. *Journal of Materials Science: Materials in Medicine*, 28.
- EPPERLEIN, N., MENZEL, F., SCHWIBBERT, K., KOTER, R., BONSE, J., SAMEITH, J., KRÜGER, J. & TOEPEL, J. 2017. Influence of femtosecond laser produced nanostructures on biofilm growth on steel. *Applied Surface Science*, 418, 420-424.
- EWALD, A., GLÜCKERMANN, S. K., THULL, R. & GBURECK, U. 2006. Antimicrobial titanium/silver PVD coatings on titanium. *BioMedical Engineering Online*, 5, 1-10.
- FADEEVA, E., TRUONG, V. K., STIESCH, M., CHICHKOV, B. N., CRAWFORD, R. J., WANG, J. & IVANOVA, E. P. 2011. Bacterial retention on superhydrophobic titanium surfaces fabricated by femtosecond laser ablation. *Langmuir*, 27, 3012-3019.
- FARKAS, A., SONG, S., DEGIULI, N., MARTIĆ, I. & DEMIREL, Y. K. 2020. Impact of biofilm on the ship propulsion characteristics and the speed reduction. *Ocean Engineering*, 199.

- FASASI, A. Y., MWENIFUMBO, S., RAHBAR, N., CHEN, J., LI, M., BEYE, A. C., ARNOLD, C. B. & SOBOYEJO, W. O. 2009. Nano-second UV laser processed micro-grooves on Ti6Al4V for biomedical applications. *Materials Science and Engineering C*.
- FLORES, C. Y., DIAZ, C., RUBERT, A., BENITEZ, G. A., MORENO, M. S., FERNANDEZ LORENZO DE MELE, M. A., SALVAREZZA, R. C., SCHILARDI, P. L. & VERICAT, C. 2010. Spontaneous adsorption of silver nanoparticles on Ti/TiO₂ surfaces. Antibacterial effect on *Pseudomonas aeruginosa*. *J Colloid Interface Sci*, 350, 402-8.
- GOMES, L. C., SAUBADE, F., M. AMIN, J. SPALL, C.M. LIAUW, J. MERGULHÃO & WHITEHEAD, K. A. 2022. BIOMIMETIC REPLICATION OF BRASSICA LEAVES AND THEIR EFFICACY TO PREVENT BIOFOULING OF *Escherichia coli* AND *Listeria monocytogenes*.
- GONZALEZ, A. S., RIEGO, A., VEGA, V., GARCIA, J., GALIE, S., GUTIERREZ DEL RIO, I., MARTINEZ DE YUSO, M. D. V., VILLAR, C. J., LOMBO, F. & DE LA PRIDA, V. M. 2021. Functional Antimicrobial Surface Coatings Deposited onto Nanostructured 316L Food-Grade Stainless Steel. *Nanomaterials (Basel)*, 11.
- GOODMAN, S. B., YAO, Z., KEENEY, M. & YANG, F. 2013. The future of biologic coatings for orthopaedic implants. *Biomaterials*.
- GOTMAN, I. & GUTMANAS, E. Y. 2014. Titanium nitride-based coatings on implantable medical devices. *Advanced Biomaterials and Devices in Medicine*, 1, 53-73.
- GOTMAN, I., GUTMANAS, E. Y. & HUNTER, G. 2011. Wear-Resistant Ceramic Films and Coatings. *Comprehensive Biomaterials*.
- HADDAD, F. S., NGU, A. & NEGUS, J. J. 2017. Prosthetic Joint Infections and Cost Analysis? In: DRAGO, L. (ed.) *A Modern Approach to Biofilm-Related Orthopaedic Implant Infections: Advances in Microbiology, Infectious Diseases and Public Health Volume 5*. Cham: Springer International Publishing.
- HUANG, Y., ZHA, G., LUO, Q., ZHANG, J., ZHANG, F., LI, X., ZHAO, S., ZHU, W. & LI, X. 2014. The construction of hierarchical structure on Ti substrate with superior osteogenic activity and intrinsic antibacterial capability. *Scientific Reports*, 4, 1-10.
- J. MUSIL, S. KADLEC, V. VALVODA, R. KUŽEL & ČERNÝ, R. 1990. Ion-assisted sputtering of TiN films. *Surface and Coatings Technology*, Volumes 43-44, 259-269.
- JÄGER, M., JENNISSEN, H. P., DITTRICH, F., FISCHER, A. & KÖHLING, H. L. 2017. Antimicrobial and osseointegration properties of nanostructured titanium orthopaedic implants. *Materials*, 10, 1-28.
- JAGGESSAR, A., SHAHALI, H., MATHEW, A. & YARLAGADDA, P. K. D. V. 2017. Bio-mimicking nano and micro-structured surface fabrication for antibacterial properties in medical implants. *Journal of Nanobiotechnology*, 15, 1-20.
- JEONG, Y. H., CHOE, H. C. & BRANTLEY, W. A. 2011. Nanostructured thin film formation on femtosecond laser-textured Ti-35Nb-xZr alloy for biomedical applications. *Thin Solid Films*, 519, 4668-4675.
- KAO, W. K., GAGNON, P. M., VOGEL, J. P. & CHOLE, R. A. 2017. Surface charge modification decreases *Pseudomonas aeruginosa* adherence in vitro and bacterial persistence in an in vivo implant model. *Laryngoscope*, 127, 1655-1661.
- KAZMERS, N. H., FRAGOMEN, A. T. & ROZBRUCH, S. R. 2016. Prevention of pin site infection in external fixation: a review of the literature. *Strategies in Trauma and Limb Reconstruction*, 11, 75-85.
- KELLY, P. & ARNELL, R. D. 2000. Magnetron sputtering: a review of recent developments and applications. *Vacuum*, 56, 159-172.
- KELLY, P. J., LI, H., BENSON, P. S., WHITEHEAD, K. A., VERRAN, J., ARNELL, R. D. & IORDANOVA, I. 2010. Comparison of the tribological and antimicrobial properties of CrN/Ag, ZrN/Ag, TiN/Ag, and TiN/Cu nanocomposite coatings. *Surface and Coatings Technology*, 205, 1606-1610.
- KELLY, P. J., LI, H., WHITEHEAD, K. A., VERRAN, J., ARNELL, R. D. & IORDANOVA, I. 2009. A study of the antimicrobial and tribological properties of TiN/Ag nanocomposite coatings. *Surface and Coatings Technology*, 204, 1137-1140.
- KELLY, P. J., WEST, G. T., RATOVA, M., FISHER, L., OSTOVARPOUR, S. & VERRAN, J. 2014. Structural formation and photocatalytic activity of magnetron sputtered titania and doped-titania coatings. *Molecules*, 19, 16327-16348.

- KELLY, P. J., WHITEHEAD, K. A., LI, H., VERRAN, J. & ARNELL, R. D. 2011. The influence of silver content on the tribological and antimicrobial properties of ZrN/Ag nanocomposite coatings. *J Nanosci Nanotechnol*, 11, 5383-7.
- KENAR, H., AKMAN, E., KACAR, E., DEMIR, A., PARK, H., ABDUL-KHALIQ, H., AKTAS, C. & KARAOZ, E. 2013. Femtosecond laser treatment of 316L improves its surface nanoroughness and carbon content and promotes osseointegration: An in vitro evaluation. *Colloids and Surfaces B: Biointerfaces*, 108, 305-312.
- KOBAYASHI, S. D., MALACHOWA, N. & DELEO, F. R. 2015. Pathogenesis of Staphylococcus aureus abscesses. *Am J Pathol*, 185, 1518-27.
- KONSTANTINIDIS, S., HEMBERG, A., DAUCHOT, J. P. & HECQ, M. 2007. Deposition of zinc oxide layers by high-power impulse magnetron sputtering. *Journal of Vacuum Science & Technology B: Microelectronics and Nanometer Structures*, 25.
- KOUZNETSOV, V. 2001. *METHOD AND APPARATUS FOR MAGNETICALLY ENHANCED SPUTTERING*.
- KOUZNETSOV, V., KAROL MACA'K, JOCHEN M. SCHNEIDER, ULF HELMERSSON & PETROV, I. 1999. A novel pulsed magnetron sputter technique utilizing very high target power densities. *Surface and Coatings Technology*, 122, 290-293.
- KUCZYŃSKA, D., KWAŚNIAK, P., MARCZAK, J., BONARSKI, J., SMOLIK, J. & GARBACZ, H. 2016. Laser surface treatment and the resultant hierarchical topography of Ti grade 2 for biomedical application. *Applied Surface Science*.
- LÉVY, F. 2016. Film Growth and Epitaxy: Methods. *Reference Module in Materials Science and Materials Engineering*.
- LI, B. J., LI, H., HUANG, L. J., REN, N. F. & KONG, X. 2016. Femtosecond pulsed laser textured titanium surfaces with stable superhydrophilicity and superhydrophobicity. *Applied Surface Science*, 389, 585-593.
- LIU, Y. H., YE, S. C. & CHENG, C. W. 2020. Two-Dimensional Periodic Nanostructure Fabricated on Titanium by Femtosecond Green Laser. *Nanomaterials (Basel)*, 10.
- LUNDIN, D. & SARAĶINOS, K. 2012. An introduction to thin film processing using high-power impulse magnetron sputtering. *Journal of Materials Research*, 27, 780-792.
- LUTEY, A. H. A., GEMINI, L., ROMOLI, L., LAZZINI, G., FUSO, F., FAUCON, M. & KLING, R. 2018. Towards laser-textured antibacterial surfaces. *Scientific Reports*, 8, 1-10.
- MOHAMED, D. S., EL-BAKY, R. M. A., SANDLE, T., MANDOOR, S. A. & AHMED, E. F. 2020. Antimicrobial activity of silver-treated bacteria against other multi-drug resistant pathogens in their environment. *Antibiotics*, 9.
- MOHD MAHAYUDDIN, N. A. H., WAHAB, J. A., MOHD SALLEH, M. A. A., RODUAN, S. F. & CHEN, H. K. 2020. Surface texturing method and roughness effect on the substrate performance: A short review. *Jurnal Tribologi*, 27.
- MOHLER, J. S., SIM, W., BLASKOVICH, M. A. T., COOPER, M. A. & ZIORA, Z. M. 2018. Silver bullets: A new lustre on an old antimicrobial agent. *Biotechnol Adv*, 36, 1391-1411.
- MOSEKE, C., GBURECK, U., ELTER, P., DRECHSLER, P., ZOLL, A., THULL, R. & EWALD, A. 2011. Hard implant coatings with antimicrobial properties. *J Mater Sci Mater Med*, 22, 2711-20.
- MÜLLER, F. A., KUNZ, C. & GRÄF, S. 2016. Bio-inspired functional surfaces based on laser-induced periodic surface structures. *Materials*, 9.
- MUSIL, J., LEŠTINA, J., VLČEK, J. & TÖLG, T. 2001. Pulsed dc magnetron discharge for high-rate sputtering of thin films. *Journal of Vacuum Science & Technology A: Vacuum, Surfaces, and Films*, 19, 420-424.
- NEPHEW, S. 2012. Ankle Spanning, Knee Spanning, Long Bone and Pelvic. In: INC., S. N. (ed.).
- OLIVEIRA, V., AUSSET, S. & VILAR, R. 2009. Surface micro/nanostructuring of titanium under stationary and non-stationary femtosecond laser irradiation. *Applied Surface Science*, 255, 7556-7560.
- PIETROCOLA, G., CAMPOCCIA, D., MOTTA, C., MONTANARO, L., ARCIOLA, C. R. & SPEZIALE, P. 2022. Colonization and Infection of Indwelling Medical Devices by Staphylococcus aureus with an Emphasis on Orthopedic Implants. *Int J Mol Sci*, 23.
- PU, X., LI, G. & HUANG, H. 2016. Preparation, anti-biofouling and drag-reduction properties of a biomimetic shark skin surface. *Biology open*, 5.

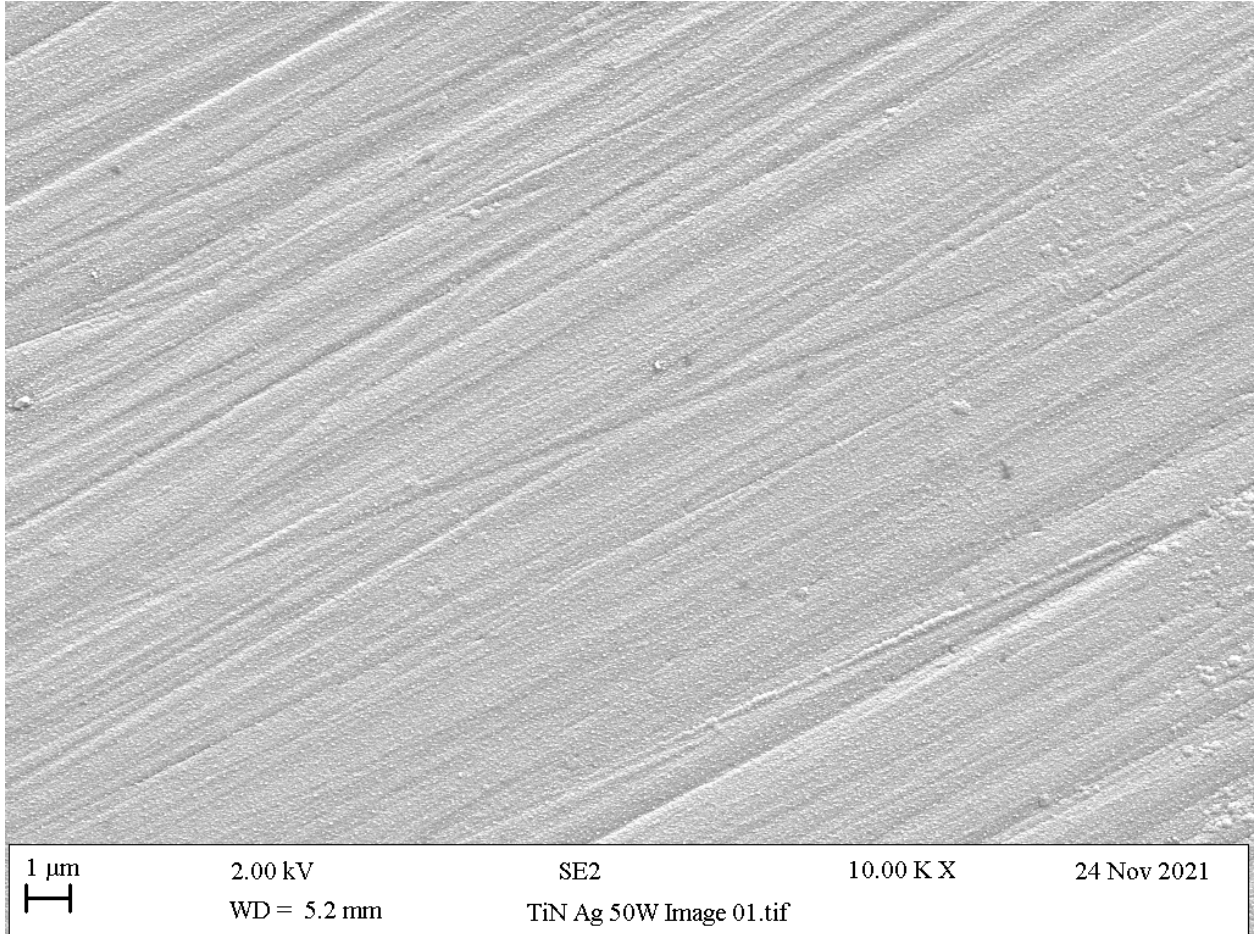
- RAI, M., YADAV, A. & GADE, A. 2009. Silver nanoparticles as a new generation of antimicrobials. *Biotechnol Adv*, 27, 76-83.
- RAJ, A., C P, P., K K, R. & U, S. 2022. Characterization of Ti biomedical implant surfaces modified by physical vapour deposition coating. *SSRN Electronic Journal*.
- RIDZWAN, M. I. Z., SHUIB, S., HASSAN, A. Y., SHOKRI, A. A. & MOHAMAD IB, M. N. 2007. Problem of Stress Shielding and Improvement to the Hip Implant Designs: A Review. *Journal of Medical Sciences*, 7, 460-467.
- RIOOL, M., DE BOER, L., JASPERS, V., VAN DER LOOS, C. M., VAN WAMEL, W. J. B., WU, G., KWAKMAN, P. H. S. & ZAAT, S. A. J. 2014. Staphylococcus epidermidis originating from titanium implants infects surrounding tissue and immune cells. *Acta Biomaterialia*, 10, 5202-5212.
- ROSENKRANZ, A., HANS, M., GACHOT, C., THOME, A., BONK, S. & MÜCKLICH, F. 2016. Direct laser interference patterning: Tailoring of contact area for frictional and antibacterial properties. *Lubricants*, 4.
- SÁENZ DE VITERI, V., BARANDIKA, G., BAYÓN, R., FERNÁNDEZ, X., CIARSOLO, I., IGARTUA, A., PÉREZ TANOIRA, R., MORENO, J. E. & PEREMARCH, C. P. J. 2016. Development of Ti-C-N coatings with improved tribological behavior and antibacterial properties. *Journal of the Mechanical Behavior of Biomedical Materials*, 55, 75-86.
- SAMUELSSON, M., LUNDIN, D., JENSEN, J., RAADU, M. A., GUDMUNDSSON, J. T. & HELMERSSON, U. 2010. On the film density using high power impulse magnetron sputtering. *Surface and Coatings Technology*, 205, 591-596.
- SAUBADE, F., PILKINGTON, L. I., LIAUW, C. M., GOMES, L. C., MCCLEMENTS, J., PEETERS, M., EL MOHTADI, M., MERGULHAO, F. J. & WHITEHEAD, K. A. 2021. Principal Component Analysis to Determine the Surface Properties That Influence the Self-Cleaning Action of Hydrophobic Plant Leaves. *Langmuir*, 37, 8177-8189.
- SAUBADE, F. J., HUGHES, S., WICKENS, D. J., WILSON-NIEUWENHUIS, J., DEMPSEY-HIBBERT, N., CROWTHER, G. S., WEST, G., KELLY, P., BANKS, C. E. & WHITEHEAD, K. A. 2019. Effectiveness of titanium nitride silver coatings against Staphylococcus spp. in the presence of BSA and whole blood conditioning agents. *International Biodeterioration and Biodegradation*, 141, 44-51.
- SCHLIE, S., FADEEVA, E., KOROLEVA, A., OVSIANIKOV, A., KOCH, J., NGEZAHAYO, A. & CHICHKOV, B. N. Laser-based nanoengineering of surface topographies for biomedical applications. *Photonics and Nanostructures - Fundamentals and Applications*, 2011.
- SELVAMANI, V., ZAREEI, A., ELKASHIF, A., MARUTHAMUTHU, M. K., CHITTIBOYINA, S., DELISI, D., LI, Z., CAI, L., POL, V. G., SELEEM, M. N. & RAHIMI, R. 2020. Hierarchical Micro/Mesoporous Copper Structure with Enhanced Antimicrobial Property via Laser Surface Texturing. *Advanced Materials Interfaces*, 7, 1-11.
- SHAH, F. A., ALI, M. A., KUMAR, V., ALAM, W. & HASAN, O. 2019. Does pin tract infection after external fixator limits its advantage as a cost-effective solution for open fractures in low-middle income countries, a prospective cohort study. *JPMA. The Journal of the Pakistan Medical Association*, 69 1), S41-S45.
- SHAIKH, S., KEDIA, S., SINGH, D., SUBRAMANIAN, M. & SINHA, S. 2019. Surface texturing of Ti6Al4V alloy using femtosecond laser for superior antibacterial performance. *Journal of Laser Applications*, 31, 022011-022011.
- SKOVAGER, A., WHITEHEAD, K., WICKENS, D., VERRAN, J., INGMER, H. & ARNEBORG, N. 2013. A comparative study of fine polished stainless steel, TiN and TiN/Ag surfaces: Adhesion and attachment strength of Listeria monocytogenes as well as anti-listerial effect. *Colloids and Surfaces B: Biointerfaces*, 109, 190-196.
- SLATE, A. J., WICKENS, D., WILSON-NIEUWENHUIS, J., DEMPSEY-HIBBERT, N., WEST, G., KELLY, P., VERRAN, J., BANKS, C. E. & WHITEHEAD, K. A. 2019. The effects of blood conditioning films on the antimicrobial and retention properties of zirconium-nitride silver surfaces. *Colloids and Surfaces B: Biointerfaces*, 173, 303-311.
- SLATE, A. J., WICKENS, D. J., EL MOHTADI, M., DEMPSEY-HIBBERT, N., BANKS, C. E. & WHITEHEAD, K. A. 2018. Antimicrobial activity of Ti-ZrN/Ag coatings for use in biomaterial applications. *Scientific Reports*, 8, 1-13.

- SPRINGER 2008. *Reactive Sputter Deposition*, Springer Berlin, Heidelberg.
- SPRINGER 2018. *Self-Assembled Molecules – New Kind of Protein Ligands*.
- TAHERI, S., CAVALLARO, A., CHRISTO, S. N., SMITH, L. E., MAJEWSKI, P., BARTON, M., HAYBALL, J. D. & VASILEV, K. 2014. Substrate independent silver nanoparticle based antibacterial coatings. *Biomaterials*, 35, 4601-4609.
- TETLOW, L. 2018. *The effect of conditioning films on the hygienic status of titanium based and antimicrobial surfaces*. PhD Doctoral, Manchester Metropolitan University.
- TETLOW, L. A., LYNCH, S. & WHITEHEAD, K. A. 2017. The effect of surface properties on bacterial retention: A study utilising stainless steel and TiN/25.65at.%Ag substrata. *Food and Bioproducts Processing*, 102, 332-339.
- THAMYONGKIT, S., BACHABI, M., THOMPSON, J. M., SHAFIQ, B. & HASENBOEHLER, E. A. 2018. Use of reprocessed external fixators in orthopaedic surgery: A survey of 243 orthopaedic trauma surgeons. *Patient Safety in Surgery*, 12, 1-7.
- TSUKAMOTO, M., ASUKA, K., NAKANO, H., HASHIDA, M., KATTO, M., ABE, N. & FUJITA, M. 2006. Periodic microstructures produced by femtosecond laser irradiation on titanium plate. *Vacuum*, 80, 1346-1350.
- VARGAS-REUS, M. A., MEMARZADEH, K., HUANG, J., REN, G. G. & ALLAKER, R. P. 2012. Antimicrobial activity of nanoparticulate metal oxides against peri-implantitis pathogens. *International Journal of Antimicrobial Agents*, 40, 135-139.
- VOROBYEV, A. Y. & GUO, C. 2013. Direct femtosecond laser surface nano/microstructuring and its applications. *Laser and Photonics Reviews*, 7, 385-407.
- WAITE, M. M., S. ISMAT SHAH & DAVID A. GLOCKER 2007. *50 Years of Vacuum Coating Technology and the growth of the Society of Vacuum Coaters*, Society of Vacuum Coaters.
- WEST, G., KELLY, P., BARKER, P., MISHRA, A. & BRADLEY, J. 2009. Measurements of deposition rate and substrate heating in a HiPIMS discharge. *Plasma Processes and Polymers*, 6, 543-547.
- WHITEHEAD, K., KELLY, P., LI, H. & VERRAN, J. 2010. Surface topography and physicochemistry of silver containing titanium nitride nanocomposite coatings. *Journal of Vacuum Science and Technology B: Microelectronics and Nanometer Structures*, 28, 180-187.
- WHITEHEAD, K. A., COLLIGON, J. & VERRAN, J. 2005. Retention of microbial cells in substratum surface features of micrometer and sub-micrometer dimensions. *Colloids and Surfaces B: Biointerfaces*, 41, 129-138.
- WHITEHEAD, K. A., LI, H., KELLY, P. J. & VERRAN, J. 2011. The antimicrobial properties of titanium nitride/silver nanocomposite coatings. *Journal of Adhesion Science and Technology*, 25, 2299-2315.
- WHITEHEAD, K. A., OLIVIER, S., BENSON, P. S., ARNEBORG, N., VERRAN, J. & KELLY, P. 2015. The effect of surface properties of polycrystalline, single phase metal coatings on bacterial retention. *Int J Food Microbiol*, 197, 92-7.
- WHITEHEAD, K. A., PILKINGTON, L. I., A.J., S., SAUBADE., F., AMIN, M., LUTEY, A., GEMINI, L., KLING, R. & ROMOLI, L. 2022. CLEANABILITY OF LASER ETCHED BIOMIMETIC SURFACES WITH REPEATED STAPHYLOCOCCUS AUREUS AND MILK FOULING.
- WHITEHEAD, K. A. & VERRAN, J. 2007. The effect of surface properties and application method on the retention of *Pseudomonas aeruginosa* on uncoated and titanium-coated stainless steel. *International Biodeterioration and Biodegradation*, 60, 74-80.
- WICKENS, D., LYNCH, S., WEST, G., KELLY, P., VERRAN, J. & WHITEHEAD, K. A. 2014. Quantifying the pattern of microbial cell dispersion, density and clustering on surfaces of differing chemistries and topographies using multifractal analysis. *Journal of Microbiological Methods*, 104, 101-108.
- WICKENS, D. J., WEST, G., KELLY, P. J., VERRAN, J., LYNCH, S. & WHITEHEAD, K. A. 2012. Antimicrobial activity of nanocomposite zirconium nitride/silver coatings to combat external bone fixation pin infections. *International Journal of Artificial Organs*, 35, 817-825.
- WU, Y., ZITELLI, J. P., TENHUISEN, K. S., YU, X. & LIBERA, M. R. 2011. Differential response of *Staphylococci* and osteoblasts to varying titanium surface roughness. *Biomaterials*, 32, 951-960.

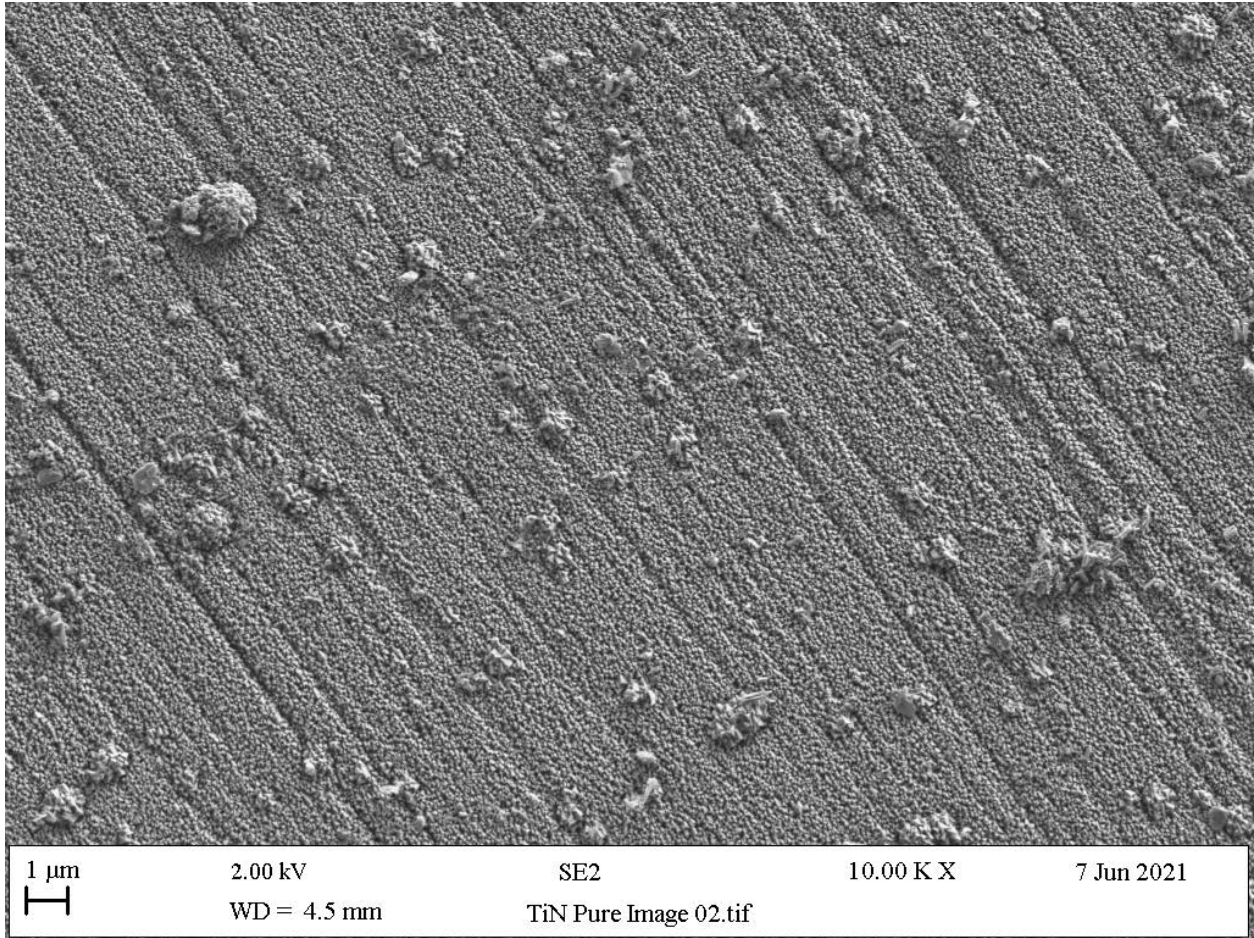
- YEH, T.-S., WU, J.-M. & HU, L.-J. 2008. The properties of TiN thin films deposited by pulsed direct current magnetron sputtering. *Thin Solid Films*, 516, 7294-7298.
- ZANDER, Z. K. & BECKER, M. L. 2018. Antimicrobial and Antifouling Strategies for Polymeric Medical Devices. *ACS Macro Letters*, 7, 16-25.
- ZHANG, M., LIU, X., SHANG, H. & LIN, J. 2019. Comparison of TiN and CN coatings on orthodontic stainless steel: Tribological and biological evaluation. *Surface and Coatings Technology*, 362, 381-387.
- ZHU, Y., KE, J. & ZHANG, L. 2020. Anti-biofouling and Antimicrobial Biomaterials for Tissue Engineering. In: LI, B., MORIARTY, T. F., WEBSTER, T. & XING, M. (eds.) *Racing for the Surface: Antimicrobial and Interface Tissue Engineering*. Cham: Springer International Publishing.

Appendices

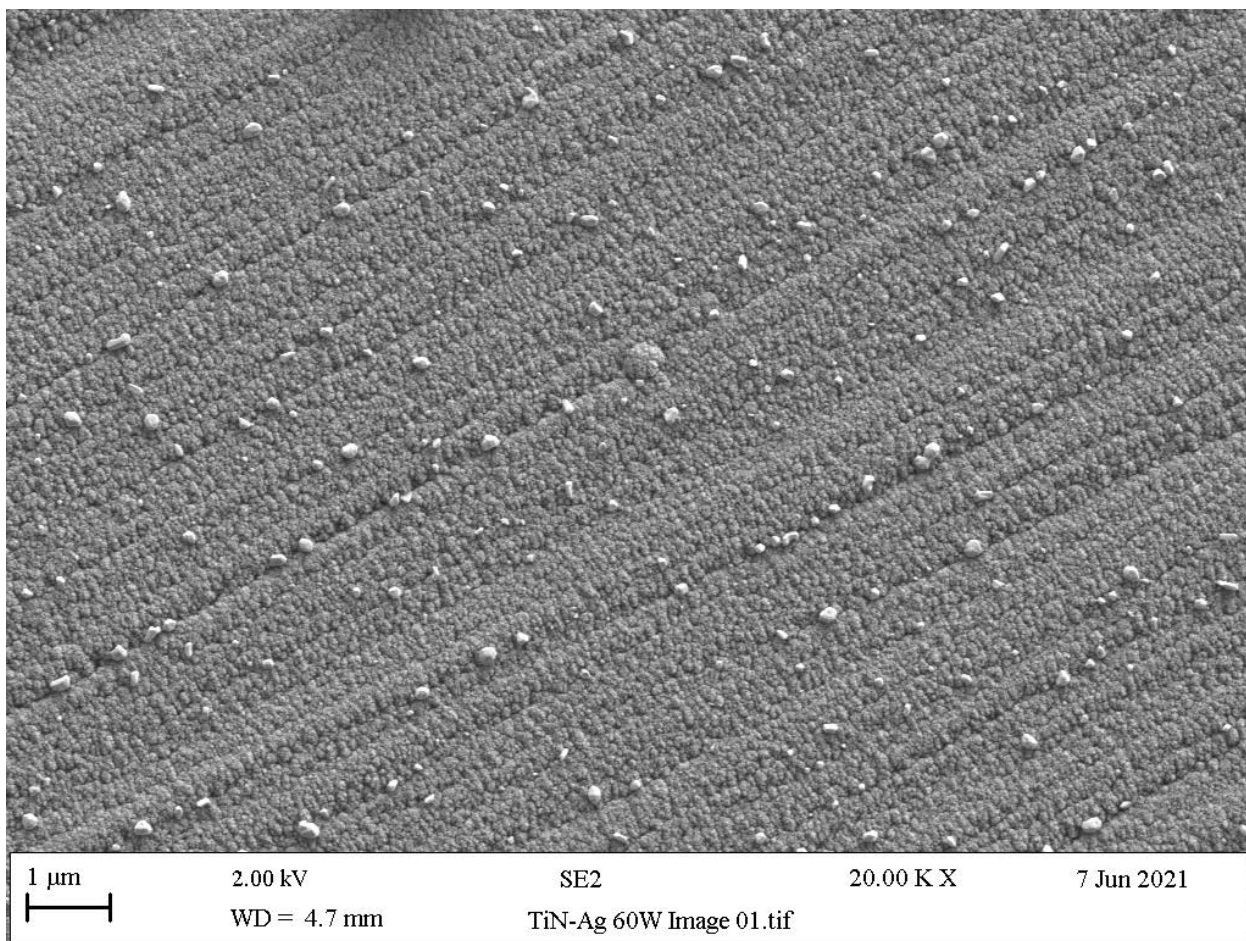
Appendix 1: TiN-Ag 50W Deposited on Stainless-Steel



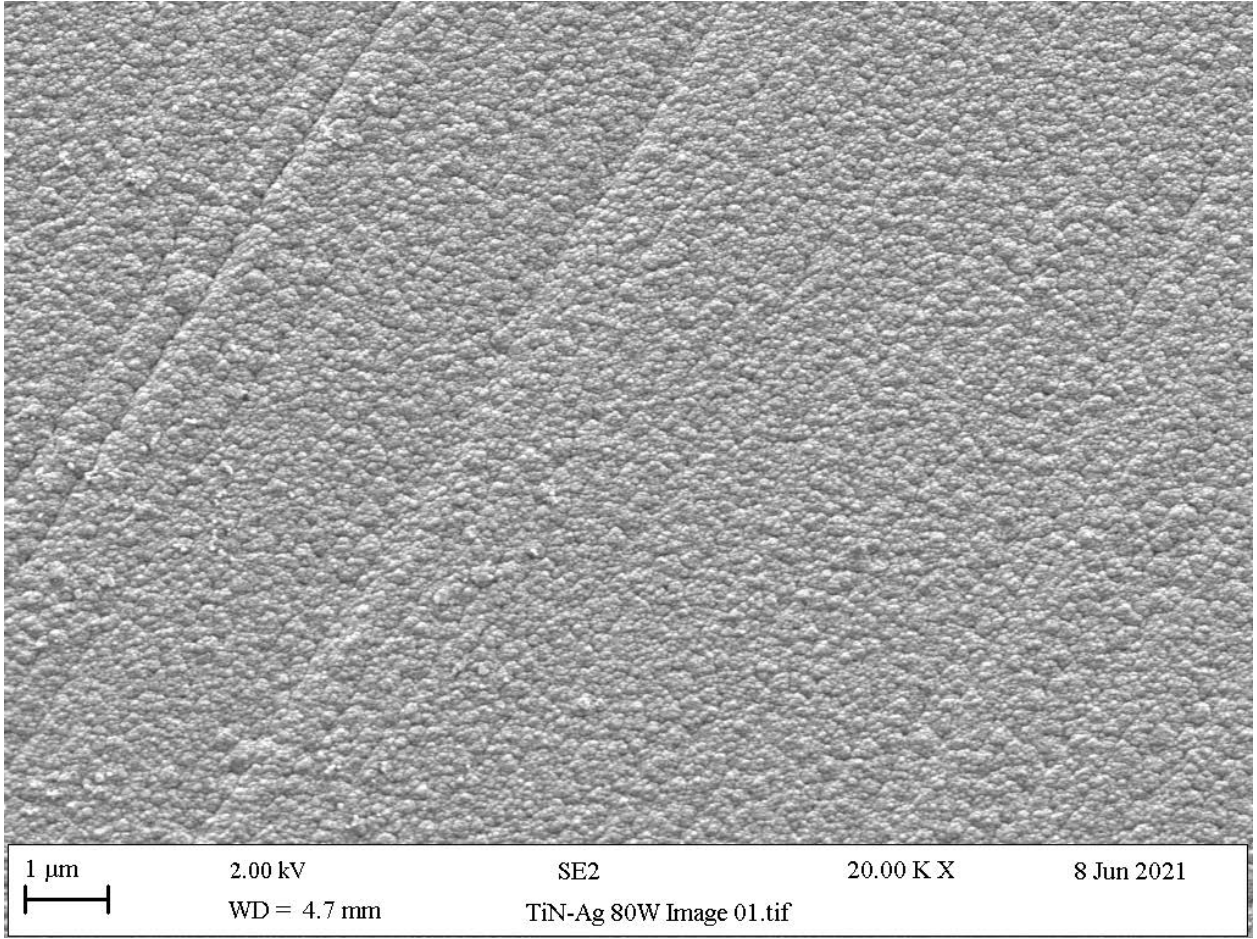
Appendix 2: TiN Deposited onto Stainless-Steel



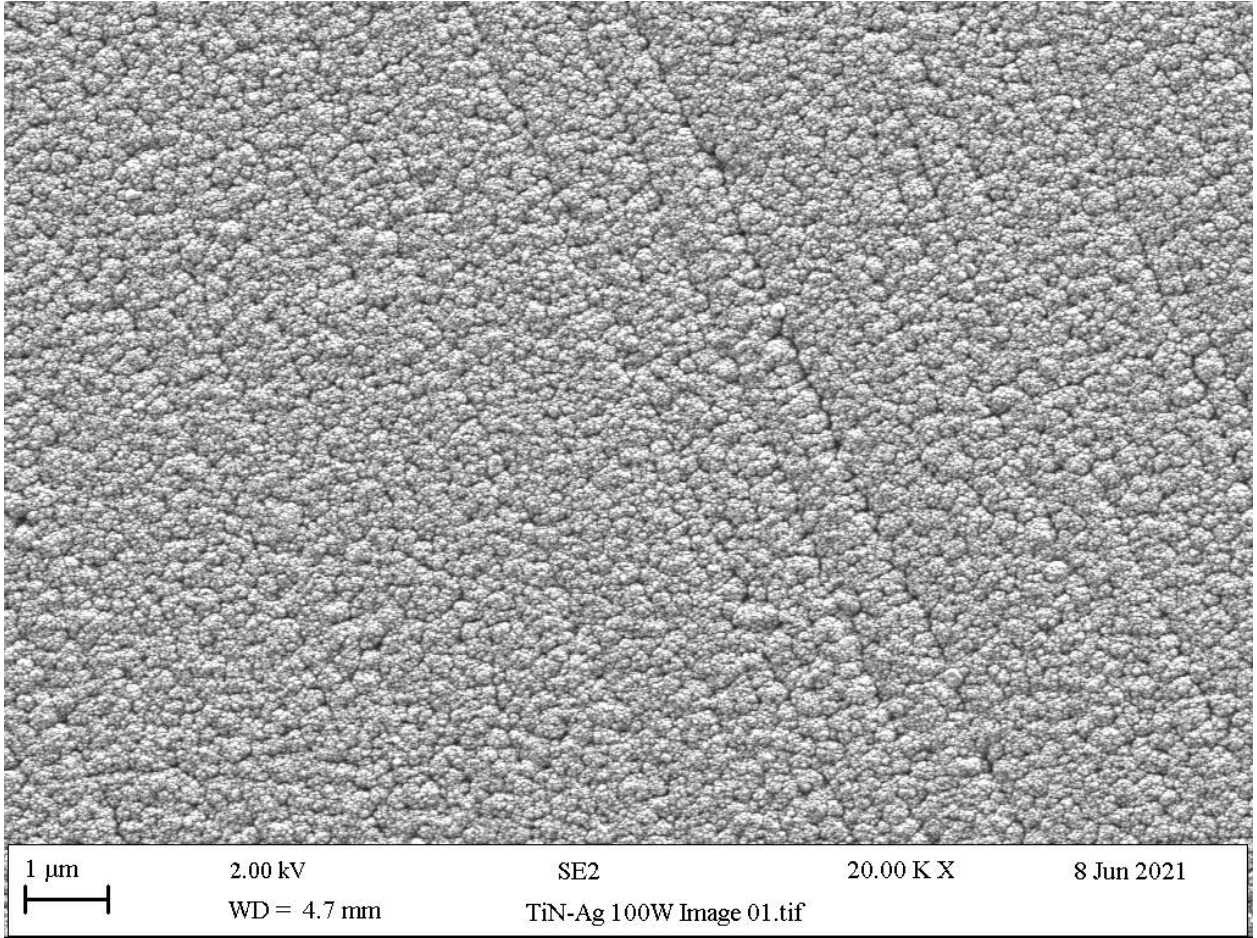
Appendix 3: TiN-Ag 60W Deposited onto Stainless-Steel



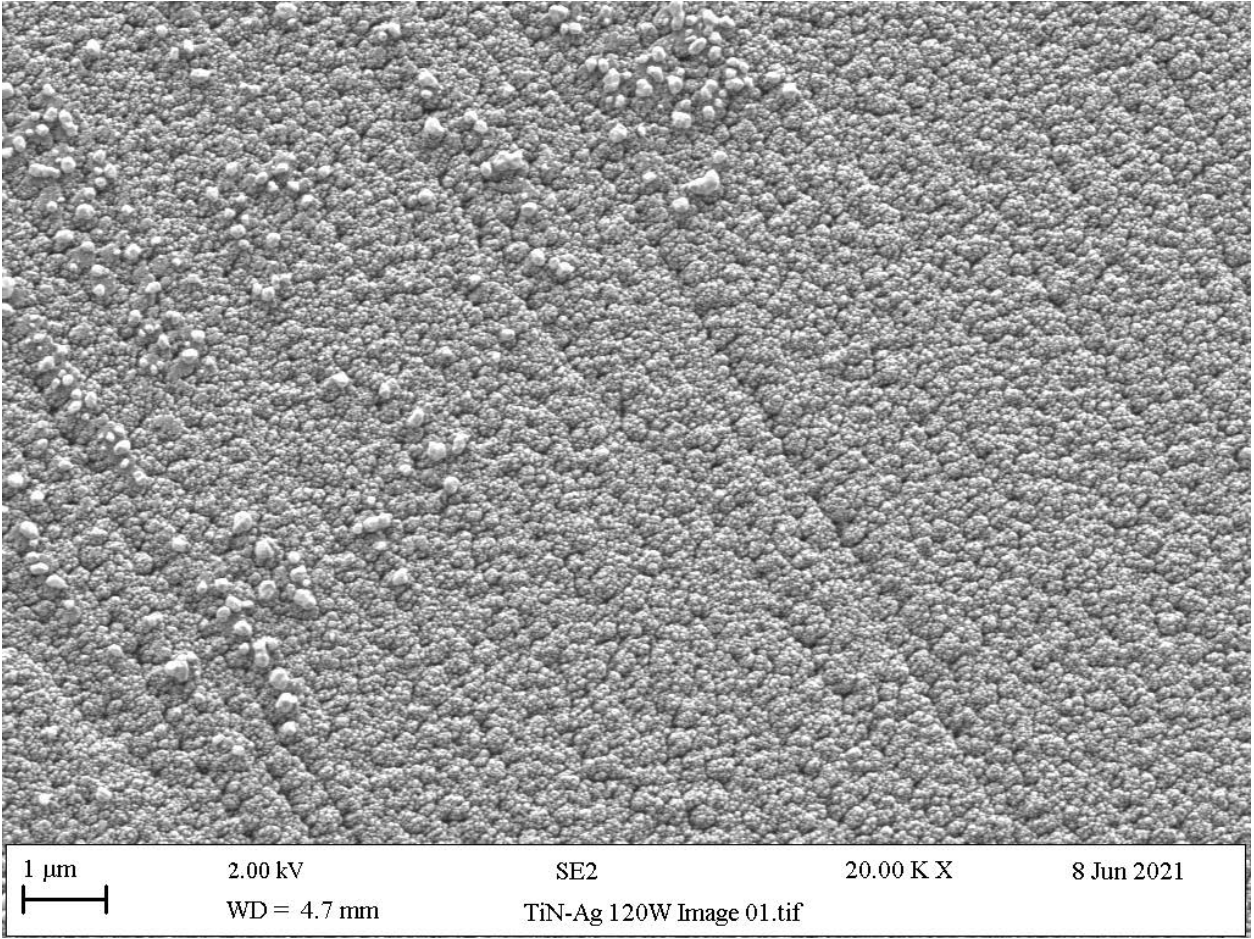
Appendix 4: TiN-Ag 80W Deposited onto Stainless-Steel



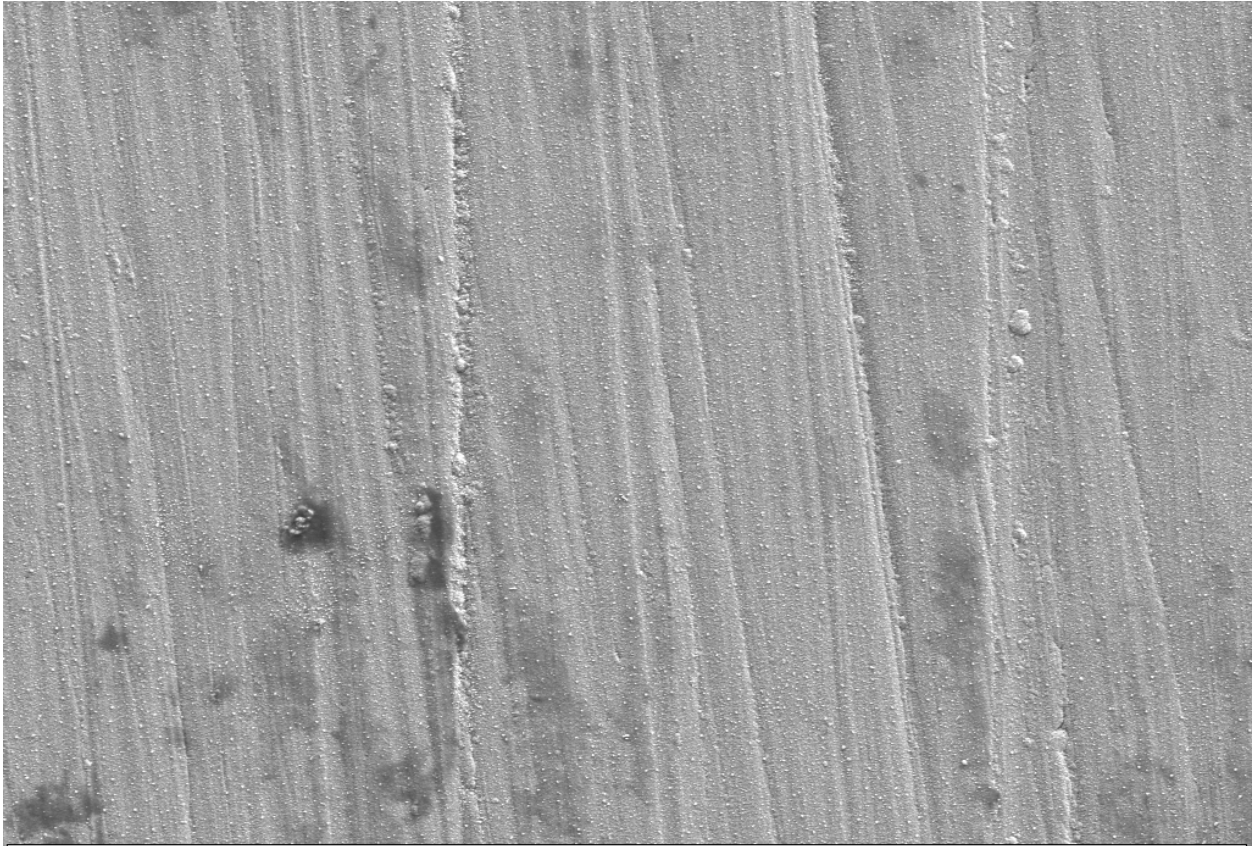
Appendix 5: TiN-Ag 100W Deposited onto Stainless-Steel

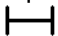


Appendix 6: TiN-Ag 120W Deposited onto Stainless-Steel

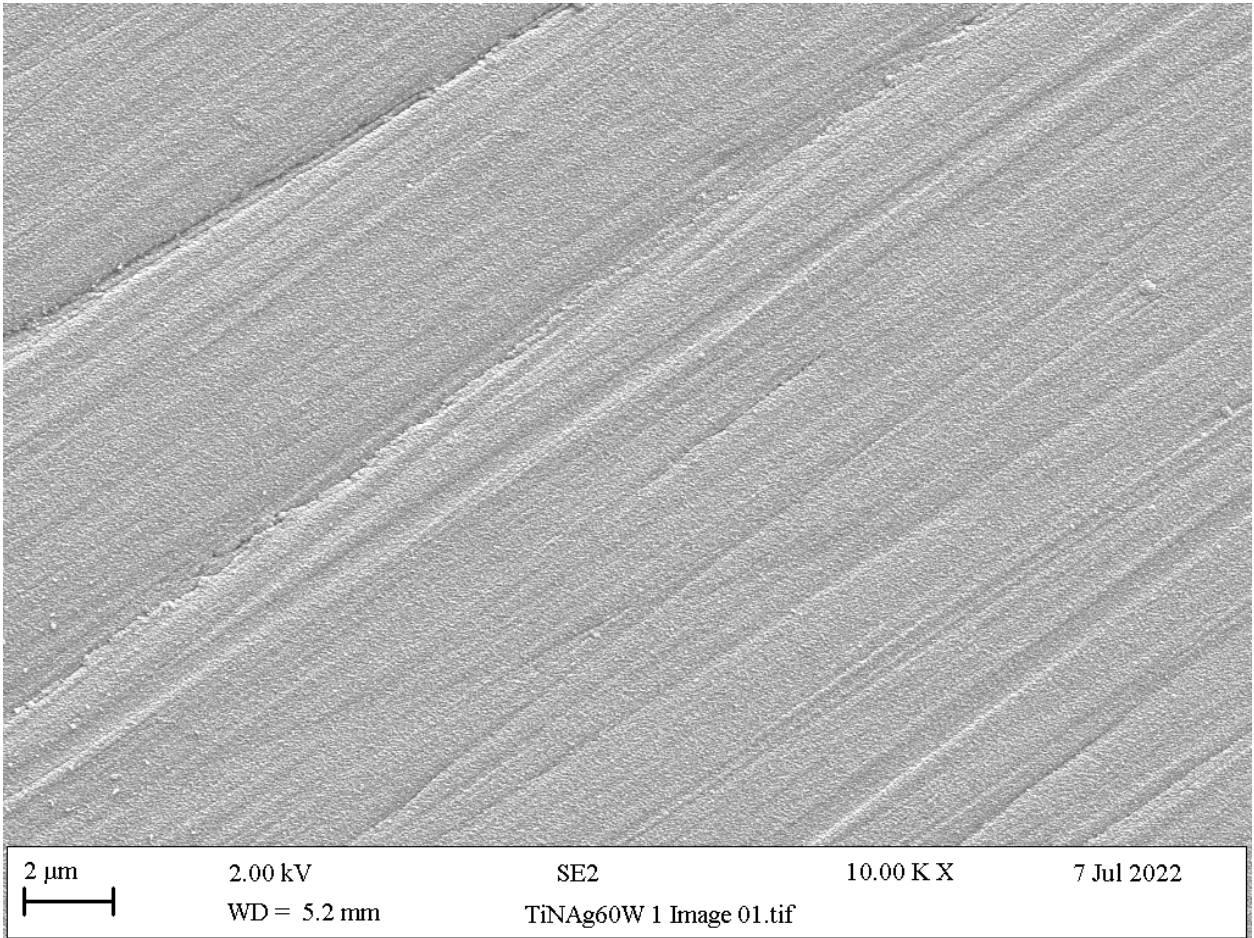


Appendix 7: TiN-Ag 50W Deposited onto Stainless-Steel

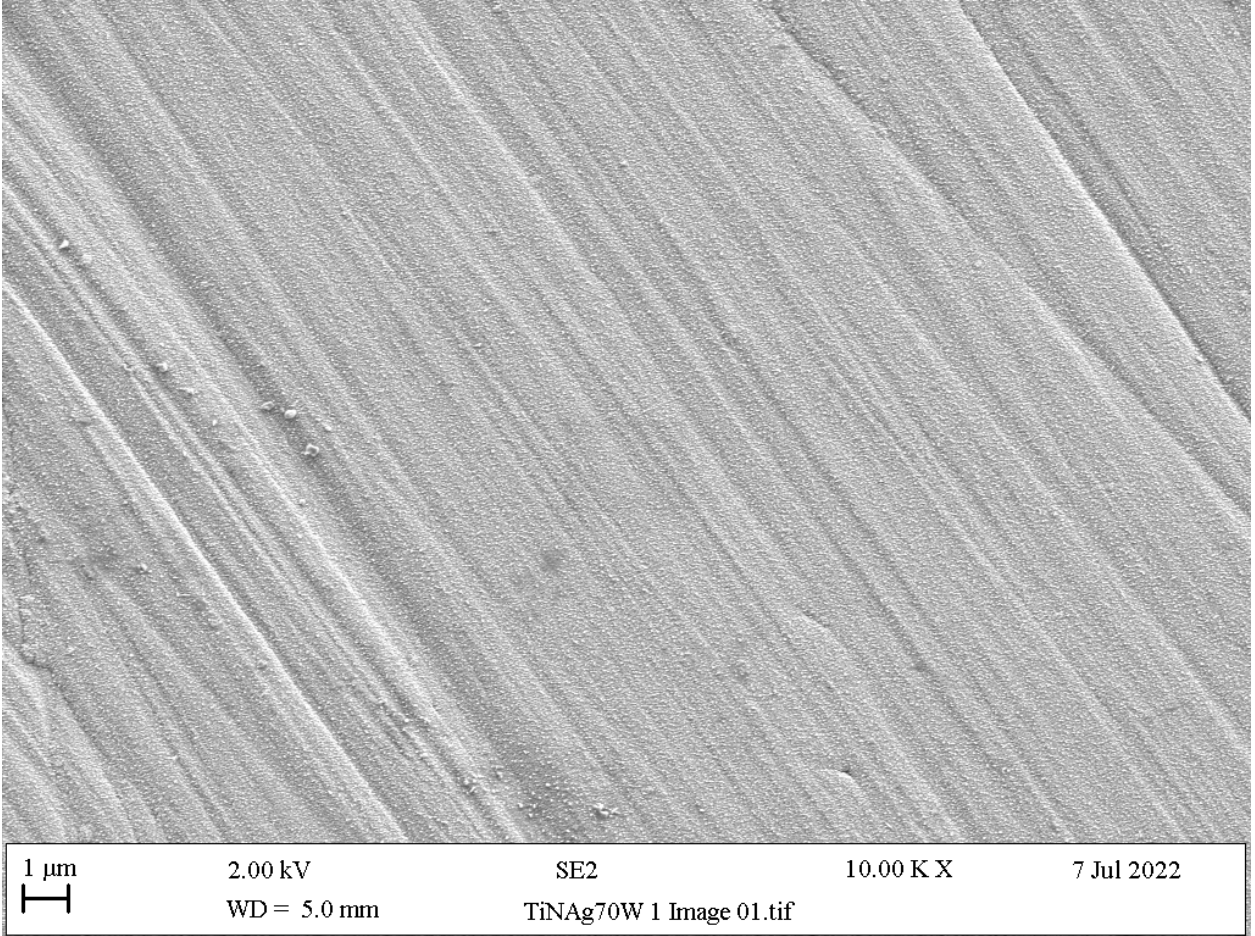


1 μm 	2.00 kV WD = 5.2 mm	SE2 TiNAg50W 1 Image 01.tif	10.00 K X	7 Jul 2022
--	------------------------	--------------------------------	-----------	------------

Appendix 8: TiN-Ag 60W Deposited onto Stainless-Steel

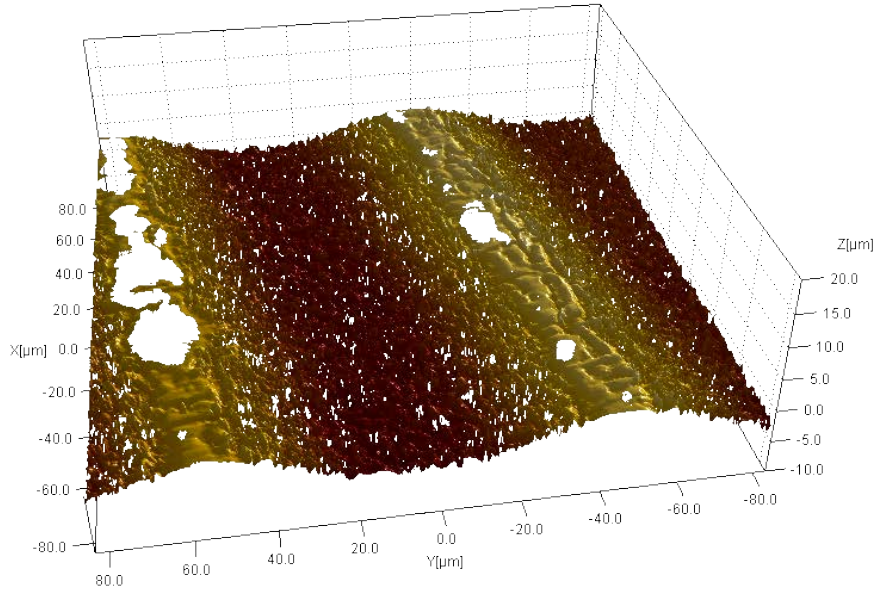


Appendix 9: TiN-Ag 70W Deposited onto Stainless-Steel



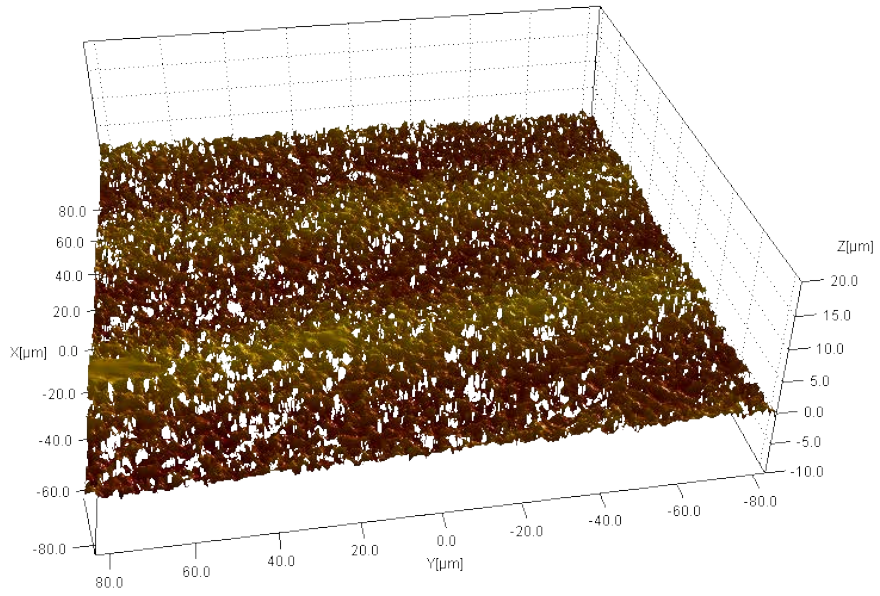
Appendix 10: WLP 3D Map of Stainless-Steel Laser Textured D20 H5 Pattern

1 3D View.zmp



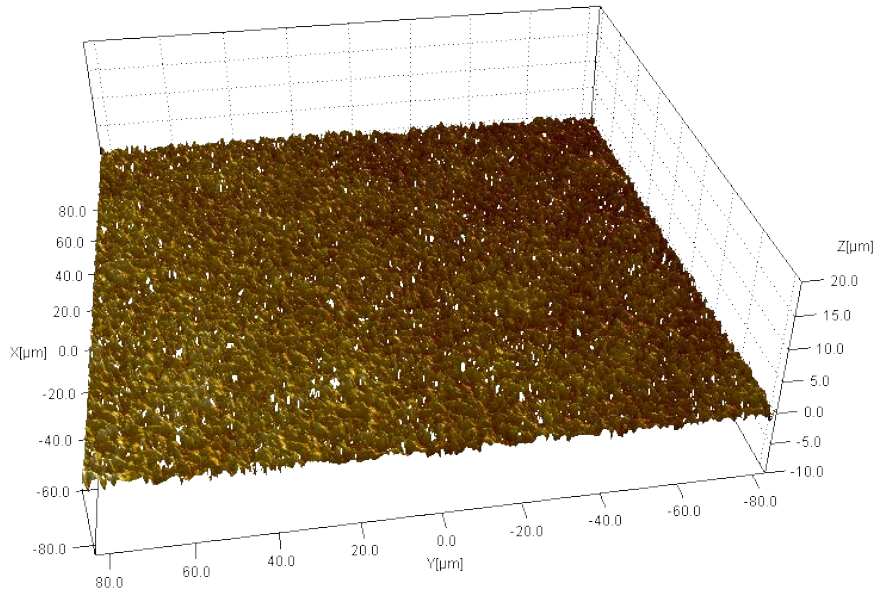
Appendix 11: WLP 3D Map of D50 H5 Laser Texture on Stainless-Steel

1 3D View.zmp



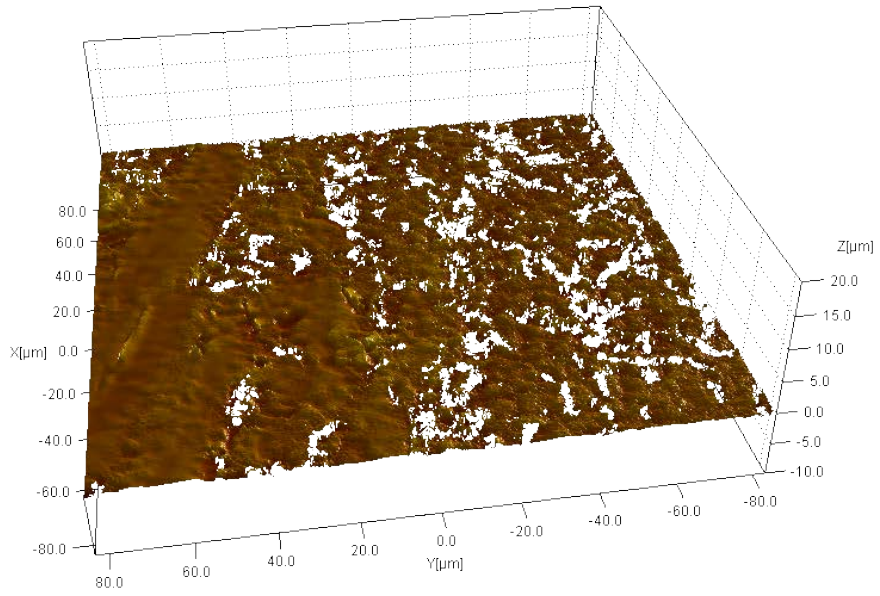
Appendix 12: WLP 3D Map of LIPSS Pattern on Stainless-Steel

2 3D View.zmp



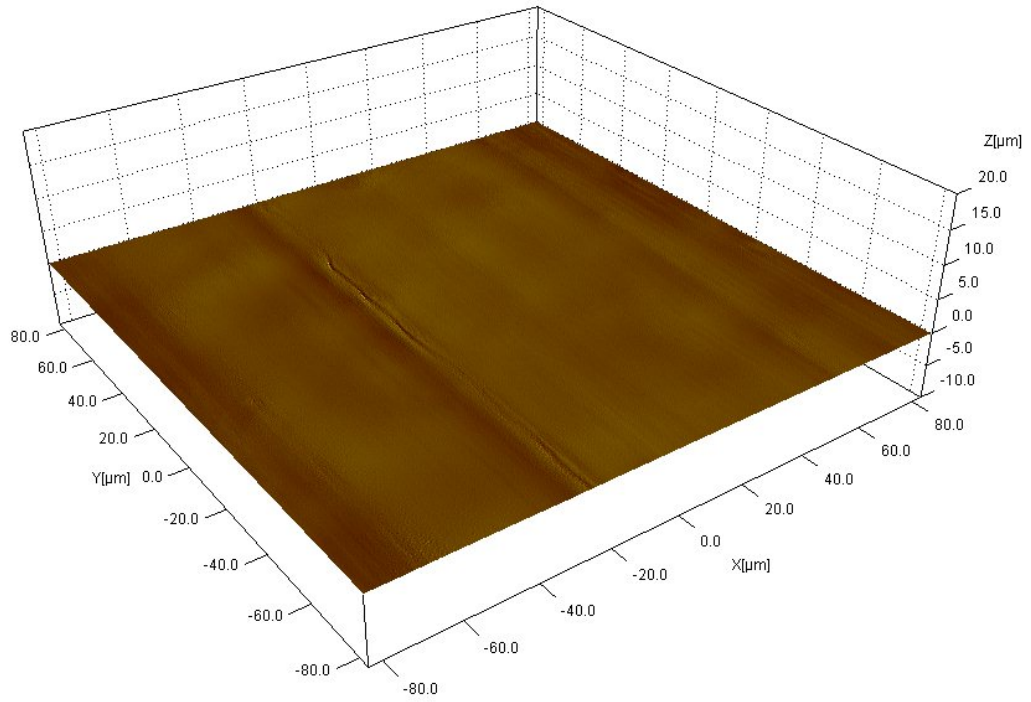
Appendix 13: WLP 3D Map of LIPSS Pattern Coated with TiN-Ag 70W on Stainless-Steel

1_3D_View.zmp



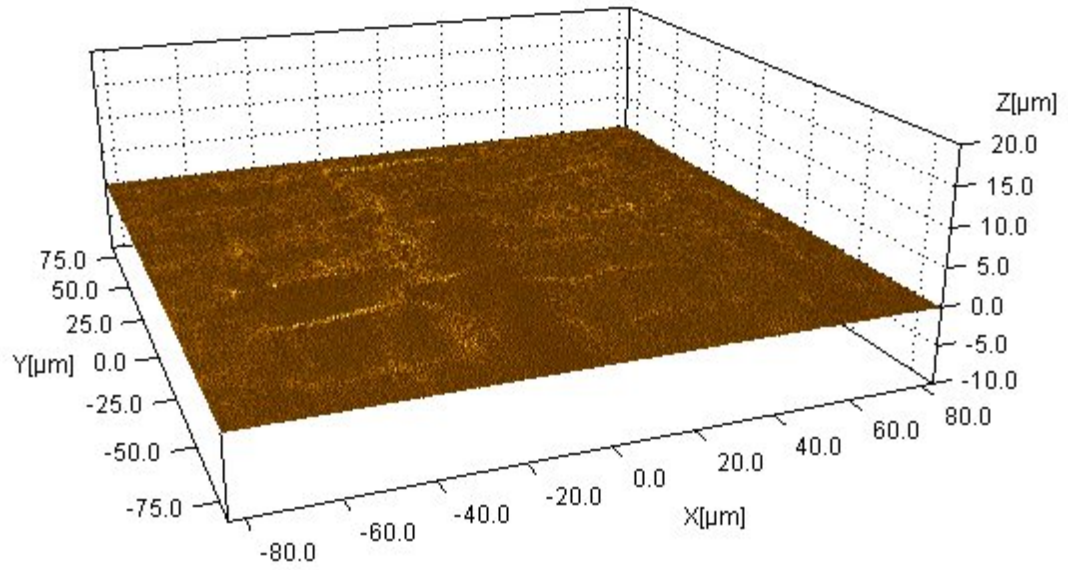
Appendix 14: WLP 3D Map of TiN Coated on Stainless-Steel

TiN 3D View.zmp



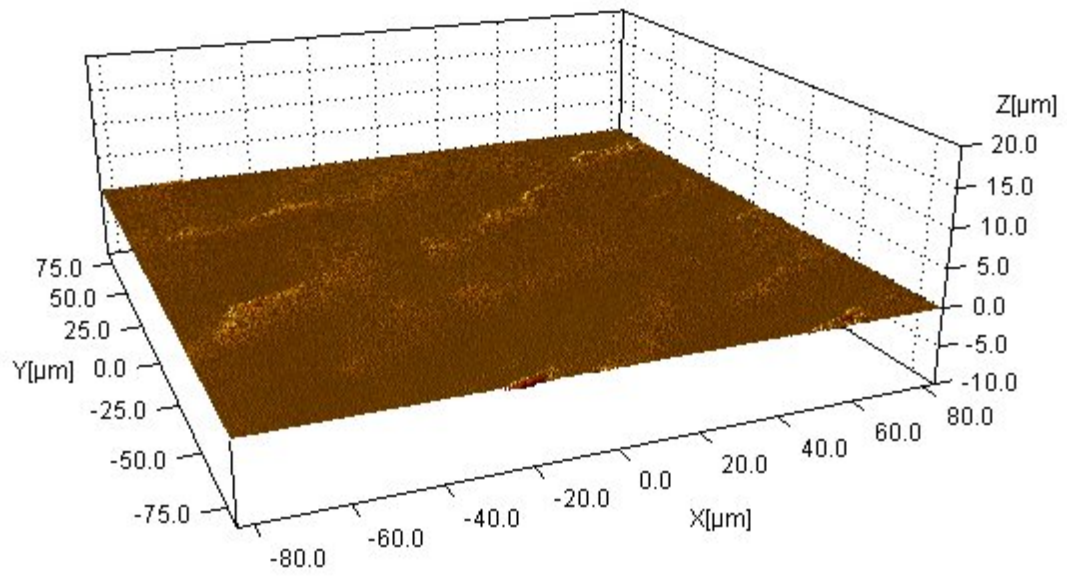
Appendix 15: WLP 3D Map of TiN-Ag 50W Deposited onto Stainless-Steel

TinAg503 3D View.zmp



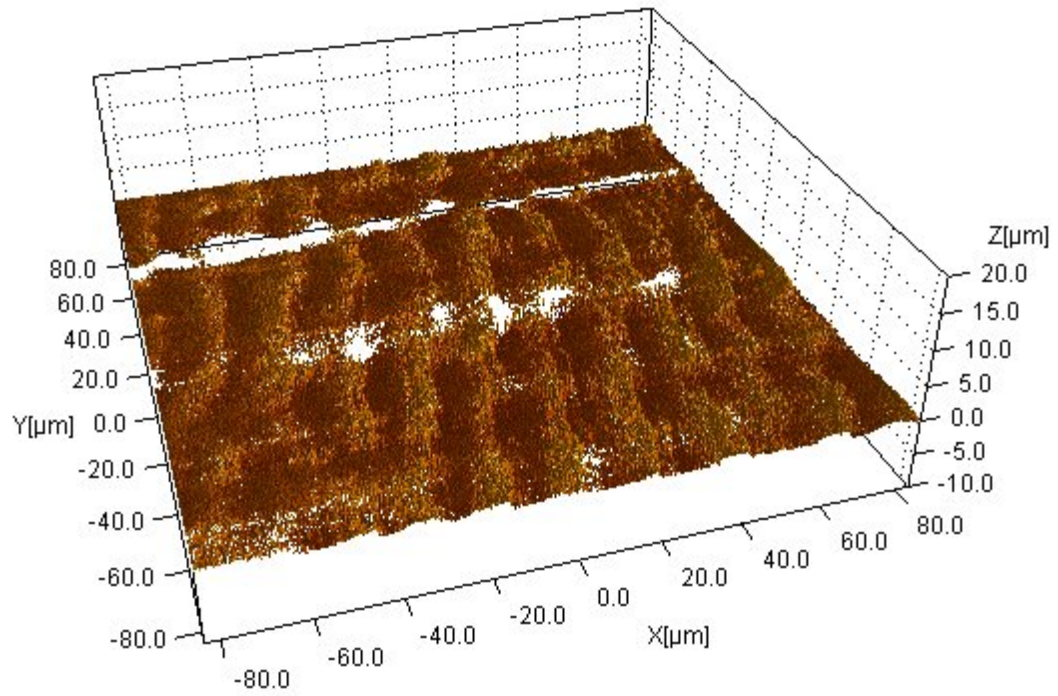
Appendix 16: WLP 3D Map of TiN-Ag 60W Deposited onto Stainless-Steel

tinag608 3D View.zmp



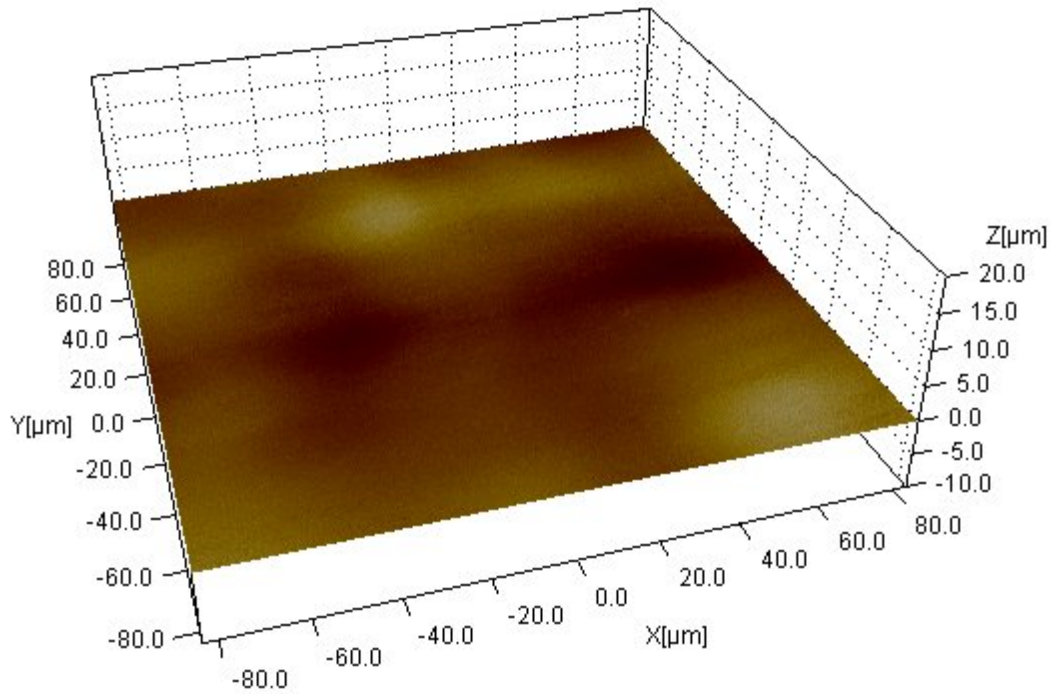
Appendix 17: WLP 3D Map of TiN-Ag 70W Deposited onto Stainless-Steel

tinag701 3D View.zmp



Appendix 18: WLP 3D Map of TiN-Ag 80W Deposited onto Stainless-Steel

tinag802 3D View.zmp



Appendix 19: Raw Data for LIVE/DEAD *S. aureus*

Sample	Total Live	Total Dead	Total Cells	% Live	% Dead
Stainless Steel	156479 ± 97.4	81862 ± 86.3	238341 ± 183.7	65.7 ± 30.4	34.4 ± 52
TiN	66998 ± 228.2	17396 ± 107.5	84394 ± 335.7	79.4 ± 6.8	20.6 ± 12.4
TiN-Ag-50	22987 ± 189.6	59985 ± 337.9	82972 ± 527.5	27.7 ± 16.5	72.3 ± 11.3
TiN-Ag-60	19332 ± 126.6	37675 ± 238.9	57007 365.5	33.9 ± 13.1	66.1 ± 12.7
TiN-Ag-70	252 ± 1.8	110055 ± 188.1	110307 ± 189.9	0.2 ± 13.9	99.8 ± 3.4
TiN-Ag-80	18579 ± 145.1	50424 ± 253.3	69003 ± 398.4	26.9 ± 15.6	73.1 ± 10.1
LIPSS Coated	84554 ± 271.4	250334 ± 406.9	334888 ± 678.3	25.2 ± 13.7	74.8 ± 11.5

Appendix 20: Raw Data for LIVE/DEAD *P. aeruginosa*

Sample	Live Cells	Dead Cells	Total Cells	% Live	% Dead
Stainles Steel	94608 ± 102.1	56356 ± 120.2	150964 ± 222.3	62.7 ± 7.0	37.3 ± 18.3
TiN	227224 ± 63.1	48346 ± 57.2	275570 ± 120.3	82.5 ± 1.7	17.5 ± 6.8
TiN-Ag 50	71013 ± 112.6	290009 ± 333.8	361022 ± 446.4	19.7 ± 11.5	80.3 ± 7.3
TiN-Ag 60	47924 ± 75.1	144135 ± 152.7	192059 ± 227.8	25.0 ± 10.3	75.0 ± 7.1
TiN-Ag 70	4338 ± 8.2	208408 ± 365.2	218991 ± 373.4	4.83 ± 16.1	95.2 ± 18.1
TiN-Ag 80	5432 ± 6.5	166150 ± 396.6	171582 ± 403.1	3.17 ± 6.5	96.8 ± 36.4
LIPSS Coated	94990 ± 167.7	241600 ± 354.8	336590 ± 522.5	28.2 ± 14.0	71.8 ± 12.6

Appendix 21: Retention Assay for Samples *S. aureus*

Staphylococcus aureus	
Sample	Cells/cm2
Stainless Steel	47404
TiN	66540
TiN-Ag 50	29589
TiN-Ag 60	22396
TiN-Ag 70	32816
TiN-Ag 80	24676
D20	91698
D50	29074
LIPSS 1	56991
LIPSS 2	52327
LIPSS Coated	91802

Appendix 22: Retention Assay for *P. aeruginosa*

P aeruginosa	
Sample	Cells/cm ²
Stainless Steel	36959
TiN	45336
TiN-Ag 50	35793
TiN-Ag 60	37063
TiN-Ag 70	43058
TiN-Ag 80	39126
D20	27017
D50	25668
LIPSS 1	29857
LIPSS 2	5530
LIPSS Coated	57221

Appendix 23: Raw Data for T-Test *S. aureus*

	P NUMBER										
	SS	TIN	TIN AG 50	TIN AG 60	TIN AG 70	TIN AG 80	D20	D50	LIPPS 1	LIPSS 2	LIPSS COATED
SS	N/A	0.00053811	6.1576E-09	5.3797E-14	0.00030997	1.6157E-12	3.6901E-06	0.00010171	0.04422478	0.39979933	2.19E-21
TIN	0.00053811	N/A	1.1551E-11	8.0272E-15	5.0878E-08	7.1934E-14	0.01286387	9.6527E-09	0.12535521	0.04666636	1.19742E-05
TINAG 50	6.1576E-09	1.1551E-11	N/A	0.00032778	0.00025424	0.00961255	1.5425E-10	0.89766843	1.4687E-09	4.9699E-05	1.09506E-39
TINAG 60	5.3797E-14	8.0272E-15	0.00032778	N/A	8.939E-11	0.25511493	2.6823E-12	0.10243164	3.877E-13	2.2539E-07	4.21717E-43
TIN AG 70	0.00030997	5.0878E-08	0.00025424	8.939E-11	N/A	6.8623E-09	3.4507E-08	0.07934901	7.314E-06	0.00599255	4.45572E-33
TIN AG 80	1.6157E-12	7.1934E-14	0.00961255	0.25511493	6.8623E-09	N/A	9.4822E-12	0.27630779	4.7007E-12	1.284E-06	2.4639E-42
D20	3.6901E-06	0.01286387	1.5425E-10	2.6823E-12	3.4507E-08	9.4822E-12	N/A	1.4737E-09	0.00045288	0.00045288	0.99096325
D50	0.00010171	9.6527E-09	0.89766843	0.10243164	0.07934901	0.27630779	1.4737E-09	N/A	1.3834E-06	0.00047375	3.91064E-25
LIPPS 1	0.04422478	0.12535521	1.4687E-09	3.877E-13	7.314E-06	4.7007E-12	0.00045288	1.3834E-06	N/A	0.4797811	8.63518E-11
LIPSS 2	0.39979933	0.04666636	4.9699E-05	2.2539E-07	0.00599255	1.284E-06	0.00045288	0.00047375	0.4797811	N/A	1.1071E-09
LIPSS COATED	2.19E-21	1.1974E-05	1.0951E-39	4.2172E-43	4.4557E-33	2.4639E-42	0.99096325	3.9106E-25	8.6352E-11	1.1071E-09	N/A

Appendix 24: Analysed Data for T-Test *S. aureus*

	P NUMBER										
	SS	TIN	TIN AG 50	TIN AG 60	TIN AG 70	TIN AG 80	D20	D50	LIPPS 1	LIPSS 2	LIPSS COATED
SS	N/A	< 0.05	< 0.05	< 0.05	< 0.05	< 0.05	< 0.05	< 0.05	0.044	0.400	< 0.05
TIN	< 0.05	N/A	< 0.05	< 0.05	< 0.05	< 0.05	< 0.05	< 0.05	0.125	0.047	< 0.05
TINAG 50	< 0.05	< 0.05	N/A	< 0.05	< 0.05	< 0.05	< 0.05	0.898	< 0.05	< 0.05	< 0.05
TINAG 60	< 0.05	< 0.05	< 0.05	N/A	< 0.05	0.255	< 0.05	0.102	< 0.05	< 0.05	< 0.05
TIN AG 70	< 0.05	< 0.05	< 0.05	< 0.05	N/A	< 0.05	< 0.05	0.079	< 0.05	< 0.05	< 0.05
TIN AG 80	< 0.05	< 0.05	< 0.05	0.255	< 0.05	N/A	< 0.05	0.276	< 0.05	< 0.05	< 0.05
D20	< 0.05	0.013	< 0.05	< 0.05	< 0.05	< 0.05	N/A	< 0.05	< 0.05	< 0.05	< 0.05
D50	< 0.05	< 0.05	0.898	0.102	0.079	0.276	< 0.05	N/A	< 0.05	< 0.05	< 0.05
LIPPS 1	0.044	0.125	< 0.05	< 0.05	< 0.05	< 0.05	< 0.05	< 0.05	N/A	0.480	< 0.05
LIPSS 2	0.400	0.047	< 0.05	< 0.05	< 0.05	< 0.05	< 0.05	< 0.05	0.480	N/A	< 0.05
LIPSS COATED	< 0.05	< 0.05	< 0.05	< 0.05	< 0.05	< 0.05	< 0.05	< 0.05	< 0.05	< 0.05	N/A

Appendix 25: Retention Assay Raw Data T-Test *P. aeruginosa*

	P NUMBER										
	Stainless-Steel	TiN	TiN-Ag 50	TiN-Ag 60	TiN-Ag 70	TiN-Ag 80	D20	D50	LIPSS 1	LIPSS 2	LIPSS Coated
Stainless-Steel	N/A	0.00064943	0.58153858	0.96307988	0.00571231	0.28498835	2.0848E-05	4.2181E-10	0.0123861	7.69128E-39	2.33084E-15
TiN	0.00064943	N/A	6.4036E-05	0.00092457	0.3353148	0.00599437	9.688E-12	2.6024E-18	6.589E-07	1.3283E-42	2.56553E-06
TiN-Ag 50	0.581538579	6.4036E-05	N/A	0.55725943	0.00062701	0.08379623	7.9587E-05	1.0064E-09	0.0310582	7.32812E-41	1.22725E-17
TiN-Ag 60	0.963079882	0.00092457	0.55725943	N/A	0.00778284	0.32075779	2.477E-05	1.0511E-09	0.0122621	1.85305E-37	8.20349E-15
TiN-Ag 70	0.005712308	0.3353148	0.00062701	0.00778284	N/A	0.04877917	3.9892E-11	1.9676E-19	5.217E-06	1.51106E-47	2.07041E-09
TiN-Ag 80	0.284988352	0.00599437	0.08379623	0.32075779	0.04877917	N/A	3.7791E-08	1.4486E-16	0.0006627	3.32399E-49	7.98634E-15
D20	2.08479E-05	9.688E-12	7.9587E-05	2.477E-05	3.9892E-11	3.7791E-08	N/A	0.42827273	0.3173216	1.65921E-24	1.94926E-25
D50	4.21812E-10	2.6024E-18	1.0064E-09	1.0511E-09	1.9676E-19	1.4486E-16	0.42827273	N/A	0.0817826	1.11899E-56	2.3284E-37
LIPSS 1	0.012386138	6.5886E-07	0.03105823	0.01226215	5.2174E-06	0.0006627	0.31732162	0.08178261	N/A	3.05858E-18	7.93845E-17
LIPSS 2	7.69128E-39	1.3283E-42	7.3281E-41	1.853E-37	1.5111E-47	3.324E-49	1.6592E-24	1.119E-56	3.059E-18	N/A	1.06253E-59
LIPSS Coated	2.33084E-15	2.5655E-06	1.2272E-17	8.2035E-15	2.0704E-09	7.9863E-15	1.9493E-25	2.3284E-37	7.938E-17	1.06253E-59	N/A

Appendix 26: Retention Assay Analysed Results T-test *P. aeruginosa*

	P NUMBER										
	Stainless-Steel	TiN	TiN-Ag 50	TiN-Ag 60	TiN-Ag 70	TiN-Ag 80	D20	D50	LIPSS 1	LIPSS 2	LIPSS Coated
Stainless-Steel	N/A	< 0.05	0.582	0.963	< 0.05	0.285	< 0.05	< 0.05	< 0.05	< 0.05	< 0.05
TiN	< 0.05	N/A	< 0.05	< 0.05	0.335	< 0.05	< 0.05	< 0.05	< 0.05	< 0.05	< 0.05
TiN-Ag 50	0.582	< 0.05	N/A	0.557	< 0.05	0.084	< 0.05	< 0.05	< 0.05	< 0.05	< 0.05
TiN-Ag 60	0.963	< 0.05	0.557	N/A	< 0.05	0.321	< 0.05	< 0.05	< 0.05	< 0.05	< 0.05
TiN-Ag 70	< 0.05	0.335	< 0.05	< 0.05	N/A	0.049	< 0.05	< 0.05	< 0.05	< 0.05	< 0.05
TiN-Ag 80	0.285	< 0.05	0.084	0.321	0.0488	N/A	< 0.05	< 0.05	< 0.05	< 0.05	< 0.05
D20	< 0.05	< 0.05	< 0.05	< 0.05	< 0.05	< 0.05	N/A	0.428	0.317	< 0.05	< 0.05
D50	< 0.05	< 0.05	< 0.05	< 0.05	< 0.05	< 0.05	0.428	N/A	0.082	< 0.05	< 0.05
LIPSS 1	< 0.05	< 0.05	< 0.05	< 0.05	< 0.05	< 0.05	0.317	0.082	N/A	< 0.05	< 0.05
LIPSS 2	< 0.05	< 0.05	< 0.05	< 0.05	< 0.05	< 0.05	< 0.05	< 0.05	< 0.05	N/A	< 0.05
LIPSS Coated	< 0.05	< 0.05	< 0.05	< 0.05	< 0.05	< 0.05	< 0.05	< 0.05	< 0.05	< 0.05	N/A

Appendix 27: NBT Results for Samples

Sample	Colony Forming Units (cm ⁻²)
SS	20.22 ± 3.07
TiN	52.71 ± 5.16
TiNAg-50W	1.33 ± 0.45
TiNAg-60W	3.33 ± 1.37
TiNAg-70W	3.56 ± 2.75
TiNAg-80W	0 ± 0